Two-way coupled meteorology and air quality models in Asia: a systematic review and meta-analysis of impacts of aerosol feedbacks on meteorology and air quality

Chao Gao[1], Aijun Xiu[1, *], Xuelei Zhang[1, *], Qingqing Tong[1], Hongmei Zhao[1], Shichun Zhang[1], Guangyi Yang[1, 2], and Mengduo Zhang[1, 2]

[1]Key Laboratory of Wetland Ecology and Environment, Northeast Institute of Geography and Agroecology, Chinese Academy of Sciences, Changchun, 130102, China
[2]University of Chinese Academy of Sciences, Beijing, 100049, China
Correspondence to: A.J. Xiu (xiuaijun@iga.ac.cn) & X.L. Zhang (zhangxuelei@iga.ac.cn)

Abstract

Atmospheric aerosols can exert influence on meteorology and air quality through aerosol-radiation interactions (ARI) and aerosol-cloud interactions (ACI) and this two-way feedback has been studied by applying two-way coupled meteorology and air quality models. As one of regions with high aerosol loading in the world, Asia has attracted many researchers to investigate the aerosol effects with several two-way coupled models (WRF-Chem, WRF-CMAQ, GRAPES-CUACE, WRF-NAQPMS and GATOR-GCMOM) over the last decade. This paper attempts to offer bibliographic analysis regarding the current status of applications of two-way coupled models in Asia, related research focuses, model performances and the effects of ARI or/and ACI on meteorology and air quality. There are total 160 peer-reviewed articles published between 2010 and 2019 in Asia meeting the inclusion criteria, with more than 79 % of papers involving the WRF-Chem model. The number of relevant publications has an upward trend annually and East Asia, India, China, as well as the North China Plain are the most studied areas. The effects of ARI and both ARI and ACI induced by natural aerosols (particularly mineral dust) and anthropogenic aerosols (bulk aerosols, different chemical compositions and aerosols from different sources) are widely investigated in Asia. Through the meta-analysis of surface meteorological and air quality variables simulated by two-way coupled models, the model performance affected by aerosol feedbacks depends on different variables, simulation time lengths, selection of two-way coupled models, and study areas. Future research perspectives with respect to the development, improvement, application, and evaluation of two-way coupled meteorology and air quality models are proposed.

1 Introduction

Atmospheric pollutants can affect local weather and global climate via many mechanisms as extensively summarized in the Intergovernmental Panel on Climate Change (IPCC) reports (IPCC, 2007, 2014, 2021), and also exhibit impacts on human health and ecosystems (Lelieveld et al., 2015; Wu and Zhang, 2018). Atmospheric pollutants can modify the radiation energy balance, thus influence meteorological conditions (Gray et al., 2010; Yiğit et al., 2016). Compared to other climate agents, the short-lived and localized aerosols could induce changes in meteorology and climate through aerosol-radiation interactions (ARI, Satheesh and Moorthy, 2005; Tremback et al., 1986) and aerosol-cloud interactions (ACI, Lohmann and Feichter, 2005; Martin and Leight, 1949) or both (Haywood and Boucher, 2000; Sud and Walker, 1990). ARI (previously known as direct effect and semi-direct effect) are based on scattering and absorbing solar radiation by aerosols as well as cloud dissipation by heating (Ackerman et al., 2000; Koch and Genio, 2010; McCormick and Ludwig, 1967; Wilcox, 2012), and ACI (known as indirect effect) are concerned with aerosols altering albedo and lifetime of clouds (Albrecht, 1989; Lohmann and Feichter, 2005; Twomey, 1977). As our knowledge base of aerosol-radiation-cloud interactions that involve extremely complex physical and chemical processes has been expanding, accurately assessing the effects of these interactions still remains a big challenge (Chung, 2012; Fan et al., 2016; Kuniyal and Guleria, 2019; Rosenfeld et al., 2019, 2008).

The interactions between air pollutants and meteorology can be investigated by observational analyses and/or air quality models. So far, many observational studies using measurement data from a variety of sources have been conducted to analyze these interactions (Bellouin et al., 2008; Groß et al., 2013; Rosenfeld et al., 2019; Wendisch et al., 2002). Yu et al. (2006) reviewed research work that adopted satellite and ground-based measurements to estimate the ARI-induced changes of radiative forcing and the associated uncertainties in the analysis. Yoon et al. (2019) analyzed the effects of aerosols on the radiative forcing based on the Aerosol Robotic Network observations and demonstrated that these effects depended on aerosol types. On the other hand, since the uncertainties in ARI estimations were associated with ACI (Kuniyal and Guleria, 2019), the simultaneous assessments of both ARI and ACI effects were needed and had gradually been conducted via satellite observations (Illingworth et al., 2015; Kant et al., 2019; Quaas et al., 2008; Sekiguchi et al., 2003). In the early stages, observational studies of ACI effects were based on several cloud parameters mainly derived from surface-based microwave radiometer (Kim et al., 2003; Liu et al., 2003) and cloud radar (Feingold et al., 2003; Penner et al., 2004). Later on, with the further development of satellite observation technology and enhanced spatial resolution of satellite measurement comparing against traditional ground observations, the satellite-retrieved cloud parameters (effective cloud droplet radius, liquid water path (LWP) and cloud cover) were utilized to identify the ACI effects studies on cloud scale. (Goren and Rosenfeld, 2014; Rosenfeld et al., 2014). Moreover, in order to clarify whether aerosols affect precipitation positively or negatively, the effects of ACI on cloud properties and precipitation were widely investigated but with various answers (Andreae and Rosenfeld, 2008; Casazza et al., 2018; Fan et al., 2018; Rosenfeld et al., 2014). Analyses of satellite and/or ground observations revealed that increased aerosols could suppress (enhance) precipitation in drier (wetter) environments (Donat et al., 2016; Li et al., 2011; Rosenfeld, 2000; Rosenfeld et al., 2008). Most recently, Rosenfeld et al. (2019) further used satellite-derived cloud information (droplet concentration and updraft velocity at cloud base, LWP at cloud cores, cloud geometrical thickness and cloud fraction) to single out ACI under a certain meteorological condition, and found that the cloudiness change caused by aerosol in marine low-level clouds was much greater than previous analyses (Sato and Suzuki, 2019). Despite the fact that aforementioned studies had significantly improved our understanding of aerosol effects, many limitations still exist, such as low temporal resolution of satellite data, low spatial resolution of ground monitoring sites and lack of vertical distribution information of aerosol and cloud (Rosenfeld et al., 2014; Sato and Suzuki, 2019; Yu et al., 2006).

Numerical models can also be used to study the interactions between air pollutants and meteorology. Air quality models simulate physical and chemical processes in the atmosphere (ATM) and are classified as offline and online models (El-Harbawi, 2013). Offline models (also known as traditional air quality models) require outputs from meteorological models to subsequently drive chemical models (Byun and Schere, 2006; ENVIRON, 2008; Seaman, 2000). Comparing to online models, offline models usually are computationally efficient but incapable of capturing two-way feedbacks between chemistry and meteorology (North et al., 2014). Online models or coupled models are designed and developed to consider the two-way feedbacks and attempted to accurately simulate both meteorology and air quality (Briant et al., 2017; Grell et al., 2005; Wong et al., 2012). Two-way coupled models can be generally categorized as integrated and access models based on whether using a coupler to exchange variables between meteorological and chemical modules (Baklanov et al., 2014). As Zhang (2008) pointed out, Jacobson (1994, 1997) and Jacobson et al. (1996) pioneered the development of a fully-coupled model named Gas, Aerosol, Transport, Radiation, General Circulation, Mesoscale, and Ocean Model (GATOR-GCMOM) in order to investigate all the processes related to ARI and ACI. Currently, there are three representative two-way coupled meteorology and air quality models, namely the Weather Research and Forecasting-Chemistry (WRF-Chem) (Grell et al., 2005), WRF coupled with Community Multiscale Air Quality (CMAQ) (Wong et al., 2012) and WRF coupled with a multi-scale chemistry-transport model for atmospheric composition analysis and forecast (WRF-CHIMERE) (Briant et al., 2017). The WRF-Chem is an integrated model that includes various chemical modules in the meteorological model (i.e., WRF) without using a coupler. For the remaining two models, which belong to access model, the WRF-CMAQ uses a subroutine called *aqprep* (Wong et al., 2012) as its coupler while the WRF-CHEMERE a general coupling software named Ocean Atmosphere Sea Ice Soil-Model Coupling Toolkit (Craig et al. 2017). With more growing interest in coupled models and their developments, applications and evaluations, two review papers thoroughly summarized the related works published before 2008 (Zhang, 2008) and 2014 (Baklanov et al., 2014). Zhang (2008) overviewed the developments and applications of five coupled models in the United States (US) and the treatments of chemical and physical processes in these coupled models with emphasis on the ACI related processes. Another paper presented a systematic review on the similarities and differences of eighteen integrated or access models in Europe and discussed the descriptions of interactions between meteorological and chemical processes in these models as well as the model evaluation methodologies involved (Baklanov et al., 2014). Some of these coupled models can not only be used to investigate the interactions between air quality and meteorology at regional scales but also at global and hemispheric scales (Grell et al., 2011; Jacobson, 2001; Mailler et al., 2017; Xing et al., 2015a), but large scale studies were not included in the two review papers by Zhang (2008) and Baklanov et al. (2014). These reviews only focused on application and evaluation of coupled models in US and Europe but there is still no systematic review targeting two-way coupled model applications in Asia.

Compared to US and Europe, Asia has been suffering more severe air pollution in the past three decades (Bollasina et al.,2011; Gurjar et al., 2016; Rohde and Muller, 2015) due to the rapid industrialization, urbanization and population growth together with unfavorable meteorological conditions (Jeong and Park, 2017; Lelieveld et al., 2018; Li M. et al., 2017). Then, the interactions between atmospheric pollution and meteorology in Asia, which have received a lot of attention from scientific community, are investigated using extensive observations and a certain number of numerical simulations (Li et al., 2016; Nguyen et al., 2019a; Wang et al., 2010). Based on airborne, ground-based, and satellite-based observations, multiple important experiments have been carried out to analyze properties of radiation, cloud and aerosols in Asia, as briefly reviewed by Lin N. et al. (2014). Recent observational studies confirmed that increasing aerosol loadings play important roles in radiation budget (Benas et al., 2020; Eck et al., 2018), cloud properties (Dahutia et al., 2019; Yang et al., 2019), precipitation intensity along with vertical distributions of precipitation types (Guo et al., 2018, 2014). According to previous observational studies in Southeast Asia (SEA), Tsay et al. (2013) and Lin N. et al. (2014) comprehensively summarized the spatiotemporal characteristics of biomass burning (BB) aerosols and clouds as well as their interactions. Li et al. (2016) analyzed how ARI or ACI influenced climate/meteorology in Asia utilizing observations and climate models. With regard to the impacts of aerosols on cloud, precipitation and climate in East Asia (EA), a detailed review of observations and modeling simulations has also been presented by Li Z. et al. (2019). Since the 2000s, substantial progresses have been made in the climate-air pollution interactions in Asia based on regional climate models simulations, which have been summarized by Li et al. (2016). Moreover, starting from year of 2010, with the development and availability of two-way coupled meteorology and air quality models, more and more modeling studies have been conducted to explore the ARI or/and ACI effects in Asia (Nguyen et al., 2019a; Sekiguchi et al., 2018; Wang et al., 2010; Wang J. et al., 2014). In recent studies, a series of WRF-Chem and WRF-CMAQ simulations were performed to assess the consequences of ARI on radiative forcing, planetary boundary layer height (PBLH), precipitation, and fine particulate matter ($PM_{2.5}$) and ozone concentrations (Huang et al., 2016; Nguyen et al., 2019a; Sekiguchi et al., 2018; J. Wang et al., 2014). Different from current released version of WRF-CMAQ model (based on WRF version 4.3 and CMAQ version 5.3.3) that only includes ARI, WRF-Chem with ACI (starting from WRF-Chem version 3.0, Chapman et al., 2009) has been implemented for analyzing the complicated aerosol effects that lead to variations of cloud properties, precipitations and $PM_{2.5}$ concentrations (Bai et al., 2020; Liu Z. et al., 2018; Park et al., 2018; Zhao et al., 2017). To quantify the individual or joint effects of ARI or/and ACI on meteorological variables and pollutants concentrations, several modeling studies have been performed in Asia (Chen et al., 2019a; Ma et al., 2016; Zhang B. et al., 2015; Zhang et al., 2018). In addition, model comparisons (including offline and online models) targeting EA have been carried out recently under the Model Inter-Comparison Study for Asia (MICS-Asia) phase III (Chen et al., 2019b; Gao M. et al., 2018a; Li J. et al., 2019). As mentioned above, even though there are already several reviews regarding the observational studies of ARI or/and ACI (Li et al., 2016; Li Z. et al., 2019S; Lin N. et al., 2014; Tsay et al., 2013) it is necessary to conduct a systematic review in Asia focusing on applications of two-way coupled meteorology and air quality models as well as simulated variations of meteorology and air quality induced by aerosol effects.

This paper is constructed as follows: Section 2 describes the methodology for literature searching, paper inclusion, and analysis; Section 3 summarizes the basic information about publications as well as developments and applications of coupled models in Asia and Section 4 provides the recent overviews of their research points. Sections 5 to 6 present systematic review and meta-analysis of the effects of aerosol feedbacks on model performance, meteorology and air quality in Asia. The summary and perspective are provided in Section 7.

2 Methodology

2.1 Criteria and synthesis

Since 2010, in Asia, regional studies of aerosol effects on meteorology and air quality based on coupled models have been increasing gradually, therefore in this study we performed a systematic search of literatures to identify relevant studies from January 1, 2010 to December 31, 2019. In order to find all the relevant papers in English, Chinese, Japanese and Korean, we deployed serval science-based search engines, including Google Scholar, the Web of Science, the China National Knowledge Infrastructure, the Japan Information Platform for S&T Innovation, the Korean Studies Information Service System. The different keywords and their combinations for paper searching are as follows: (1) model-related keywords including "coupled model", "two-way", "WRF", "NU-WRF", "WRF-Chem", "CMAQ", "WRF-CMAQ", "CAMx", "CHIMERE", "WRF-CHIMERE" and "GATOR-GCMOM"; (2) effect-related keywords including "aerosol radiation interaction", "ARI", "aerosol cloud interaction", "ACI", "aerosol effect" and "aerosol feedback"; (3) air pollution-related keywords including "air quality", "aerosol", "PM2.5", "O3", "CO", "SO2", "NO2", "dust", "BC", "black carbon", "blown carbon", "carbonaceous", "primary pollutants"; (4) meteorology-related keywords including "meteorology", "radiation", "wind", "temperature", "specific humidity", "relative humidity", "planetary boundary layer", "cloud" and "precipitation"; (5) region-related keywords including "Asia", "East Asia", "Northeast Asia", "South Asia", "Southeast Asia", "Far East", "China", "India", "Japan", "Korea", "Singapore", "Thailand", "Malaysia", "Nepal", "North China Plain", "Yangtze River Delta", "Pearl River Delta", "middle reaches of the Yangtze River", "Sichuan Basin", "Guanzhong Plain", "Northeast China", "Northwest China" "East China", "Tibet Plateau", "Taiwan", "northern Indian", "southern Indian", "Gangetic Basin", "Kathmandu Valley".

After applying the search engines and the keywords combinations mentioned above, we found 946 relevant papers. In order to identify which paper should be included or excluded in this paper, following criteria were applied: (1) duplicate literatures were deleted; (2) studies of using coupled models in Asia with aerosol feedbacks turned on were included, and observational studies of aerosol effects were excluded; (3) publications involving coupled climate model were excluded. According to these criteria, not only regional studies, but also studies using the coupled models at global or hemispheric scales involving Asia or its subregions were included. Then, we carefully examined all the included papers and further checked the listed reference in each paper to make sure that no related paper was neglected. A flowchart that illustrated the detailed procedures applied for article identification is presented in Appendix Figure A1 (Note: Although the deadline for literature searching is 2019, any literature published in 2020 is also included.). There was a total of 160 publications included in our study.

2.2 Analysis method

To summarize the current status of coupled models applied in Asia and quantitatively analyze the effects of aerosol feedbacks on model performance as well as meteorology and air quality, we carried out a series of analyses based on data extracted from the selected papers. We firstly compiled the publication information of the included papers as well as the information regarding model name, simulated time period, study region, simulation design, and aerosol effects. Secondly, we summarized the important findings of two-way coupled model applications in Asia according to different aerosol sources and components to clearly acquire what are the major research focuses in past studies. Finally, we gathered all the simulated results of meteorological and air quality variables with/out aerosol effects and their statistical indices (SI). For questionable results, the quality assurance was conducted after personal communications with original authors to decide whether they were deleted and/or corrected. All the extracted publication and statistical information were exported into an Excel file, which was provided in Table S1. Moreover, we performed quantitative analyses of the effects of aerosol feedbacks through following steps. (1) We discussed whether meteorological and air quality variables were overestimated or underestimated based on their SI. Then, variations of the SI of these variables were further analyzed in detail with/out turning on ARI or/and ACI in two-way coupled models. (2) We investigated the SI of simulation results at different simulation time lengths and spatial resolutions in coupled models. (3) More detailed inter-model comparisons of model performance based on the compiled SI among different coupled models are conducted. (4) Differences in simulation results with/out aerosol feedbacks were grouped by study regions and time scales (yearly, seasonal, monthly, daily and hourly). Toward a better understanding of the complicated interactions between air quality and meteorology in Asia, the results sections in this paper are organized following above analysis methods (1) - (3) and represented in Section 5, and the results following method (4) were represented in Section 6. In addition, Excel and Python were used to conduct data processing and plotting in this study.

3 Basic overview

3.1 Summary of applications of coupled models in Asia

A total of 160 articles were selected according to the inclusion criteria, and their basic information was compiled in Table 1. In Asia, five two-way coupled models are applied to study the ARI and ACI effects. These include GATOR-GCMOM, two commonly used models, i.e., WRF-Chem and WRF-CMAQ, and two locally developed models, i.e., the global-regional assimilation and prediction system coupled with the Chinese Unified Atmospheric Chemistry Environment forecasting system (GRAPES-CUACE) and WRF coupled with nested air-quality prediction modeling system (WRF-NAQPMS). 127 out of total 160 papers involved the applications of WRF-Chem in Asia since its two-way coupled version was publicly available in 2006 (Fast et al., 2006). WRF-CMAQ was applied in only 16 studies due to its later initial release in 2012 (Wong et al., 2012). GRAPES-CUACE was developed by the China Meteorological Administration and introduced in details in Zhou et al. (2008, 2012, 2016), then firstly utilized in Wang et al. (2010) to estimate impacts of aerosol feedbacks on meteorology and dust cycle in EA. The coupled version of WRF-NAQPMS was developed by the Institute of Atmospheric Physics, Chinese Academy of Sciences and could improve the prediction accuracy of haze pollution in the North China Plain (NCP) (Wang Z.F. et al., 2014). Note that GRAPES-CUACE and WRF-NAQPMS were only applied in China. There were only three published papers about the applications of GATOR-GCMOM in Northeast Asia (NEA), NCP and India. In the included papers, 93, 33, 31 studies targeted various areas in China, EA and India, respectively. There were 79 papers regarding effects of ARI (7 health), 63 both ARI and ACI (1 health) and 18 ACI. ACI studies were much less than ARI related ones, which indicated that ACI related studies need to be paid with more attention in the future. Considering that the choices of cloud microphysics and radiation schemes can affect coupled models' results (Baró et al., 2015; Jimenez et al., 2016), these schemes used in the selected studies were also summarized in Table 1. This table presents a concise overview of coupled models' applications in Asia with the purpose of providing basic information regarding models, study periods and areas, aerosol effects, scheme selections, and reference. More complete information is summarized Table S1 including model version, horizontal resolution, vertical layer, aerosol and gas phase chemical mechanisms, photolysis rate, PBL, land surface, surface layer, cumulus, urban canopy schemes, meteorological initial and boundary conditions (ICs and BCs), chemical ICs and BCs, spin-up time, and anthropogenic natural emissions.

It should be noted that in Table 1 there were four model inter-comparison studies that aimed at evaluating model performance, identifying error sources and uncertainties, and providing optimal model setups. By comparing simulations from two coupled models (WRF-Chem and Spectral Radiation-Transport Model for Aerosol Species) (Takemura et al., 2003) in India (Govardhan et al., 2016), it was found that the spatial distributions of various aerosol species (black carbon (BC), mineral dust and sea salt) were similar with the two models. Based on the intercomparisons of WRF-Chem simulations in different areas, Yang et al. (2017) revealed that aerosol feedbacks could enhance $PM_{2.5}$ concentrations in the Indo-Gangetic Plain but suppress the concentrations in the Tibetan Plateau (TP). Targeting China and India, Gao M. et al. (2018b) also applied the WRF-Chem model to quantify the contributions of different emission sectors to aerosol radiative forcings, suggesting that reducing the uncertainties in emission inventories were critical, especially for India. Moreover, for the NCP region, Gao M. et al. (2018a) presented a comparison study with multiple online models under the MICS-Asia Phase III and pointed out noticeable discrepancies in the simulated secondary inorganic aerosols under heavy haze conditions and the importance of accurate wind speed at 10 meters above surface (WS10) predictions by these models. Comprehensive comparative studies for Asia have been emerging lately but are still limited, comparing to those for North America and Europe, such as the Air Quality Model Evaluation International Initiative Phase II (Brunner et al., 2015; Campbell et al., 2015; Forkel et al., 2016; Im et al., 2015a, 2015b; Kong et al., 2015; Makar et al., 2015a, 2015b; Wang K. et al., 2015).

Table 1. Basic information of coupled model applications in Asia during 2010-2019.

No.	Model	Study period	Region	Aerosol effect	Short/long-wave radiation scheme	Microphysics scheme	Reference
1	WRF-Chem	2013	India	ARI	Dudhia/RRTM	Thompson	Singh et al. (2020)*
2	WRF-Chem	12/2015	India	ARI	Goddard/RRTM	Lin	Bharali et al. (2019)
3	WRF-Chem	10/13/2016 to 11/20/2016	India	ARI	RRTMG	†	Shahid et al. (2019)
4	WRF-Chem	12/27/2017 to 12/30/2017	NCP	ARI	RRTMG	Lin	Wang D. et al. (2019)
5	WRF-Chem	12/05/2015 to 01/04/2016	NCP	ARI	Goddard	WSM 6-class graupel	Wu et al. (2019a)
6	WRF-Chem	12/05/2015 to 01/04/2016	NCP	ARI	Goddard	WSM 6-class graupel	Wu et al. (2019b)
7	WRF-Chem	06/01/2006 to 12/31/2011	NWC	ARI	RRTMG	Morrison	Yuan et al. (2019)
8	WRF-Chem	07/2016, 10/2016, 01/2017, 04/2017	NCP	ARI	Goddard/RRTM	Lin	Zhang et al. (2019)
9	WRF-Chem	02/17/2014 to 02/26/2014, 10/21/2014 to 10/25/2014, 11/05/2014 to 11/11/2014, 12/18/2015 to 12/24/2015	NCP	ARI	RRTMG	Morrison	Zhou et al. (2019)
10	WRF-Chem	03/15/2012 to 03/25/2012	WA	ARI	RRTMG	Morrison	Bran et al. (2018)
11	WRF-Chem	2013	China & India	ARI	RRTMG	Lin	Gao M. et al. (2018b)
12	WRF-Chem	05/01/2007 to 05/07/2007	CA	ARI	RRTM	Lin	Li and Sokolik (2018)
13	WRF-Chem	06/02/2012 to 06/15/2012	YRD	ARI	RRTMG	Lin	Li M. et al. (2018)
14	WRF-Chem	12/15/2016 to 12/21/2016	NCP	ARI	RRTMG	Morrison	Liu Q. et al. (2018)
15	WRF-Chem	11/30/2016 to 12/04/2016	NCP	ARI	RRTMG	Lin	Miao et al. (2018)
16	WRF-Chem	2010	India	ARI	RRTMG	Morrison	Soni et al. (2018)
17	WRF-Chem	01/01/2013 to 01/31/2013	NCP	ARI	Goddard/RRTM	Lin	Wang L. et al. (2018)
18	WRF-Chem	12/2013	EC	ARI	RRTMG	Lin	Wang Z. et al. (2018)
19	WRF-Chem	2013	TP	ARI	RRTMG	Morrison	Yang et al. (2018)
20	WRF-Chem	03/11/2015 to 03/26/2015	EA	ARI	RRTMG	Lin	Zhou et al. (2018)
21	WRF-Chem	01/2013	EC	ARI	RRTMG	Lin	Gao et al. (2017a)
22	WRF-Chem	03/16/2014 to 03/18/2014	YRD	ARI	RRTMG	Lin	Li M. M. et al. (2017a)
23	WRF-Chem	10/15/2015 to 10/17/2015	YRD	ARI	Goddard/RRTM	Lin	Li M. M. et al. (2017b)
24	WRF-Chem	02/21/2014 to 02/27/2014	NCP	ARI	RRTMG	Lin	Qiu et al. (2017)
25	WRF-Chem	07/21/2012	NCP	ARI	RRTMG	Lin	Yang and Liu (2017a)
26	WRF-Chem	07/21/2012	NCP	ARI	RRTMG	Lin	Yang and Liu (2017b)
27	WRF-Chem	05/30/2013 to 06/27/2013	EC	ARI	RRTMG	Lin	Yao et al. (2017)
28	WRF-Chem	11/15/2013 to 12/30/2013	SEC	ARI	RRTMG	Lin	Zhan et al. (2017)
29	WRF-Chem	03/2012	India	ARI	RRTMG	Thompson	Feng et al. (2016)
30	WRF-Chem	1960-2010	NCP	ARI	Goddard/RRTM	Lin	Gao M. et al. (2016a)
31	WRF-Chem	01/2008, 04/2008, 07/2008, 10/2008	EA	ARI	Goddard/RRTM	Lin	Liu X. et al. (2016)
32	WRF-Chem	04/2011	NCP	ARI	RRTMG	Single-Moment 5-class	Liu L. et al. (2016)
33	WRF-Chem	09/21/2011 to 09/23/2011	NCP	ARI	RRTMG	Lin	Miao et al. (2016)
34	WRF-Chem	03/2005	EA	ARI	Goddard/RRTM	Morrison	Wang et al. (2016)
35	WRF-Chem	06/23/2008 to 07/20/2008	NWC	ARI	RRTMG	Morrison	Yang et al. (2016)
36	WRF-Chem	01/2007, 04/2007, 07/2007, 10/2007	EA	ARI	RRTM	Lin	Zhong et al. (2016)
37	WRF-Chem	05/2011, 10/2011	India	ARI	RRTMG	Thompson	Govardhan et al. (2015)
38	WRF-Chem	2006	China	ARI	RRTMG	Lin	Huang et al. (2015)
39	WRF-Chem	2007 to 2011	EA	ARI	Goddard/RRTM	Lin	Chen et al. (2014)
40	WRF-Chem	11/2007 to 12/2008	EA	ARI	RRTMG	Lin	Gao et al. (2014)
41	WRF-Chem	10/2006	SEA	ARI	RRTM	Lin	Ge et al. (2014)

42	WRF-Chem	04/17/2010 to 04/22/2010	India	ARI	RRTM	Thompson	Kumar et al. (2014)
43	WRF-Chem	01/11/2013 to 01/14/2013	NCP	ARI	Goddard/RRTM	Lin	Li and Liao (2014)
44	WRF-Chem	03/15/2008 to 03/18/2008	EA	ARI	RRTMG	Morrison	Lin C. et al. (2014)
45	WRF-Chem	07/21/2006 to 07/30/2006	NWC	ARI	RRTMG	Morrison	Chen et al. (2013)
46	WRF-Chem	05/12/2009 to 05/22/2009	India	ARI	Goddard/RRTM	Milbrandt-Yau	Dipu et al. (2013)
47	WRF-Chem	2008	India	ARI	Goddard/RRTM	Thompson	Kumar et al. (2012a)
48	WRF-Chem	2008	India	ARI	Goddard/RRTM	Thompson	Kumar et al. (2012b)
49	WRF-Chem	1999	India	ARI	Goddard/*	Lin	Seethala et al. (2011)
50	WRF-Chem	2006	China	ARI	†	†	Zhuang et al. (2011)
51	WRF-Chem	12/14/2013 to 12/16/2013	PRD	ARI & ACI	RRTMG	Morrison	Liu et al. (2020)*
52	WRF-Chem	11/30/2009 to 12/01//2009	NCP	ARI & ACI	Goddard/RRTM	Morrison	Jia et al. (2019)
53	WRF-Chem	11/25/2013 to 12/26/2013	EC	ARI & ACI	RRTMG	Lin	Wang Z. et al. (2019)
54	WRF-Chem	01/2014	China	ARI & ACI	RRTMG	Morrison	Archer-Nicholls et al. (2019)
55	WRF-Chem	12/01/2016 to 12/09/2016, 12/19/2016 to 12/24/2016	YRD	ARI & ACI	RRTMG	Lin	Li M. et al. (2019)
56	WRF-Chem	05/06/2013 to 20/06/2013 & 24/08/2014 to 08/09/2014	India	ARI & ACI	RRTM	Lin	Kedia et al. (2019a)
57	WRF-Chem	06/2010 to 09/2010	India	ARI & ACI	RRTM	Lin, Morrison, Thompson	Kedia et al. (2019b)
58	WRF-Chem	04/2013	PRD	ARI & ACI	RRTMG	Lin	Huang et al. (2019)
59	WRF-Chem	11/30/2013 to 12/10/2013	EC	ARI & ACI	RRTMG	Morrison	Ding et al. (2019)
60	WRF-Chem	12/01/2015	NCP	ARI & ACI	RRTMG	Lin	Chen et al. (2019a)
61	WRF-Chem	04/12/2015 to 27/12/2015	EA	ARI & ACI	Goddard	WSM 6-class graupel	An et al. (2019)
62	WRF-Chem	06/2015 to 02/2016	MRYR	ARI & ACI	Goddard/RRTM	WSM 6-class graupel	Liu L. et al. (2018)
63	WRF-Chem	06/2008, 06/2009, 06/2010, 06/2011, 06,2012	PRD	ARI & ACI	RRTMG	Morrison	Liu Z. et al. (2018)
64	WRF-Chem	01/2014, 04/2014, 07/2014, 10/2014	China	ARI & ACI	RRTMG	Lin	Zhang et al. (2018)
65	WRF-Chem	10/01/2015 to 10/26/2015	YRD	ARI & ACI	RRTMG	Lin	Gao J. et al. (2018)
66	WRF-Chem	2001, 2006, 2011	EA	ARI & ACI	RRTMG	Morrison	Zhang et al. (2017)
67	WRF-Chem	06/01/2011 to 06/06/2011	EC	ARI & ACI	Goddard/RRTM	Lin	Wu et al. (2017)
68	WRF-Chem	11/27/2013 to 12/12/2013	YRD	ARI & ACI	Goddard/RRTM	Single-Moment 5-class	Sun et al. (2017)
69	WRF-Chem	2005 & 2009	YRD	ARI & ACI	RRTMG	Morrison	Zhong et al. (2017)
70	WRF-Chem	11/05/2014 to 11/11/2014	NCP	ARI & ACI	Goddard/RRTM	Lin	Gao et al. (2017b)
71	WRF-Chem	01/2013	NCP	ARI & ACI	Goddard/RRTM	Lin	Gao et al. (2017c)
72	WRF-Chem	01/2010, 07/2010	China	ARI & ACI	†	†	Ma and Wen (2017)
73	WRF-Chem	06/01/2008 to 07/05/2008	India	ARI & ACI	†	†	Lau et al. (2017)
74	WRF-Chem	01/2013	NCP	ARI & ACI	Goddard/RRTM	Morrison	Kajino et al. (2017)
75	WRF-Chem	03/01/2009 to 03/31/2009	TP & India	ARI & ACI	RRTMG	Morrison	Yang et al. (2017)
76	WRF-Chem	2001, 2006, 2011	EA	ARI & ACI	RRTMG	Morrison	He et al. (2017)
77	WRF-Chem	05/2008 to 08/2008	YRD	ARI & ACI	†	†	Campbell et al. (2017)
78	WRF-Chem	12/07/2013 to 12/09/2013	EC	ARI & ACI	Goddard/RRTM	Morrison	Zhang Yue et al. (2016)
79	WRF-Chem	01/2006, 04/2006, 07/2006, 10/2006	China	ARI & ACI	Goddard/RRTM	Lin	Ma et al. (2016)
80	WRF-Chem	01/2005, 04/2005, 07/2005, 10/2005	EC	ARI & ACI	Goddard/RRTM	Lin	Zhang Yang et al. (2016a)
81	WRF-Chem	01/2005, 04/2005, 07/2005, 10/2005	EC	ARI & ACI	Goddard/RRTM	Lin	Zhang Yang et al. (2016b)
82	WRF-Chem	06/2012	EC	ARI & ACI	RRTMG	Lin	Huang et al. (2016)
83	WRF-Chem	01/2010, 07/2010	YRD	ARI & ACI	Goddard/RRTM	Lin	Xie et al. (2016)
84	WRF-Chem	11/12/2012 to 11/16/2012, 11/02/2013 to 11/06/2013	India	ARI & ACI	Goddard/RRTM	Lin	Srinivas et al. (2016)
85	WRF-Chem	07/2010	India	ARI & ACI	RRTMG	Lin	Kedia et al. (2016)

86	WRF-Chem	05/20/2008 to 08/31/2015	India	ARI & ACI	Goddard/RRTM	Lin	Jin et al. (2016a)
87	WRF-Chem	05/20/2008 to 08/31/2015	India	ARI & ACI	Goddard/RRTM	Lin	Jin et al. (2016b)
88	WRF-Chem	01/2010	NCP	ARI & ACI	Goddard/RRTM	Lin	Gao M. et al. (2016b)
89	WRF-Chem	01/05/2008 to 01/09/2008	NCP	ARI & ACI	RRTMG	Lin	Gao Y. et al. (2016)
90	WRF-Chem	12/2013	EC	ARI & ACI	RRTMG	Lin	Ding et al. (2016)
91	WRF-Chem	02/15/2013 to 02/17/2013	NCP	ARI & ACI	Goddard/RRTM	†	Yang et al. (2015)
92	WRF-Chem	01/2010, 04/2010, 07/2010, 10/2010	NCP	ARI & ACI	Goddard/RRTM	Lin	Shen et al. (2015)
93	WRF-Chem	2006 & 2011	EA	ARI & ACI	RRTMG	Morrison	Zhang Y. et al. (2015a)
94	WRF-Chem	2006 & 2011	EA	ARI & ACI	RRTMG	Morrison	Chen Y. et al. (2015)
95	WRF-Chem	06/27/2008 to 06/28/2008	NCP	ARI & ACI	RRTM	Lin	Zhong et al. (2015)
96	WRF-Chem	05/20/2008 to 08/31/2015	India	ARI & ACI	Goddard/RRTM	Lin	Jin et al. (2015)
97	WRF-Chem	03/2005, 04/2005, 05/2005	India	ARI & ACI	Goddard/RRTM	Thompson	Jena et al. (2015)
98	WRF-Chem	01/02/2013 to 01/26/2013	NCP	ARI & ACI	RRTMG	Morrison	Gao Y. et al. (2015)
99	WRF-Chem	07/08/2013 to 07/09/2013	SWC	ARI & ACI	RRTMG	†	Fan et al. (2015)
100	WRF-Chem	01/2010, 04/2010, 07/2010, 10/2010	NCP	ARI & ACI	Goddard/RRTM	Lin	Chen D. et al. (2015)
101	WRF-Chem	01/2013	EC	ARI & ACI	Goddard/RRTM	Lin	Zhang B. et al. (2015)
102	WRF-Chem	2006 & 2007	EA	ARI & ACI	Goddard/†	Lin	Wu et al. (2013)
103	WRF-Chem	09/27/2010 to 10/22/2010	India	ARI & ACI	Goddard/RRTM	Lin	Beig et al. (2013)
104	WRF-Chem	12/1/2009	NCP	ARI & ACI	Goddard/RRTM	Lin	Jia and Guo, (2012)
105	WRF-Chem	01/2001, 07/2001	EA	ARI & ACI	Goddard/RRTM	Lin	Zhang et al. (2012)
106	WRF-Chem	11/10/2007 to 01/01/2008	China	ARI & ACI	RRTMG	Lin	Gao et al. (2012)
107	WRF-Chem	06/18/2018 to 06/19/2018	MRYR	ACI	Goddard/RRTM	†	Bai et al. (2020)*
108	WRF-Chem	06/07/2017 to 06/12/2017	YRD	ACI	RRTMG	Morrison	Liu et al. (2019)
109	WRF-Chem	03/2010 to 05/2010	EA	ACI	RRTMG	Morrison	Wang K. et al. (2018)
110	WRF-Chem	03/09/2012 to 04/30/2012	EA	ACI	RRTMG	Thompson	Su and Fung (2018a)
111	WRF-Chem	03/09/2012 to 04/30/2012	EA	ACI	RRTMG	Thompson	Su and Fung (2018b)
112	WRF-Chem	05/18/2015 to 06/13/2015	NEA	ACI	RRTMG	Morrison	Park et al. (2018)
113	WRF-Chem	08/2008	EC	ACI	RRTMG	Lin	Gao and Zhang (2018)
114	WRF-Chem	10/03/2013 to 10/07/2013	SEC	ACI	RRTMG	Morrison	Shen et al. (2017)
115	WRF-Chem	01/2013, 07/2013	China	ACI	Fu-Liou-Gu	Morrison	Zhao et al. (2017)
116	WRF-Chem	06/04/2004 to 07/10/2004	India	ACI	Goddard	Lin	Bhattacharya et al. (2017)
117	WRF-Chem	09/20/2013 to 09/23/2013	PRD	ACI	RRTMG	Lin	Jiang et al. (2016)
118	WRF-Chem	2005 & 2010	EA	ACI	RRTMG	Morrison	Y. Zhang et al. (2015b)
119	WRF-Chem	08/20/2009 to 08/29/2008	India	ACI	Goddard/RRTM	Morrison	Sarangi et al. (2015)
120	WRF-Chem	01/2001, 04/2001, 07/2001, 10/2001, 01/2005, 04/2005, 07/2005, 10/2005, 01/2008, 04/2008, 07/2008, 10/2008	EA	ACI	†	†	Zhang et al. (2014)
121	WRF-Chem	07/2008	EC	ACI	RRTMG	Morrison	Lin et al. (2014)
122	WRF-Chem	1980 to 2010	SEC	ACI	†	†	Bennartz et al. (2011)
123	WRF-Chem	2008 & 2050	China	ARI (Health)	†	†	Zhong et al. (2019)
124	WRF-Chem	2015 & 2050	India	ARI (Health)	RRTM	Thompson	Conibear et al. (2018a)
125	WRF-Chem	2014	India	ARI (Health)	RRTM	Thompson	Conibear et al. (2018b)
126	WRF-Chem	2011	India	ARI (Health)	Goddard/RRTM	Thompson	Ghude et al. (2016)
127	WRF-Chem	2013	NCP	ARI (Health)	RRTMG	†	Gao M. et al. (2015)
128	WRF-CMAQ	03/2006 & 04/2006 to 03/2010 & 04/2010	EA	ARI	†	†	Dong et al. (2019)
129	WRF-CMAQ	04/10/2016 to 06/19/2016	NEA	ARI	RRTMG	Single-Moment 3-class	Jung et al. (2019)

130	WRF-CMAQ	2014	EA	ARI	RRTMG	Morrison	Nguyen et al. (2019a)
131	WRF-CMAQ	2014	SEA	ARI	RRTMG	Morrison	Nguyen et al. (2019b)
132	WRF-CMAQ	02/2015	NEA	ARI	RRTMG	Single-Moment 5-class	Yoo et al. (2019)
133	WRF-CMAQ	01/2014, 02/2014, 03/2014	EA	ARI	RRTMG	Morrison	Sekiguchi et al. (2018)
134	WRF-CMAQ	2006 to 2010, 2013	EA	ARI	RRTMG	Morrison	Hong et al. (2017)
135	WRF-CMAQ	01/2013, 07/2013	China	ARI	RRTMG	Morrison	Xing et al. (2017)
136	WRF-CMAQ	1990 to 2010	EA	ARI	RRTMG	Morrison	Xing et al. (2016)
137	WRF-CMAQ	1990 to 2010	EC	ARI	RRTMG	Morrison	Xing et al. (2015a)
138	WRF-CMAQ	1990 to 2010	EC	ARI	RRTMG	Morrison	Xing et al. (2015b)
139	WRF-CMAQ	1990 to 2010	EC	ARI	RRTMG	Morrison	Xing et al. (2015c)
140	WRF-CMAQ	01/2013	China	ARI	RRTMG	Morrison	J. Wang et al. (2014)
141	WRF-CMAQ	01/2013, 04/2013, 07/2013, 10/2013	China	ACI	RRTMG	Morrison	Chang (2018)
142	WRF-CMAQ	2050	China	ARI (Health)	RRTMG	Morrison	Hong et al. (2019)
143	WRF-CMAQ	1990 to 2010	EA & India	ARI (Health)	RRTMG	Morrison	Wang et al. (2017)
144	GRAPES-CUACE	12/15/2016 to 12/24/2016	NCP	ARI	Goddard	†	H. Wang et al. (2018)
145	GRAPES-CUACE	07/07/2008 to 07/11//2008	EC	ARI	CLIRAD	†	H. Wang et al. (2015)
146	GRAPES-CUACE	04/26/2006	EA	ARI	Goddard/†	†	Wang and Niu .(2013)
147	GRAPES-CUACE	04/26/2006	EA	ARI	Goddard/†	†	Wang et al. (2013)
148	GRAPES-CUACE	07/13/2008 to 07/31/2008	NCP	ARI	†	†	Zhou et al. (2012)
149	GRAPES-CUACE	04/26/2006	EA	ARI	Goddard/†	†	Wang et al. (2010)
150	GRAPES-CUACE	01/2013	EC	ACI	†	Single-Moment 6-class	Zhou et al. (2016)
151	WRF-NAQPMS	2013	EA	ARI	†	†	Li J. et al. (2018)
152	WRF-NAQPMS	09/27/2013 to 10/01/2013	NCP	ARI	Goddard/RRTM	Lin	Wang Z. et al. (2014)
153	WRF-NAQPMS	01/01/2013	EC	ARI	Goddard/RRTM	Lin	Wang Z. F. et al. (2014)
154	GATOR-GCMOM	2000 & 2009	NEA	ARI & ACI	†	†	Ten Hoeve and Jacobson, 2012
155	GATOR-GCMOM	2002 & 2009	India	ARI & ACI	†	†	Jacobson et al. (2019)
156	GATOR-GCMOM	2000 & 2009	NCP	ARI & ACI	†	†	Jacobson et al. (2015)
157	Multi-model comparison	†	EA	ARI & ACI	†	†	Chen et al. (2019b)
158	Multi-model comparison	2010	EA	ARI & ACI	†	†	Li J. et al., (2019)
159	Multi-model comparison	01/2010	NCP	ARI & ACI	†	†	Gao et al. (2018a)
160	Multi-model comparison	05/2011	India	ARI & ACI	†	†	Govardhan et al. (2016)

†: Unclear; *: A preprint version of this study was available online on October 31, 2019, and was formally published on January 1, 2020. (EA: East Asia, NEA: Northeast Asia, SEA: Southeast Asia, EC: East China, NCP: North China Plain, YRD: Yangtze River Delta, SEC: Southeast China, NWC: Northwest China, TP: Tibetan Plateau, MRYR: middle reaches of the Yangtze River, SWC: Southwest China; PRD: Pearl River Delta).

3.2 Spatiotemporal distribution of publications

To gain an overall understanding of applications of coupled models in Asia, the spatial distributions of study areas of the selected literatures and the temporal variations of the annual publication numbers were extracted from Table 1 and summarized. Figure 1 illustrates the spatial distributions of study regions as well as the number of papers involving coupled models in Asia (Fig. 1a) and China (Fig. 1b). In this figure, the color and number in the pie charts represent individual (WRF-Chem, WRF-CMAQ, GRAPES-CUACE, WRF-NAQPMS, and GATOR-GCMOM) or multiple coupled models and the quantity of corresponding articles, respectively. At subregional scales, most studies targeted EA where high anthropogenic aerosol loading occurred in recent decades, mainly using WRF-Chem and WRF-CMAQ (Fig. 1a). For other subregions, such as NEA, SEA, Central Asia (CA), and West Asia (WA), there were rather limited research activities taking into account aerosol feedbacks with two-way coupled models. National scale applications of two-way coupled models targeted mostly modeling domains covering India and China but much less work were carried out in other countries, such as Japan and Korea, where air pollution levels are much lower. With respect to various areas in China (Fig. 1b), the research activities concentrated mostly in NCP and secondly in the East China (EC), then in the Yangtze River Delta (YRD) and Pearl River Delta (PRD) areas. WRF-Chem was the most popular model applied in all areas, but there were a few applications of GPRAPES-CUACE and WRF-NAQPMS in EC and NCP.

Figure 2 depicts the temporal variations of research activities with two-way coupled models in Asia over the period of 2010 to 2019. The total number of papers related to two-way coupled models had an obvious upward trend in the past decade. Prior to 2014, applications of two-way coupled models in Asia were scarce, with about 1 to 6 publications per year. A noticeable increase of research activities emerged starting from 2014 and the growth was rapid from 2014 to 2016, at a rate of 7-9 more papers per year, especially in China. It could be related to the Action Plan on Prevention and Control of Atmospheric Pollution (2013-2017) implemented by the Chinese government. The growth was rather flat during 2016-2018 before reaching a peak of 31 articles in 2019. In addition, the pie charts in Fig. 2 indicates that modeling activities had been picking up with a diversified pattern in study domain from 2010 to 2019. The modeling domains extended from EA to China and India and then several subregions in Asia and various areas in China. For EA and India, investigations of aerosol feedbacks based on two-way coupled models rose from 1-2 papers per year during 2010-2013 to 4-8 during 2014-2019. Since 2014, most model simulations were carried out towards areas with severe air pollution in China, especially the NCP area where attracted 5-7 publications per year.

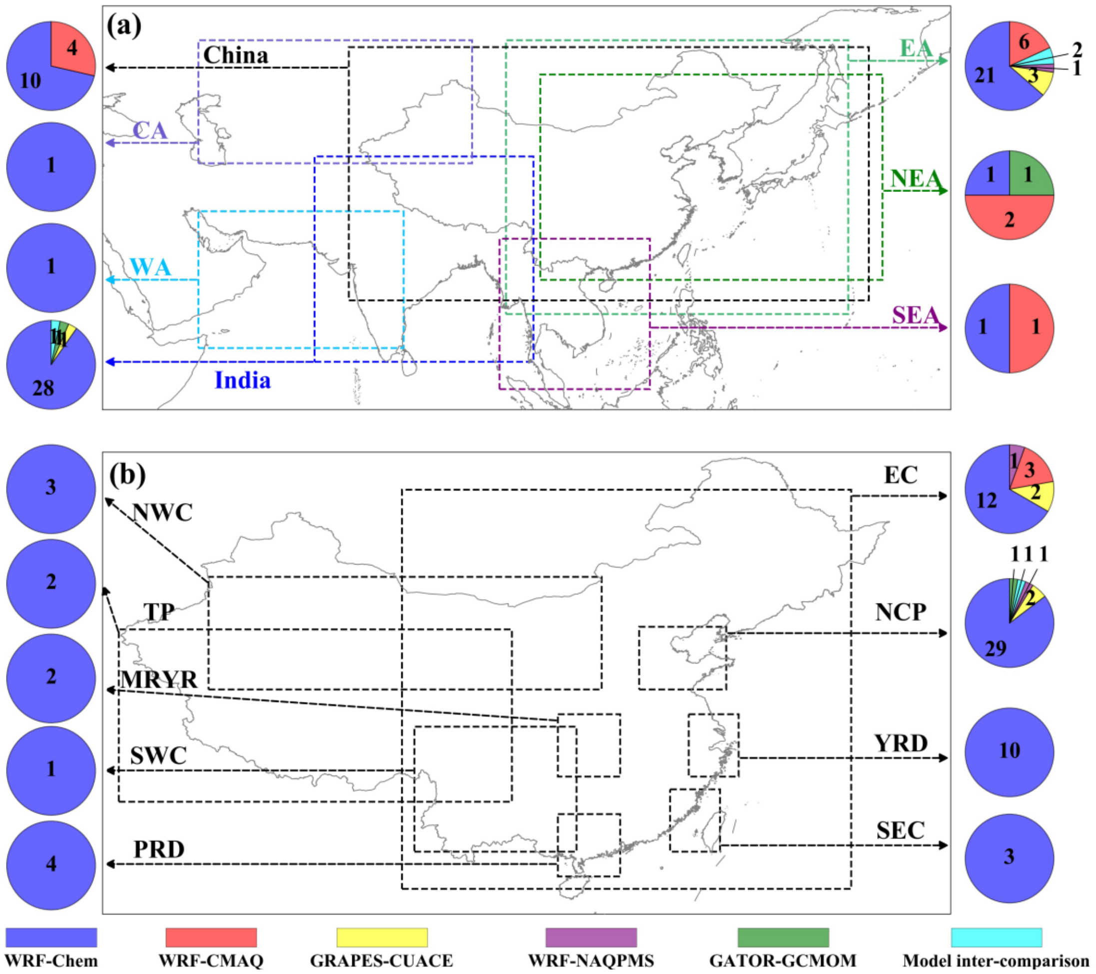

Figure 1. The spatial distributions of study domains as well as the two-way coupled modeling publication numbers in different subregions or countries of Asia (a) and areas of China (b). (EA: East Asia, NEA: Northeast Asia, SEA: Southeast Asia, EC: East China, NCP: North China Plain, YRD: Yangtze River Delta, SEC: Southeast China, NWC: Northwest China, TP: Tibetan Plateau, MRYR: middle reaches of the Yangtze River, SWC: Southwest China; PRD: Pearl River Delta).

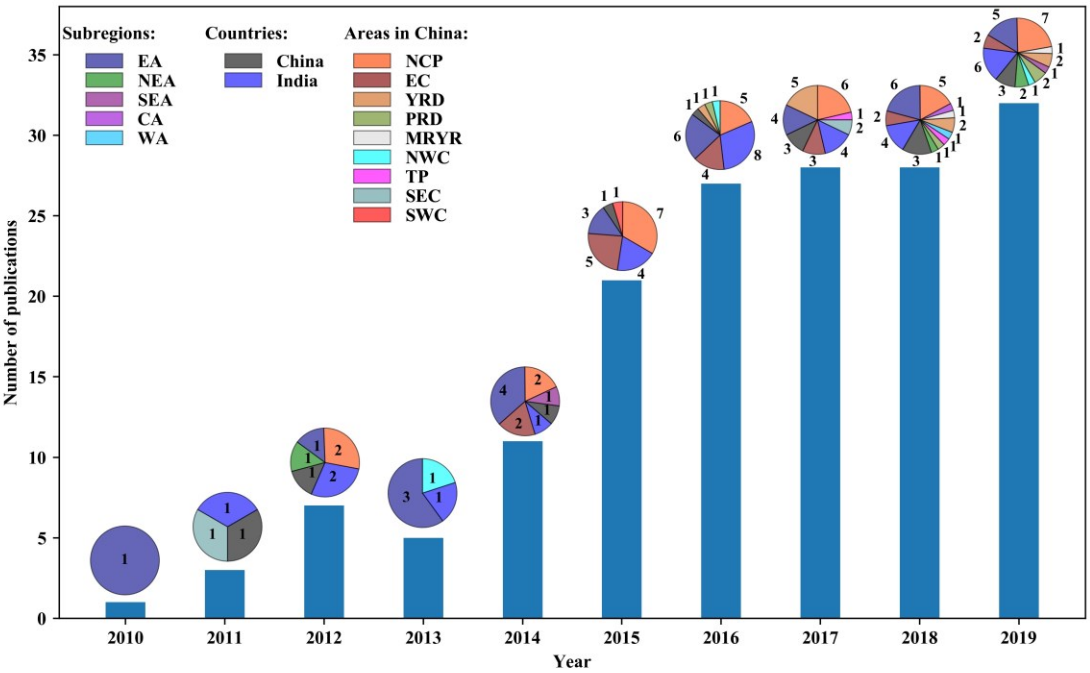

Figure 2. The temporal variations of study activities adopting two-way coupled models in Asia during 2010-2019. (EA: East Asia, NEA: Northeast Asia, SEA: Southeast Asia, EC: East China, NCP: North China Plain, YRD: Yangtze River Delta, SEC: Southeast China, NWC: Northwest China, TP: Tibetan Plateau, MRYR: middle reaches of the Yangtze River, SWC: Southwest China; PRD: Pearl River Delta).

3.3 Summary of modeling methodologies

The physiochemical processes involved with ARI and ACI are sophisticated in actual conditions of atmospheric environment but their representations in two-way coupled models can be rather different. Also, simulation results depend on how these models are configured and set up. Therefore, the treatments of aerosol and cloud microphysics, and aerosol-radiation-cloud interactions in WRF-Chem, WRF-CMAQ, GRAPES-CUACE, WRF-NAQPMS and GATOR-GCMOM applied in Asia, as well as the various aspects of how the modeling studies being set up in the selected papers are summarized in Tables 2-5, respectively, and outlined in this section.

Aerosol microphysics processes consist of particle nucleation, coagulation, condensation/evaporation, gas/particle mass transfer, inorganic aerosol thermodynamic equilibrium, aqueous chemistry and formation of secondary organic aerosol (SOA). Their representations in a variety of aerosol mechanisms offered in the five two-way coupled models applied in Asia and relevant references are compiled in Table 2. Note that the GOCART scheme in WRF-Chem is based on a bulk aerosol mechanism that is not able to consider the details of these microphysics processes. The binary homogeneous nucleation schemes with/out hydration developed by different authors are applied in the five coupled models for simulating the new particle formation and GATOR-GCMOM also adopts the ternary nucleation parameterization scheme for H_2SO_4, NH_3 and H_2O vapors. All the five coupled models calculate the aerosol-aerosol coagulation rate coefficients based the Brownian coagulation theory, with certain enhancements in GATO-GCMOM as stated in details by Jacobson (1999). The dynamic condensation/evaporation approaches of inorganic gases (e.g., H_2SO_4, NH_3, HNO_3, and HCl) and organic gases (VOCs) based on the Fuchs-Sutugin expression are implemented in various aerosol mechanisms offered by WRF-Chem, WRF-CMAQ, GRAPES-CUACE, and WRF-NAQPMS, while GATOR-GCMOM deploys the condensation/evaporation approach in which several terms of processes are factored in the 3-D equations of discrete size-resolved aerosol growth (Jacobson, 2012). The mass transfer between gaseous and aerosol particles are treated via two typical methods (i.e., bulk equilibrium and kinetic) in most coupled models, and the hybrid and Henry's law equilibrium methods are also applied in the MADRID (WRF-Chem) and the 6th/7th generation CMAQ aerosol modules (AERO6/AERO7) (WRF-CMAQ), respectively. Different versions of the ISORROPIA module, the Model for an Aerosol Reacting System-version A (MARS-A), the Multicomponent Equilibrium Solver for Aerosols with the Multicomponent Taylor Expansion Method (MESA-MTEM), and the EQUIlibrium SOLVer version 2 (EQUISOLV

II) modules are implemented for computing the inorganic aerosol thermodynamic equilibrium in these two-way coupled models. For aqueous chemistry, the bulk aqueous chemistry scheme and variations of the CMAQ's standard aqueous chemistry module (AQCHEM) are the most applied, and the CBM-IV aqueous chemistry scheme, the Regional Acid Deposition Model (RADM) aqueous chemistry module, and the size-resolved aqueous chemistry module are utilized as well. Multiple approaches have been incorporated into the five coupled models for calculating the SOA formation and include the volatility basis set (VBS) approach, approaches considering reversible absorption or combined absorption and dissolution, fixed or bulk two-product yield approaches, and the approach of time-dependent organics condensation/evaporation with considering vapor pressure.

Table 2. Treatments of aerosol microphysics processes in two-way coupled models (WRF-Chem, WRF-CMAQ, GRAPES-CUACE, WRF-NAQPMS and GATOR-GCMOM) applied in Asia.

	WRF-Chem						WRF-CMAQ			GRAPES-CUACE	WRF-NAQPMS	GATOR-GCMOM
	GOCART	MADE/SORGAM	AERO5	MAM3/MAM7	MOSAIC	MADRID	AERO5	AERO6	AERO7	CUACE※	AERO5	GATOR2012*
New particle formation/if with hydration	None	H_2SO_4-H_2O binary homogeneous nucleation (Kulmala et al., 1998)/Yes	H_2SO_4-H_2O binary homogeneous nucleation (Kulmala et al., 1998)/Yes	H_2SO_4-H_2O binary homogeneous nucleation (Vehkamäki et al., 2002)/Yes	H_2SO_4-H_2O binary homogeneous nucleation (Wexler, et al., 1994)/Yes	H_2SO_4-H_2O binary homogeneous nucleation (McMurry and Friedlander, 1979)/Unclear	H_2SO_4-H_2O binary homogeneous nucleation (Kulmala et al., 1998)/Yes	H_2SO_4-H_2O binary homogeneous nucleation (Vehkamäki et al., 2002)/Yes	H_2SO_4-H_2O binary homogeneous nucleation (Vehkamäki et al., 2002)/Yes	H_2SO_4-H_2O binary homogeneous nucleation (Kulmala et al., 1998)/Yes	H_2SO_4-H_2O binary homogeneous nucleation (Yu, 2006)/Yes	H_2SO_4-H_2O binary homogeneous nucleation (Vehkamäki et al., 2002)/Yes; H_2SO_4-NH_3-H_2O ternary homogeneous nucleation (Napari et al., 2002)/Yes
Coagulation	None	Brownian motion (Binkowski and Shankar, 1995)	Brownian motion (Binkowski and Roselle, 2003)	Brownian motion (Whitby, 1978)	Brownian motion (Jacobson et al., 1994)	Brownian motion (Jacobson et al., 1994)	Brownian motion (Binkowski and Roselle, 2003)	Brownian motion (Binkowski and Roselle, 2003)	Brownian motion (Binkowski and Roselle, 2003)	Brownian motion (Jacobson et al., 1994)	Brownian motion (Jacobson et al., 1994; Chen et al., 2017)	Brownian motion, Brownian diffusion enhancement, turbulent shear, turbulent inertial motion, gravitational setting, Van der Waals forces, viscous forces, fractal geometry (Jacobson, 2003)
Condensation/ Evaporation	None	Dynamical condensation/ evaporation of H_2SO_4 vapor and VOCs based on Fuchs-Sutugin expression (Binkowski and Shankar, 1995)	Dynamical condensation/ evaporation of H_2SO_4 vapor and VOCs based on Fuchs-Sutugin expression (Binkowski and Shankar, 1995); Condensation/ evaporation of volatile inorganic gases to/from the gas-phase concentrations of coarse particle surfaces using ISORROPIA in reverse mode (CMAQ User's Guide)	Dynamical condensation of H_2SO_4 vapor, NH_3 (7 modes) and semi-volatile organics; Condensation/ evaporation of SOA gas (Liu et al., 2012)	Dynamical condensation/ evaporation of H_2SO_4 vapor, methanesulfonic acid, HNO_3, HCl and NH_3 with adaptive step time-split Euler approach (Zaveri et al., 2008)	Dynamical condensation/ evaporation of semi-volatile species for analytical predictor of condensation with moving-center approach (Zhang et al., 2010)	Dynamical condensation/ evaporation of H_2SO_4 vapor and VOCs based on Fuchs-Sutugin expression (Binkowski and Shankar, 1995); Condensation/ evaporation of volatile inorganic gases to/from the gas-phase concentrations of coarse particle surfaces using ISORROPIA in reverse mode (CMAQ User's Guide)	Same as in AERO5	Same as in AERO5	Dynamical condensation/ evaporation of H_2SO_4 vapor and gaseous precursors based on modified Fuchs-Sutugin expression (Jacobson, et al., 1994; Gong et al., 2003)	Condensation/ evaporation of H_2SO_4 with advanced particle microphysics approach (Li et al., 2018; Yu and Luo, 2009; Chen et al., 2019; Yu, 2006)	Dynamical condensation of H_2O and involatile species with Analytical Predictor of Nucleation, Condensation, and Dissolution scheme (Jacobson, 2002); Evaporation of a volatile component over a single particle (Jacobson and Turco, 1995)
Gas/particle mass transfer	None	1. Bulk equilibrium approach for HNO_3 and NH_3 (Zhang et al., 2005) 2. Kinetic approach for H_2SO_4 (Zhang et al., 2016)	Kinetic approach for all species (Foley et al., 2010)	Bulk equilibrium approach for $(NH_4)_2SO_4$ (Hu and Zhang, 2014)	Kinetic approach for all species (Zaveri et al., 2008)	1. Bulk equilibrium approach for HNO_3 and NH_3 (Zhang et al., 2010) 2. Kinetic approach for all species (Zhang et al., 2010) 3. Hybrid approach (Zhang et al., 2010)	Kinetic approach for all species (Foley et al., 2010)	1. Henry's law equilibrium (Foley et al., 2017) 2. Kinetic approach for all species (Foley et al., 2017)	Same as in AERO6	Kinetic approach for all species (Zhou et al., 2021)	Kinetic for all species (Chen et al., 2021)	Kinetic approach for all species (Jacobson, 1999)
Inorganic aerosol thermodynamic equilibrium	None	MARS-A (Binkowski and Shankar, 1995)	ISORROPIA (Byun and Kenneth, 2006)	ISORROPIA II (Hu and Zhang, 2014)	MESA-MTEM (Zaveri et al., 2008)	ISORROPIA (Zhang et al., 2010)	ISORROPIA (Byun and Kenneth, 2006)	ISORROPIA II (Appel et al., 2013)	ISORROPIA II (Appel et al., 2013)	ISSOROPIA (Zhou et al., 2012)	ISSOROPIA (Li et al., 2011)	EQUISOLV II (Jacobson, 1999)
Aqueous chemistry	None	Bulk cloud-chemistry scheme (Fahey and Pandis, 2001; Zhang et al., 2015)	AQCHEM (Fahey et al., 2017)	Based on algorithm developed by Barth et al. (2001) (He and Zhang, 2014)	Same as in MADE/ SORGAM (Fahey and Pandis, 2001; Chapman et al., 2009)	Same as in MADE/ SORGAM (Fahey and Pandis, 2001; Zhang et al., 2004)	1. AQCHEM 2. AQCHEM-KMT (Fahey et al., 2017)	1. AQCHEM-KMT 2. AQCHEM-KMTI (Fahey et al., 2017)	1. AQCHEM-KMT 2. AQCHEM-KMTI (Fahey et al., 2017)	Based on aqueous chemistry in CBM-IV mechanism by Gery et al. (1989)	Based on the RADM mechanism used in CMAQ v4.6 (AERO5) (Li et al., 2011)	Bulk or size-resolved cloud-chemistry module (GATOR2012)
SOA formation	None	1. Reversible absorption of 8 classes volatile organic compounds (VOCs) based on Caltech smog-chamber data (Odum et	Combined absorption and dissolution approaches for 9 parent VOCs and 32 SOA species (Carlton, et al., 2010)	Treatment of SOA from fixed mass yields for anthropogenic and biogenic precursor VOCs (Liu et al., 2012)	1. Based on ambient ageing measurement of organic aerosols by Hodzic and Jimenez (2011) 2. Based on volatility basis set approach	1. Absorptive approach for 14 parent VOCs and 38 SOA species 2. Combined absorption and	Combined absorption and dissolution approaches for 9 parent VOCs and 32 SOA species (Carlton, et al., 2010)	On the basis of SOA scheme in AERO5, adding parameterization of in-cloud SOA formation from biogenic VOCs (Foley et al., 2017)	On the basis of SOA scheme in AERO5/6, updated parametrization of monoterpene SOA yielded from photooxidation	Reversible absorption of 8 classes VOCs based on Caltech smog-chamber data (Zhou et al., 2012)	Bulk two-product yield parametrization (Fu et al., 2016; Odum et al., 1997)	Using Henry's Law to determine vapor pressure of organics and perform either time-dependent condensation or evaporation calculations.

al., 1997; Griffin et al., 1999) 2. Based on volatility basis set approach (Ahmadov et al., 2012)	(Knote et al., 2014)	dissolution approaches for 42 hydrophilic and hydrophobic VOCs (Zhang et al., 2004)	(Foley et al., 2021)	(Jacobson, 2002)

※CUACE is the aerosol mechanism implemented in the GRAPES-CUACE model (Zhou et al., 2012).

* GATOR2012 is the aerosol mechanism implemented in the GATOR-GCMOM model (Jacobson et al., 2012).

In addition to aerosol microphysics processes, the cloud properties included in cloud microphysics schemes and the treatment of aerosol-cloud processes in the five two-way coupled models are different in terms of hydrometeor classes, cloud droplet size distribution, aerosol water uptake, in-/below-cloud scavenging, hydrometeor-aerosol coagulations, and sedimentation of aerosols and cloud droplets (Table 3). Among the microphysics schemes implemented in the five coupled models, mass concentrations of different hydrometeors (including cloud water, rain, ice, snow or graupel) are included but their number concentrations are only considered if the cloud microphysics schemes are two-moment or three-moment. The single modal approach with either lognormal or gamma distribution and the sectional approach with discrete size distributions for cloud droplets are applied in different microphysics schemes. Based on the Mie theory, WRF-Chem, WRF-CMAQ, GRAPES-CUACE, WRF-NAQPMS and GATOR-GCMOM calculate cloud radiative properties (including extinction/scattering/absorption coefficient, single scattering albedo and asymmetry factor of liquid and ice clouds) in their radiation schemes (e.g., RRTMG, GODDARD, GATOR2012). In atmosphere, the hygroscopic growth of aerosols due to water uptake is parameterized based on the Köhler or Zdanovskii-Stokes-Robinson theory and the hysteresis effects depending on the deliquescence and crystallization RH are taken into account in the five coupled models. The removal processes of aerosol particles include wet removal and sedimentation. Aerosol particles in accumulation and coarse modes can act as CCN or IN via activations in cloud, which can further develop to different types of hydrometeors (cloud water, rain, ice, snow and graupel), and then gradually form precipitations. These processes are named as in-cloud scavenging or rainout. The aerosol particles below cloud base also can be coagulated with the falling hydrometeors, which are known as below-cloud scavenging or wash out. Both representations of in- and below-cloud scavenging processes are based on scavenging rate approach in aerosol mechanisms of WRF-Chem, WRF-CMAQ, GRAPES-CUACE and WRF-NAQPMS except GATOR-GCMOM. Size-resolved sedimentation of aerosols are computed from one model layer to layers below down to the surface layer using setting velocity in most coupled models and the MOSAIC aerosol mechanism in WRF-Chem only considers the sedimentation in the lowest model level (Marelle et al., 2017).

Table 3. Compilation of cloud properties and aerosol-cloud processes in two-way coupled models (WRF-Chem, WRF-CMAQ, GRAPES-CUACE, WRF-NAQPMS and GATOR-GCMOM) applied in Asia.

	WRF-Chem	WRF-CMAQ	GRAPES-CUACE	WRF-NAQPMS	GATOR-GCMOM
Hydrometeor (Cloud microphysics scheme)	Mass concentrations: Cloud water, rain, ice, snow and graupel (Morrison, Lin, Thompson, WSM 6 class and Milbrandt-Yau) Cloud water, rain, ice and snow (WSM 5 class) Number concentrations: Rain, ice, snow and graupel (Morrison and Milbrandt-Yau) Rain and ice (Thompson) None (Lin, WSM 5 class and WSM 6 class)	Mass concentrations: Cloud water, rain, ice, snow and graupel (Morrison) Cloud water, rain, ice and snow (WSM 5 class) Cloud water and rain (WSM 3 class) Number concentrations: Rain, ice, snow and graupel (Morrison) None (WSM 3 class and WSM 5 class)	Mass concentrations: Cloud water, rain, ice, snow and graupel (WSM 6 class) Number concentrations: None (WSM 6 class)	Mass concentrations Cloud water, rain, ice, snow and graupel (Lin) Number concentrations: None (Lin)	Mass concentrations: Cloud water, ice and graupel (GATOR2012) Number concentrations: Cloud water, ice and graupel (GATOR2012)
Cloud droplet size distribution (Cloud microphysics scheme)	1. Single, modal approach with lognormal distribution (Morrison and Lin) 2. Gamma distribution (Thompson, WSM 5 class and WSM 6 class)	1. Single, modal approach with lognormal distribution (Morrison) 2. Gamma distribution (WSM 3 class and WSM 5 class)	Gamma distribution (WSM 6 class)	Single, modal approach with lognormal distribution (Lin)	Sectional approach with multiple size distributions (GATOR2012*) (Jacobson, et al., 2007)
Cloud radiative properties (Radiation scheme)	Extinction coefficient, single scattering albedo and asymmetry factor of liquid and ice clouds based on Mie scattering theory (RRTMG SW) Absorption coefficient of liquid and ice clouds using constant values (RRTMG LW) Extinction coefficient, single scattering albedo and asymmetry factor of liquid and ice clouds from lookup tables (Goddard SW and LW)	Extinction coefficient, single scattering albedo and asymmetry factor of liquid and ice clouds based on Mie scattering theory (RRTMG SW) Absorption coefficient of liquid and ice clouds using constant values (RRTMG LW)	Extinction coefficient, single scattering albedo and asymmetry factor of liquid and ice clouds using lookup tables (Goddard SW) Extinction coefficient, single scattering albedo and asymmetry factor of liquid and ice clouds from lookup tables (Goddard LW)	Extinction coefficient, single scattering albedo and asymmetry factor of liquid and ice clouds using lookup tables (Goddard SW) Clear sky optical depth from lookup table (RRTM LW)	Integrating spectral optical properties over each size bin of each hydrometeor particle size distribution (Toon SW and LW) (Jacobson and Jadhav, 2018)
Aerosol water uptake	Equilibrium with RH based on Köhler theory, and hysteresis is treated (Ghan and Zaveri, 2007)	The empirical equations of deliquescence and crystallization RH developed by Martin et al (2003), and hysteresis is treated (CMAQ source code)	Equilibrium with the mutual deliquescence and crystallization RH using the Zdanovskii-Stokes-Robinson equation, and hysteresis is treated (Personal communication)	Equilibrium with the mutual deliquescence and crystallization RH using the Zdanovskii-Stokes-Robinson equation, and hysteresis is treated (Nenes et al., 1998; Li et al., 2011)	Size-resolved equilibrium with the mutual deliquescence and crystallization RH using the Zdanovskii-Stokes-Robinson equation, and hysteresis is treated (Jacobson et al., 1996)
In-cloud scavenging (Aerosol mechanism)	Scavenging via nucleation, Brownian diffusion, collection and autoconversion in both grid-scale and sub-grid clouds with a first-order removal rate (MADE/SORGAM, MOSAIC, MAM3 and MAM7) (Easter et al., 2004)	Scavenging of interstitial aerosol in the Aitken mode and nucleation scavenging of aerosol in the accumulation and coarse modes by the cloud droplets in both grid-scale and sub-grid clouds (AERO5, AERO6 and AERO7) (Binkowski and Roselle, 2004; Fahey et al., 2017)	Algorithm of rainout removal tendency by Giorgi and Chameides (1986)	Employing a scavenging coefficient approach based on relationships described by Seinfeld and Pandis (1998), only hydrophilic particles can be scavenged (Chen et al., 2017)	Size-resolved aerosol activation; nucleation scavenging and autoconversion for size-resolved cloud droplets (GATOR2012) (Jacobson, 2003)

Below-cloud scavenging (Aerosol mechanism)	Scavenged aerosols are instantly removed by interception and impaction but not resuspended by evaporating rain (MADE/SORGAM, MOSAIC, MAM3 and MAM7) (Slinn, 1984; Easter et al., 2004)	All aqueous species are scavenged from the cloud top to the ground in both grid-scale and sub-grid clouds (AERO5, AERO6 and AERO7) (CMAQ User's Guide; Fahey et al., 2017)	Aerosol particles between sizes ranging from 0.5 to 1 μm radius are instantly removed with considering cloud fraction, and scavenged rate depends on aerosol and hydrometeor sizes (Slinn, 1984; Gong et al., 2003)	Employing a scavenging coefficient approach based on relationships described by Seinfeld and Pandis (1998), considering accretion of in-cloud droplets particles into precipitation and impaction of ambient particles into precipitation	Discrete size-resolved coagulation between hydrometeors and aerosol particles (aerosol-liquid, aerosol-ice and aerosol-graupel) (GATOR2012) (Jacobson, 2003)
Sedimentation of aerosols (Aerosol mechanism)	Sedimentation with considering mass and number concentrations of aerosols at surface (MOSAIC) (Marelle et al., 2017)	Only considering gravitational sedimentation for aerosols (AERO5, AERO6 and AERO7)	Size-resolved sedimentation of aerosol particles above surface layer is computed with the setting velocity (CUACE) (Gong et al., 2003)	Using size-resolved sedimentation velocity to simulate sedimentation of aerosols (AERO5)	Sedimentation of size-resolved aerosols is computed from one model layer to layers below down to the surface, and the sedimentation velocities are calculated by two-step iterative method (GATOR2012) (Bear, 1976; Jacobson, 1997, 2003)

* GATOR2012 refers to either the aerosol or cloud microphysics scheme used in Jacobson (2012).

Table 4 further lists various aspects with regards to how ARI and ACI being calculated in the five two-way coupled models (WRF-Chem, WRF-CMAQ, GRAPES-CUACE, WRF-NAQPMS, and GATOR-GCMOM) applied in Asia. Note that the information in this table was extracted from the latest released version of WRF-Chem (version 4.3.3) and WRF-CMAQ (based on WRF v4.3 and CMAQ v5.3.3) as well as relevant references for GRAPES-CUACE (Wang et al., 2015), WRF-NAQPMS (Wang et al., 2014) and GATOR-GCMOM (Jacobson et al., 2010; 2012). These models all use the Mie theory to compute ARI effects but differ in representations of aerosol optical properties and radiation schemes. To simplify the calculation, aerosol species simulated by the chemistry module/model are put into different groups (Table 4) and the refractive indices of these groups are directly from the Optical Properties of Aerosols and Clouds (OPAC) database (Hess et al., 1998) in WRF-Chem and WRF-CMAQ (Table B6 in Appendix B). In WRF-Chem, the aerosol optical properties (AOD, extinction/scattering/absorption coefficient, single scattering albedo and asymmetry factor) are calculated in terms of four spectral intervals (listed in Table B6 in Appendix B) and then inter/extrapolated to 11 (14) SW intervals defined in the GODDARD (RRTMG) scheme. For SW and LW radiation in both WRF-CMAQ and WRF-Chem, these optical parameters are computed at each of corresponding spectral intervals in the RRTMG scheme. The aerosol optical property for LW radiation is considered only at 5 thermal windows (listed in Table B6) in WRF-CMAQ. No detailed information regarding how aerosol optical property and relevant parameters being calculated in GRAPES-CUACE and WRF-NAQPMS can be found from the relevant references.

With respect to ACI effects, the simulated aerosol characteristics (such as mass, size distribution and species) are utilized for the calculation of cloud droplet activation and aerosol resuspension based on the Köhler theory (Abdul-Razzak and Ghan, 2002) in several (one) microphysics schemes (scheme) in WRF-Chem (GRAPES-CUACE). GATOR-GCMOM is the first two-way coupled model adding IN activation processes including heterogeneous and homogeneous freezing (Jacobson et al., 2003). None of the other four two-way coupled models considers the IN formation processes (including immersion freezing, deposition freezing, contact freezing, and condensation freezing) but they have been included in some specific versions of WRF-Chem (Keita et al., 2020; Lee et al., 2020), which are not yet in the latest release version 4.3.3 of WRF-Chem.

Table 4. Summary of relevant information regarding calculations of aerosol-radiation interactions (ARI) and aerosol-cloud interactions (ACI) in two-way coupled models (WRF-Chem, WRF-CMAQ, GRAPES-CUACE, WRF-NAQPMS and GATOR-GCMOM) applied in Asia.

Model	ARI					ACI	
	Aerosol species groups	Aerosol size distribution (Aerosol mechanism)	Mixing state‡	SW scheme (# of spectral intervals)	LW scheme (# of spectral intervals)	CCN (Microphysics scheme)	IN (Microphysics scheme)
WRF-Chem	1. Water 2. Dust 3. BC 4. OC 5. Sea-salt 6. Sulfate	1. Bulk (GOCART) 2. Modal (MADE/SORGAM, AERO5, MAM3 and MAM7) 3. Sectional (MOSAIC (4bins and 8 bins) and MADRID (8bins))	Internal mixing (Volume averaging, Core-shell, and Maxwell-Garnett)	1. Goddard (11) 2. RRTMG (14)	RRTMG (16)	Activation under a certain supersaturation in an air parcel based on Köhler theory (Morrison, Lin, Thompson, WSM 6/5/3 class and Milbrandt-Yau)	Ice heterogeneous nucleation of mineral dust aerosols in based on classical nucleation theory (Milbrandt-Yau and Morrison)†
WRF-CMAQ	1. Water 2. Water-soluble 3. BC 4. Insoluble 5. Sea-salt	Modal (AERO5, AERO6 and AERO7)	Internal mixing (Core-shell)	RRTMG (14)	RRTMG (16)	None	None
GRAPES-CUACE	1. Nitrate 2. Dust 3. BC 4. OC 5. Sea-salt 6. Sulfate 7. Ammonium	Sectional (CUACE (12 bins))	External mixing	Goddard (11)	Goddard (10)	Activation under a certain supersaturation in an air parcel based on Köhler theory (WSM 6-class)	None
WRF-NAQPMS	1. Nitrate 2. Dust 3. BC 4. OC 5. Sea-salt 6. Sulfate	Modal (AERO5)	External mixing	Goddard (11)	RRTM (16)	Activation under a certain supersaturation in an air parcel based on Köhler theory (Lin)	None

	7. Ammonium 8. Other primary particles						
GATOR-GCMOM	1. Water 2. Dust 3. BC 4. HCO_3^- 5. SOA 6. Sulfate … 42. $MgCO_3(s)$	Sectional (GATOR2012* (17-30 bins))	Internal mixing (Core-shell‡)	Toon※ (318)	Toon※ (376)	Activation under a certain supersaturation in an air parcel based on Köhler theory (GATOR2012*)	Ice heterogeneous and homogeneous nucleation (GATOR2012*)

‡ Specific version of WRF-Chem, WRF-NAQPMS and GOTAR-GCMOM have the ability of simulating aerosol aging (Zhang et al., 2014;Chen et al., 2017; Li et al., 2018; Jacobson, 2012).

† Some specific versions of WRF-Chem consider IN (Keita et al., 2020; Lee et al., 2020).

※The short- and long-wave radiation calculations in GATOR-GCMOM are based on the algorithm of Toon et al. (1989).

* GATOR2012 refers to either the aerosol or cloud microphysics scheme used in Jacobson (2012).

How accurately ARI and ACI are simulated also rely on the representation of aerosol composition and size distribution in two-way coupled models. Table 5 presents the treatments of aerosol compositions and size distributions in the five two-way coupled models applied in Asia. As shown in Tables 4 and 5, GATOR-GCMOM considered more detailed aerosol species groups as high as 42 kinds, and others coupled models different numbers of species groups (such as 6, 5, 7, 8 aerosol species groups in WRF-Chem, CMAQ, NAQPMS and CUACE, respectively). Three typical representation approaches of size distribution (bulk, modal and sectional methods) are adopted by the five two-way coupled models and WRF-Chem offers all the three approaches, but other models only support one specific option. The Global Ozone Chemistry Aerosol Radiation and Transport (GOCART) model (Ginoux et al., 2001) in WRF-Chem is the only one that is based on a combination of bulk (for water, BC, OC, and sulfate aerosols) and sectional (for dust and sea salt aerosols) approaches. The widely used modal and sectional approaches in five coupled models and their detailed numerical settings of aerosol size distribution (namely, geometric diameter and standard deviation for modal approach or bin ranges for sectional method) are listed in Table 5. Regarding the modal method, same parameter values for Aitken and accumulation modes and geometric diameters for coarse mode in the latest version of WRF-Chem (v4.3.3) and older version of WRF-CMAQ (before v5.2) are set as default, except the standard deviations for coarse mode are slightly different. In the official version of WRF-CMAQ released after v5.2, there are some modifications to the default setting of geometric diameters in Aitken, accumulation and coarse modes, from 0.01 to 0.015 μm, 0.07 to 0.08 μm and 1.0 to 0.6 μm, respectively. For the GRAPES-CUACE model, the parameters of size distribution for certain aerosol species in the accumulation mode were updated from its older version (Zhou et al., 2012) to newer one (Zhang et al., 2021). With respect to the sectional approach, 4 or 8 (from 0.039 to 10 μm), 12 (from 0.005 to 20.48 μm) and 14 (from 0.002 to 50 μm) particle size bins are defined in WRF-Chem, CUACE and GATOR-GCMOM, respectively.

Table 5. Summary of numerical representations of aerosol size distribution and composition in two-way coupled models (WRF-Chem, WRF-CMAQ, GRAPES-CUACE, WRF-NAQPMS and GATOR-GCMOM) applied in Asia.

Model	Aerosol mechanism	Modal approach						Compositions	Reference
		Aitken		Accumulation		Coarse			
		Geometric diameters (μm)	Standard deviations (μm)	Geometric diameters (μm)	Standard deviations (μm)	Geometric diameters (μm)	Standard deviations (μm)		
WRF-Chem v4.3.3	MADE/ SORGAM	0.010	1.7	0.07	2.0	1.0	2.5	Water, BC, OC, and sulfate, dust and sea salt	WRF-Chem codes֍
WRF-Chem$^{\Delta}$	MAM3	0.013 (Sulfate and secondary OM)	1.6 (Sulfate and secondary OM)	0.068 (Sulfate, secondary OM, primary OM, BC, dust and sea salt)	1.8 (Sulfate, secondary OM, primary OM, BC, dust and sea salt)	2.0 (Sea salt), 1.0 (Dust)	1.8 (Sea salt and dust)	Sulfate, methane sulfonic acid (MSA), OM, BC, sea salt and dust	Easter et al. (2004) Liu et al. (2012)
WRF-Chem$^{\Delta}$	MAM7	0.013 (Sulfate and secondary OM and BC)	1.6 (Sulfate, OM and BC)	0.068 (Sulfate and BC) 0.068 (Primary OM) 0.2 (Sea salt) 0.11 (Dust)	1.8 (Sulfate and BC) 1.6 (Primary OM) 1.8 (Sea salt) 1.8 (Dust)	2.0 (Sea salt) 1.0 (Dust)	2.0 (Sea salt) 1.8 (Dust)	Sulfate, methane sulfonic acid (MSA), OM, BC, sea salt and dust	Easter et al. (2004) Liu et al. (2012)
WRF-CMAQ	AERO5	0.010	1.7	0.07	2.0	1.0	2.2	Water, water-soluble BC,	CMAQ codes*

(before CMAQ v5.2)								insoluble, sea salt	
WRF-CMAQ (after CMAQ v5.2)	AERO6 and AERO7	0.015	1.7	0.08	2.0	0.60	2.2	Water, water-soluble BC, insoluble, sea salt	CMAQ codes†
WRF-NAQPMS	AERO5	0.052	1.9	0.146	1.8	0.80	1.9	Nitrate, dust, BC, OC, sea-salt, sulfate, ammonium, other primary particles	Wang et al. (2014)
GRAPES-CUACE	CUACE	0.10 (BC and OC)	1.7 (BC and OC)	0.25 (Sulfate and nitrate)	1.7 (Sulfate and nitrate)	3.0 (Dust)	1.7 (Dust)	Nitrate, dust, BC, OC, sea-salt, sulfate, ammonium*	Zhou et al. (2012)
GRAPES-CUACE	CUACE	Unclear	Unclear	0.37 (BC and OC)	0.42 (BC and OC)	Unclear	Unclear	Nitrate, dust, BC, OC, sea-salt, sulfate, ammonium ‡	Zhang et al. (2021)
		Sectional approach							
WRF-Chem v4.3.3	MOSAIC	0.039-0.156, 0.156-0.625, 0.625-2.5, 2.5-10.0 μm (4 bins) 0.039-0.078, 0.078-0.156, 0.156-0.312, 0.312-0.625, 0.625-1.25, 1.25-2.5, 2.5-5.0, 5.0-10.0 μm (8 bins)						Water, BC, OC, sulfate, dust and sea salt	WRF-Chem codes✿
WRF-Chem$^{\Delta}$	MADRID	0.0216-10 μm (8 bins)						Water, BC, OC, and sulfate, dust and sea salt	Zhang et al. (2016)
WRF-Chem v4.3.3	GOCART	0.1-1.0, 1.0-1.8, 1.8-3.0, 3.0-6.0, 6.0-10.0 (5 bins for dust) 0.1-0.5, 0.5-1.5, 1.5-5.0, 5.0-10.0 (4 bins for sea salt)						Dust and sea salt	WRF-Chem codes✿
GRAPES-CUACE	CUACE	0.005-0.01, 0.01-0.02, 0.02-0.04, 0.04-0.08, 0.08-0.16, 0.16-0.32, 0.32-0.64, 0.64-1.28, 1.28-2.56, 2.56-5.12, 5.12-10.24, 10.24-20.48 μm (12 bins)						Nitrate, dust, BC, OC, sea-salt, sulfate, ammonium	Zhou et al. (2012)
GATOR-GCMOM	GATOR2012	0.002-50 μm (14 bins)						42 species‡	Jacobson (2002, 2012)

✿ Official released version of WRF-Chem.

$^{\Delta}$ Specific version of WRF-Chem.

* https://github.com/USEPA/CMAQ/blob/5.1/models/CCTM/aero/aero6/AERO_DATA.F.

† https://github.com/USEPA/CMAQ/blob/5.2/CCTM/src/aero/aero6/AERO_DATA.F.

‡ More detailed components were presented in the first column of Table 2.

* Initial size distribution is tri-modal log-normal distribution.

Not only the choice of methodologies for ARI and ACI calculations can impact simulation results, but also the various aspects regarding the setup of modeling studies by applying two-way coupled models. The extra/auxiliary information about model configuration, including horizontal and vertical resolutions, aerosol and gas phase chemical mechanisms, PBL schemes, meteorological and chemical initial conditions (ICs) and boundary conditions (BCs), anthropogenic and natural emissions, were extracted from the 160 papers and presented in Table S4 of Supplement, which is organized in the same order as Table 1.

For two-way coupled model applications in Asia, horizontal resolutions were set from a few to several hundred kilometers, sometimes with nests, and vertical resolutions were from 15 to about 50-70 levels, with only one study performed at 100 levels for studying a fog case (Wang Z. L. et al., 2018). Wang K. et al. (2018) evaluated the impacts of horizontal resolutions on simulation results and found out surface meteorological variables were better modeled at finer resolution but no significant improvements of ACI related meteorological variables and certain chemical species between different grid resolutions. Through applying a single column model and then WRF-Chem with ARI, Wang et al. (2019) unraveled that better representation of PBL structure and relevant variables with finer vertical resolution from the surface to PBL top could reduce model biases noticeably, but balancing between vertical resolution and computational resource was important as well. Among the 160 applications of two-way coupled models in Asia, the frequently used aerosol module and gas-phase chemistry mechanism in WRF-CMAQ (WRF-Chem) were AERO6 (MOSAIC and MADE/SOGARM) and CB05 (CBMZ and RADM2), respectively. For PBL schemes, most studies selected YSU in WRF-Chem and ACM2 in WRF-CMAQ. Regarding to meteorological ICs and BCs, the FNL data were the first choice, and outputs from the Model for Ozone and Related Chemical Tracer (MOZART) were used to generate chemical ICs and BCs by most researchers. Georgiou et al. (2018) also unraveled that boundary conditions of dust and O_3 played an important role in WRF-Chem simulations. The modeling applications in Asia utilized global (EDGAR), regional (e.g., MIX, INTEX-B, and REAS), and national (e.g., MEIC and JEI-DB) anthropogenic emission inventories. Natural emission sources, such as mineral dust (Shao, 2004), biomass burning (FINN (Wiedinmyer et al., 2011) and GFED (Guido et al., 2010)), biogenic VOCs (MEGAN (Guenther et al., 2006)), and sea salt (Gong et al., 1997) were also considered. It should be noted that only one paper by Gao et al. (2017) reported that the WRF-Chem model with the Gridpoint Statistical Interpolation (GSI) data assimilation could improve the simulation accuracy during a wintertime pollution period.

4 Overview of research focuses in Asia

4.1 Feedbacks of natural aerosols

4.1.1 Mineral dust aerosols

Due to the fact that dust storm events frequently occurred over Asia during 2000-2010, the research community has focused on dust transportation and associated climatic effects (Choobari et al., 2014; Gong et al., 2003; Lee et al., 2010; Yasunari and Yamazaki, 2009; Zhang et al., 2003a, 2003b). Also the detailed processes and physiochemical mechanisms of dust storms had been well understood and reviewed in detail (Chen et al., 2017a; Huang et al., 2014; Shao and Dong, 2006; Uno et al., 2006). To probe into the radiative feedbacks of dust aerosols in Asia, Wang et al. (2013, 2010) initiated modeling studies by a two-way coupled model, i.e., the GRAPES-CUAUE model, to simulate direct radiative forcing (DRF) of dust, and revealed that the feedback effects of dust aerosols could lead to decreasing of surface wind speeds and then suppress dust emissions. Further modeling simulations by the same model (Wang and Niu, 2013) indicated that considering dust radiative effects did not substantially improve the model performance of the air temperature at 2 meters above the surface (T2), even with assimilating data from in-situ and satellite observations into the model. Subsequently, several similar studies based on another two-way coupled model (WRF-Chem with The Georgia Tech/Goddard Global Ozone Chemistry Aerosol Radiation and Transport scheme) were conducted to investigate dust radiative forcing (including shortwave radiative forcing (SWRF) and longwave radiative forcing (LWRF)) and ARI effects of dust on meteorological variables (PBLH, T2 and WS10) in different regions of Asia (Bran et al., 2018; Chen et al., 2014; Jin et al., 2016a, 2015; Kumar et al., 2014; Liu L. et al., 2016; Su and Fung, 2018a, 2018b; Zhou et al., 2018). These studies demonstrated that dust aerosols could induced negative radiative forcing (cooling effect) at top of atmosphere (TOA) as well as the surface (including both Earth's and sea surfaces) and positive radiative forcing (warming effect) in the ATM (Bran et al., 2018; Chen et al., 2014; Kumar et al., 2014; Li and Sokolik, 2018; Li M.M. et al., 2017a; Su and Fung, 2018a; Wang et al., 2013). More thorough analyses of the radiative effects of dust in Asia (Li and Sokolik, 2018; Wang et al., 2013) pointed out that dust aerosols played opposite roles in the shortwave and longwave bands, so that the dust SWRF at TOA and the surface (cooling effects) as well as in the ATM (warming effects) was offset partially by the dust LWRF (warming effects at TOA and the surface but cooling effects in the ATM). It was noteworthy that adding more detailed mineralogical composition into the dust emission for WRF-Chem could alter the dust SWRF at TOA from cooling to warming and then lead to a positive net radiative forcing at TOA (Li and Sokolik, 2018). These different conclusions showed some degrees of uncertainties in the coupled model simulations of dust aerosols' radiative forcing that need to be further investigated in the future.

Dust aerosols can act not only as water-insoluble cloud condensation nuclei (CCN) (Kumar et al., 2009) but also as ice nuclei (IN) (Lohmann and Diehl, 2006) since they are referred to as ice friendly (Thompson and Eidhammer, 2014). Therefore, activation and heterogeneous ice nucleation parameterizations (INPs) with respect to dust aerosols were developed and incorporated into WRF-Chem to explore ACI effects as well as both ARI and ACI effects of dust aerosols in Asia (Jin et al., 2016a, 2015; Su and Fung, 2018a, 2018b; Wang K. et al., 2018; Zhang Y. et al., 2015b). During dust storms, including the adsorption activation of dust particles played vital roles in the simulations of ACI-related cloud properties and a 45 % of increase of cloud droplet number concentration (CDNC), comparing to a simpler aerosols activation scheme in WRF-Chem (Wang K. et al., 2018). More sophisticated INPs implemented in WRF-Chem that taking dust particles into account as IN resulted in substantial modifications of cloud and ice properties as well as surface meteorological variables and air pollutant concentrations in model simulations (Su and Fung, 2018b; Zhang Y. et al., 2015b). Zhang Y. et al. (2015b) delineated that dust aerosols acting either as CCN or IN made model results rather different regarding radiation, T2, precipitation, and number concentrations of cloud water and ice. Su and Fu (2018b) described that the ACI effects of dust had less impacts on the radiative forcing than its ARI effects and dust particles could promote (demote) ice (liquid) clouds in mid-upper (low-mid) troposphere over EA. With turning on both ARI and ACI effects of dust, less low-level clouds and more mid- and high-level clouds were detected that contributed to cooling at the Earth's surface and in the lower atmosphere and warming in the mid-upper troposphere (Su and Fung, 2018b). Mineral dust particles transported by the westerly and southwesterly winds from the Middle East (ME) affected the radiative forcing at TOA and the Earth's surface and in the ATM by the dust-induced ARI and ACI in the Arabian Sea and the India subcontinent, and subsequently changed the circulation patterns, cloud properties, and characteristics related to the India summer monsoon (ISM; Jin et al., 2015, 2016b). Moreover, the effects of dust on precipitation are not only complex but also highly uncertain, evidencing from several modeling investigations targeting a variety of areas in Asia (Jin et al., 2016a, 2016b, 2015; Su and Fung, 2018b; Zhang Y. et al., 2015b). Less precipitation from model simulations including dust effects was found at EA and dust particles acting mainly as CCN or IN influenced precipitation in a rather different way (Zhang Y. et al., 2015b). A positive response of ISM rainfall to dust particles from the ME was reported by Jin et al. (2015) and less affected by dust storms from the local sources and NWC (Jin et al., 2016a). Jin et al. (2016b) further elucidated that the impacts of ME dust on ISM rainfall were highly sensitive to the imaginary refractive index of dust setting in the model, so that accurate simulations of the dust-rainfall interaction depended on more precise representation of radiative absorptions of dust in two-way coupled models. About 20 % of increase or decrease in rainfall due to the dust effects were detected in different areas over EA from the WRF-Chem simulations (Su and Fung, 2018b). However, it should be mentioned that a few studies that targeting DRF of dust in Asia based on WRF-Chem simulations but without enabling aerosol-radiation feedbacks (Ashrafi et al., 2017; Chen S. et al., 2017b; Tang et al., 2018) were not included in this paper.

Along with the modeling research on the effects of dust aerosols on meteorology, their impacts on air quality in Asia were explored using two-way coupled models (Chen et al., 2014; Kumar et al., 2014; Li and Sokolik, 2018; Li M. M. et al., 2017a; Wang et al., 2013). Many early modeling research work involving two-way coupled models with dust only looked into the ARI or direct radiative effects of dust particles, which are described as follows. Taking a spring-time dust storm from the Thar Desert into consideration in WRF-Chem, the modeled aerosol optical depth (AOD) and Angstrom exponent (as indicators of aerosol optical properties and unique proxies of the surface particulate matter pollution) demonstrated that turning on the ARI effects of dust could reduce biases in their simulations, but were underestimated in North India (Kumar et al., 2014). Wang et al. (2013) pointed out that in EA, including the longwave radiative effects of dust in the GRAPES-CUACE/dust model lowered relative errors of the modeled AOD by 15 %, as compared to simulations that only considering shortwave effects of dust. Comparisons against both satellite and in situ observations depicted that the WRF-Chem model was able to capture the general spatiotemporal variations of the optical properties and size distribution of dust particles over the main dust sources in EA, such as the Taklimakan Desert and Gobi Desert, but overestimated AOD during summer and fall and also exhibited positive (negative) biases in the fine (coarse) mode of dust particles (Chen et al., 2014). Besides the ARI effects of dust, the heterogeneous chemistry on dust particles' surface added in WRF-Chem was accounted for 80 % of the net reductions of O_3, NO_2, NO_3, N_2O_5, HNO_3, ·OH, HO_2· and H_2O_2 when a springtime dust storm striking the Nanjing megacity of EC (Li M. M. et al., 2017a). In CA, AOD was overestimated by WRF-Chem model but its simulation was improved when more detailed mineral components of dust particles were incorporated in the model (Li and Sokolik, 2018). Later on, more investigations started to focus on both ARI and ACI effects of dust aerosols. With consideration of ARI as well as both ARI and ACI of dust particles from the ME, during the ISM period, the WRF-Chem model reproduced AOD's spatial distributions but underpredicted (overpredicated) AOD over the Arabian Sea (the Arabian Peninsula) comparing with satellite observations and AOD reanalysis data (Jin et al., 2016a, 2016b, 2015). In EA, Wang K. et al. (2018) demonstrated that including both ARI and ACI effects of dust in WRF-Chem caused lower O_3 concentrations and by incorporating INPs, the WRF-Chem model well simulated the surface PM_{10} concentrations (Su and Fung, 2018a) with reduced (elevated) surface concentrations of OH, O_3, SO_4^{2-}, and $PM_{2.5}$ (CO, NO_2, and SO_2) (Zhang Y. et al., 2015b). It is worth noting that how to partition dust particles into fine mode and coarse mode or initialize their size distribution in coupled models can affect simulations in many ways and requires more detailed measurements at the source areas and further modeling studies.

4.1.2 Wildfire, sea salt and volcanic ash

In the Maritime SEA region, peat and forest fire triggered by El Niño induced drought conditions released huge amount of smoke particles, which promoted dire air pollution problems in the downstream areas, and their ARI effects simulated by WRF-Chem enhanced radiative forcing at the TOA and the atmospheric stability (Ge et al., 2014). Ge et al. (2014) also pointed out the ARI effects of these fires impaired (intensified) sea breeze at daytime (land breeze at nighttime) over this region so that their impacts on cloud cover could be positive or negative in different areas and time period (day or night). Sea salt and volcanic ash are also important natural aerosols for regions near seashores and active volcanoes and surrounding areas but modeling studies of their ARI and ACI effects are relatively scarce in Asia. Based on WRF-Chem simulations, Kedia et al. (2019a) demonstrated that the feedbacks of sea salt aerosols impacted convective and nonconvective precipitation rather variously in different areas of the India subcontinent. Jiang et al. (2019a, 2019b) also used WRF-Chem with/without sea-salt emissions to evaluate the effects of sea salt on rainfall in Guangdong Province of China, but unfortunately, no feedbacks were considered in the simulations. So far there is no investigation targeting aerosol effects of volcanic ash from volcano eruptions in Asia using coupled models.

4.2 Feedbacks of anthropogenic aerosols

Atmospheric pollutants from anthropogenic sources are the leading causes of heavy pollution events occurring in Asia due to the acceleration of urbanization, industrialization, and population growth in recent decades, particularly in China and India, and their ARI or/and ACI effects on meteorology and air quality had been quantitatively examined using two-way coupled models (Archer-Nicholls et al., 2019; Bharali et al., 2019; Gao M. et al., 2016b; Kumar et al., 2012a, 2012b; Li and Liao, 2014; Wang J. et al., 2014; Wang Z. et al., 2018; Zhang B. et al., 2015; Yao et al., 2017; Zhong et al., 2016). These modeling research work had been primarily focused on the ARI or/and ACI effects of anthropogenic aerosols, their specific chemical components (especially the light-absorbing aerosols, i.e., BC and brown carbon (BrC)) and aerosols originated from different sources. The major findings are outlined as follows, with respect to the effects of anthropogenic aerosol feedbacks on meteorology and air quality.

Concerning the meteorological responses, most papers treated anthropogenic aerosols as a whole to explore their effects on meteorological variables based on coupled model simulations with enabling ARI or/and ACI in WRF-Chem, WRF-CMAQ, WRF-CMAQ, GRAPES-CUACE and WRF-NAQPMS (Bai et al., 2020; Gao M. et al., 2016b; Kumar et al., 2012a; Nguyen et al., 2019a, 2019b; Wang H. et al., 2015; J. Wang et al., 2014; Wang Z. F. et al., 2014; Zhang B. et al., 2015; Zhang et al., 2018; Zhao et al., 2017). Generally, the main ARI effects of anthropogenic aerosols resulted in decreases of SWRF, T2 and WS10, and PBLH, as well as increases of surface relative humidity (RH2) and temperature in the ATM, which further suppressed PBL development (Gao Y. et al., 2015; Li M. M. et al., 2017b; Nguyen et al., 2019a, 2019b; Xing et al., 2015c; Zhang et al., 2018). Wang H. et al. (2015) utilized GRAPES-CUACE with ARI to study a summer haze case in the NCP area and discovered that the ARI effects made the subtropical high less intense (-14 hPa) to help pollutants in the area to dissipate. In Asia, ACI effects of anthropogenic aerosols on cloud properties and precipitation are relatively complex. On the one hand, anthropogenic aerosols, that being activated as CCN, enhanced CDNC and LWP and then slowed down the precipitation onset, but their impacts on precipitation amounts varied in different seasons and areas in China (Zhao et al., 2017). Targeting a summertime rainstorm in the middle reaches of the Yangtze River (MRYR) in China, sensitivity studies using WRF-Chem unveiled that CDNC, cloud water contents, and precipitation decreased (increased) with low (high) anthropogenic emission scenarios due to the ACI effects and these variations tended to depend on atmospheric humidity (Bai et al., 2020). The modeling investigations with WRF-Chem aiming at the ISM (Kedia et al., 2019) and a disastrous flood event in Southwest China (SWC) (Fan et al., 2015) pointed out that the simulated convective process was suppressed and convective (nonconvective) precipitation was inhibited (enhanced) by the ARI and ACI effects of accumulated anthropogenic aerosols, but these effects could invigorate convection and rainfall in the downwind mountainous area at nighttime (Fan et al., 2015). On the other hand, how anthropogenic aerosols act in the ice nucleation processes is still open to question (Zhao et al., 2019) and these processes need to be represented accurately in two-way coupled models, however until now no study had been performed to simulate the ACI effects of anthropogenic aerosol serving as IN in Asia using two-way coupled models. Therefore, in Asia, further investigations are needed that targeting cloud or/and ice processes involving anthropogenic aerosols (including their size, composition, and mixing state) in two-way coupled models. Meanwhile, several studies not only discussed aerosol feedbacks but also focused on the additional effects of topography or urban heat island on meteorology (Wang D. et al., 2019; Zhong et al., 2017, 2015). Utilizing the GATOR-GCMOM model at global and local scales, Jacobson et al. (2015, 2019) explored the impacts of landuse changes due to the unprecedented expansions of megacities, such as Beijing and New Delhi in Asia, from 2000 to 2009 on meteorology and air quality.

Hitherto there were several attempts to ascertain the effects of different chemical components of anthropogenic aerosols on meteorology in Asia (Archer-Nicholls et al., 2019; Ding et al., 2019; Ding et al., 2016; Gao J. et al., 2018; Huang et al., 2015; Wang Z. et al., 2018). First of all, Asia is the region in the world with the highest BC emissions due to burning of large amount of fossil fuels and biomass and this has increasingly attracted many researchers to probe into the ARI or/and ACI effects of BC (Boucher et al., 2013). As the most important absorbing aerosol, BC induced the largest positive, positive and negative mean DRF at the TOA, in the ATM, and at the surface, respectively, over China during 2006 (Huang et al., 2015). Ding et al. (2016) and Wang Z. et al. (2018) further applied WRF-Chem with feedbacks to investigate how aerosol-PBL interactions involving BC suppressed the PBL development, which deteriorated air quality in Chinese cities and was described as “dome effect” (namely BC warms the atmosphere and cools the surface, suppresses the PBL development and eventually results in more accumulation of pollutants). This “dome effect” of BC promoted the advection-radiation fog and fog-haze formation in the YRD area through altering the land-sea circulation pattern and increasing the moisture level (Ding et al., 2019). Gao J. et al. (2018) also pointed out BC in the ATM modified the vertical profiles of heating rate and equivalent potential temperature in Nanjing, China. In India, the ARI effects of BC enhanced convective activities, meridional flows, and rainfall in North-East India during the pre-monsoon season but could either enhance or suppress precipitation during the monsoon season in different parts of the India subcontinent (Soni et al., 2018). Moreover, the ARI effects of BC on surface meteorological variables were larger than its ACI effects in EC (Archer-Nicholls et al., 2019; Ding et al., 2019). Besides BC, the BrC portion of organic aerosols (OA) emitted from agriculture residue burning (ARB) were included in WRF-Chem with the parameterization scheme suggested by Saleh et al. (2014) and the model simulations in EC revealed that at the TOA, the net DRF of OA was -0.22 $W \cdot m^{-2}$ (absorption and scattering DRF were +0.21 $W \cdot m^{-2}$ and -0.43 $W \cdot m^{-2}$ respectively), but the BC’s DRF was still the highest (+0.79 $W \cdot m^{-2}$) (Yao et al., 2017). As mentioned above, it is obvious that ARI and ACI effects of different aerosol components are substantially distinctive, and many other aerosol compositions (e.g., sulfate, nitrate and ammonium) besides BC and BrC should be taken into considerations in future modeling studies in Asia.

ARB is a common practice in many Asian countries after harvesting and before planting and can deteriorate air quality quickly as one of the most important sources of anthropogenic aerosols, so that it has been attracting much attention among the public and scientists worldwide (Chen J. et al., 2017; Hodshire et al, 2019; Koch and Del Genio, 2010; Reid et al., 2005; Yan et al., 2018). Recently, the effects of ARB aerosols on meteorology had widely been explored using the two-way coupled model (WRF-Chem) in many Asian countries and regions, such as EC (Huang et al., 2016; Li M. et al., 2018; Wu et al., 2017; Yao et al., 2017), South China (SC) (Huang et al., 2019), and South Asia (SA) (Singh et al., 2020). In general, when ARB occurred, the WRF-Chem simulations from all the studies showed that the changes in radiative forcing induced by ARB aerosols were greater than by those from other anthropogenic sources, especially in the ATM. Also all the modeling studies indicated that ARB aerosols reduced (increased) radiative forcing at the surface (in the ATM), cooled (warmed) the surface (the atmosphere), and increased (decreased) atmospheric stability (PBLH). Furthermore, the WRF-Chem simulations with ARI demonstrated that light-absorbing carbonaceous aerosols (CAs) from ARB caused daytime (nighttime) precipitation decreased (increased) over Nanjing in EC during a post-harvest ARB event (Huang et al., 2016). Yao et al. (2017) pointed out their WRF-Chem simulations in EC exhibited larger DRE induced by BC from

ARB at the TOA than previous studies. Lately, several modeling studies using WRF-Chem had targeted the effects of ARI and both ARI and ACI due to ARB aerosols from countries in the Indochina, SEA, and SA regions during the planting and harvesting time (Dong et al., 2019; Huang et al., 2019; Singh et al., 2020; Zhou et al., 2018). Zhou et al. (2018) investigated how ARB aerosols from SEA mixed with mineral dust and other anthropogenic aerosols while being lifted to the mid-low troposphere over the source region and transported to the YRD area and then affected meteorology and air quality there. The influences of ARI and ACI caused by ARB aerosols from Indochina were contrary, namely, the ARI (ACI) effects made the atmosphere over SC warmer (cooler) and drier (wetter), and the ARI effects hindered cloud formation and suppressed precipitation there (Huang et al., 2019). Dong et al. (2019) found the warming ARI effects of ARB aerosols were smaller over the source region (i.e., SEA) than the downwind region (i.e., SC) with cloudier conditions. Annual simulations regarding the ARI effects of ARB aerosols from SA (especially Myanmar and Punjab) indicated that CAs released by ARB reduced the radiative forcing at the TOA but did not change the precipitation processes much when only the ARI effects were considered in WRF-Chem (Singh et al., 2020).

Besides ARB, to our best knowledge, there were only a few research work quantitatively assessing the effects of anthropogenic aerosols from different emission sources on meteorology using WRF-Chem. Gao M. et al. (2018b) evaluated the responses of radiative forcing in China and India to aerosols from five emission sectors (power, industry, residential, BB, and transportation), and found that the power (residential) sector was the dominate contributor to the negative (positive) DRF at the TOA over both countries due to high emissions of sulfate and nitrate precursors (BC) and the total sectoral contributions were in the order of power > residential > industry > BB > transportation (power > residential > transportation > industry > BB) for China (India) during 2013. To pinpoint the ARI and ACI effects, Archer-Nicholls et al. (2019) reported that during January 2014, the aerosols from the residential emission sector induced larger SWRF (+1.04 $W \cdot m^{-2}$) than LWRF (+0.18 $W \cdot m^{-2}$) at the TOA and their DRF (+0.79 $W \cdot m^{-2}$) was the largest, followed by their semidirect effects (+0.54 $W \cdot m^{-2}$) and indirect effects (-0.29 $W \cdot m^{-2}$) over EC. This study further emphasized a realistic ratio of BC to total carbon from the residential emission was critical for accurate simulations of the ARI and ACI effects with two-way coupled models.

In terms of anthropogenic aerosol effects on air quality, the responses of $PM_{2.5}$ had been widely investigated (Chen et al., 2019a; Gao J. et al., 2018; Gao M. et al., 2016b; Gao Y. et al., 2015; Nguyen et al., 2019a, 2019b; Wang H. et al., 2015; Wang J. et al., 2014; Wang Z. F. et al., 2014; Wu et al., 2019a; Zhang B. et al., 2015; Zhang et al., 2018; Zhao et al., 2017) but less studies explored the responses of O_3 and other species (Kumar et al., 2012b; Li J. et al., 2018; Nguyen et al., 2019a, 2019b; Xing et al., 2017; Zhang B. et al., 2015). As summarized by Wu et al. (2019a) in their Table 1, observations and model simulations with WRF-Chem, WRF-CMAQ, WRF-CMAQ, GRAPES-CUACE, and WRF-NAQPMS all pointed out that the ARI effects promoted higher $PM_{2.5}$ concentrations in China (Chen et al., 2019a; Gao M. et al., 2016b; Gao Y. et al., 2015; Wang H. et al., 2015; Wang J. et al., 2014; Wang Z.F. et al., 2014; Zhang B. et al., 2015; Zhang et al., 2018) and this was also true in other areas of Asia (e.g., India, EA, Continental SEA) (Gao M. et al., 2018b; Nguyen et al., 2019a, 2019b) during different seasons. At the same time, all the modeling investigations revealed that the positive aerosol-meteorology feedbacks could further exacerbate pollution problems during heavy haze episodes. Based on WRF-Chem simulations, the ACI effects on $PM_{2.5}$ was negligible comparing to the ARI effects over EC (Zhang B. et al., 2015) but was subject to a certain degree of uncertainty if no consideration of the ACI effects induced by cumulus clouds in the model (Gao Y. et al., 2015). Annual WRF-Chem simulations for 2014 by Zhang et al. (2018) indicated that even though the ARI effects had bigger impacts on $PM_{2.5}$ during wintertime than the ACI effects, the ARI and ACI impacts on $PM_{2.5}$ were similar during other seasons and the increase of $PM_{2.5}$ due to the ACI effects was more noticeable in wet season than dry season. Using the process analysis method to distinguish the contributions of different physical and chemical processes to $PM_{2.5}$ over the NCP area, Chen et al. (2019a) applied WRF-Chem with ARI and ACI and found that besides local emissions and regional transport processes, vertical mixing contributed the most to the accumulation and dispersion of $PM_{2.5}$, comparing to chemistry and advection, and the ARI effects changed the vertical mixing contribution to daily $PM_{2.5}$ variation from negative to positive. Regarding surface O_3 concentrations, all the two-way coupled models with ARI, ACI, and both ARI and ACI predicted reduced photolysis rate and O_3 concentrations under heavy pollution conditions, through the radiation attenuation induced by aerosols and clouds. Further analyses indicated that the ARI effects impacted O_3 positively through reducing vertical dispersions (WRF-CMAQ, Xing et al., 2017), reduced O_3 more during wintertime than summertime in EC (WRF-NAQPMS, Li J. et al., 2018), and suppressed (enhanced) O_3 in dry (wet) season in continental SEA (WRF-CMAQ, Nguyen et al., 2019b). Xing et al. (2017) applied the process analysis method in WRF-CMAQ with ARI and revealed that the impacts of ARI on the contributions of atmospheric dynamics and photochemistry processes to O_3 over China varied in winter and summer months and ARI induced largest changes in photochemistry (dry deposition) of surface O_3 at noon time in January (July). The process analysis in WRF-Chem with ARI and ACI identified that the vertical mixing process played the most important role among the other physical and chemical processes (advection and photochemistry) in surface O_3 growth during 10-14 local time in Nanjing, China (Gao J. et al., 2018). ARI and ACI not only affected $PM_{2.5}$ and O_3, but also other chemical species. For instance, CO and SO_2 increased due to ARI and ACI over EC (Zhang B. et al., 2015), ARI caused midday (daily average) OH increased (decreased) in July (January) over China (Xing et al., 2017), SO_2, NO_2, BC, SO_4^{2-}, NO_3^- were enhanced but OH was reduced over China by ACI (Zhao et al., 2017), and ARI impacted SO_2 and NO_2 positively over EA (Nguyen et al., 2019a). Wu et al. (2019b) further analyzed how the aerosol liquid water involved in ARI and chemical processes (i.e., photochemistry and heterogeneous reactions) and influenced radiation and $PM_{2.5}$ (esp. secondary aerosols) over NCP during an intense haze event. Moreover, evaluations and sensitivity studies indicated that turning on aerosol feedbacks could improve the model performance for surface $PM_{2.5}$, particularly during severe haze episodes (Li J. et al., 2018; Wang H. et al., 2018; Zhang B. et al., 2015; Zhang et al., 2018).

With reference to the feedback effects of anthropogenic aerosol compositions on air quality, most modeling research work with WRF-Chem had focused on the ARI and ACI effects of BC and BrC, especially the "dome effect" that prompted the accumulation of pollutants (aerosols and O_3) near surface and in PBL (Ding et al., 2016; Ding et al., 2019; Gao J. et al., 2018; Li and Liao, 2014; Wang Z. et al., 2018). At the same time, the ARI effects of BC undermined the low-level wind convergence and then led to decrease of aerosols (sulfate and nitrate) and O_3 (Li and Liao, 2014). With the process analysis methodology in WRF-Chem, Gao J. et al. (2018) indicated that comparing to simulations without BC, the BC and PBL interaction slowed the O_3 growth from late morning to early afternoon somewhat before O_3 reaching its maximum value at noon due to less vertical mixing in PBL.

Studies on the feedback effects of aerosols from different emission sectors on air quality were relatively limited and mainly involved with ARB emissions and assessments of emission controls during certain major air pollution events. Jena et al. (2015) applied WRF-Chem with aerosol feedbacks and investigated O_3 and its precursors in SA due to regional ARB. Based on WRF-Chem simulations with enabling ARI and ACI, Wu et al. (2017) denoted that aerosols emitted from ARB could be mixed or/and coated with urban aerosols while being transported to cities and contributed to heavy air pollution events there, such as in Nanjing, China. The ARI effects induced by ARB aerosols on O_3 and NO_2 concentrations (-1 % and 2 %, respectively) were small compared to the contribution of precursors emitted from ARB to O_3 chemistry (40 %) in the ARB zone (Li M. et al., 2018). Pollutants emitted from natural and anthropogenic BB over Indochina affected pollution levels over SC and their ACI effects removed aerosols more efficiently than the ARI effects that could make BB aerosols last longer in the ATM (Huang et al., 2019). Gao et al. (2017a) and Zhou et al. (2019) both utilized WRF-Chem to evaluate what role the ARI effects played when dramatic emission reductions implemented during the week of Asia Pacific Economic Cooperation Summit and concluded that the ARI reduction induced by decreased emission led to 6.7-10.9 % decline in $PM_{2.5}$ concentrations in Beijing.

4.3 Human health effects

Poor air quality posts risks to human health (Brunekreef and Holgate, 2002; Manisalidis et al., 2020), therefore, in the past several decades, air quality models had been used in epidemiology related research to establish quantitative relationships between concentrations of various pollutants and burden of disease (including mortality or/and morbidity) as well as associated economic loss (Conti et al., 2017). In Asia, there were several studies that applied coupled air quality models with feedbacks to assess human health effects of air pollutants under historical and future scenarios (Conibear et al., 2018a, 2018b; Gao et al., 2017b; Gao M. et al., 2015; Ghude et al., 2016; Hong et al., 2019; Wang et al., 2017; Xing et al., 2016; Zhong et al., 2019). By applying WRF-Chem with

ARI and ACI, M. Gao et al. (2015) estimated the health and financial impacts induced by an intense air pollution event happened in the NCP area during January, 2013 and concluded that the mortality, morbidity, and financial loss over Beijing area were 690, 69070, and 253.8 million US$, respectively. Targeting the same case, Gao M. et al. (2017b) pointed out that turning on the data assimilation of surface $PM_{2.5}$ observations in WRF-Chem not only improved model simulations but also made the premature death numbers increased by 2 % in the NCP area, comparing to simulations without the $PM_{2.5}$ data assimilation. In India, WRF-Chem simulations with aerosol feedbacks and updated population data revealed that the premature (COPD related) deaths caused by $PM_{2.5}$ (O_3) were 570,000 (12,000), resulting in shortened life expectancy (3.4±1.1 years) and financial expenses (640 million US$) during 2011 (Ghude et al., 2016). Based on WRF-CMAQ simulations with ARI for 21 years (1990-2010), Xing et al. (2016) pointed out that in EA the population-weighted $PM_{2.5}$ induced mortality had an upward trend from 1990 (+3187) to 2010 (+3548) and the mean mortality caused by ARI-enhanced $PM_{2.5}$ was 3.68 times more than that decreased by ARI-reduced temperature. The same 21 year simulations also showed that from 1990 to 2010, the $PM_{2.5}$ related mortalities in EA and SA rose by 21 % and 85 %, respectively, while they declined in Europe and high-income North America by 67 % and 58 %, respectively (Wang et al., 2017). Conibear et al. (2018a) applied WRF-Chem with ARI to study how different emission sectors affected human health in India and demonstrated that the residential energy use sector played the most critical role among other sectors and could cause 511,000 premature deaths in 2014. Furthermore, Conibear et al. (2018b) investigated future $PM_{2.5}$ pollution levels as well as health impacts in India under different emission scenarios (business as usual and two emission control pathways) and deduced that the burden of disease driven by $PM_{2.5}$ and population factors (growth and aging) in 2050 increased by 75 % under the business as usual scenario but decreased by 9 % and 91 % under the International Energy Agencies New Policy Scenario and Clean Air Scenario, respectively, comparing with that in 2015. The sensitivity study using WRF-Chem with ARI under a variety of emission scenarios, population projections, and concentration-response functions (CRFs) for the years of 2008 and 2050 demonstrated that CRFs (future emission projections) were the main sources of uncertainty in the total mortality estimations related to $PM_{2.5}$ (O_3) in China (Zhong et al., 2019). Applying a suite of models, including WRF-CMAQ with ARI, climate and epidemiology, Hong et al. (2019) inferred that under Representative Concentration Pathway 4.5, the future mortalities could be 12100 and 8900 per year in China led by $PM_{2.5}$ and O_3, respectively, and the climate-driven weather extremes could add 39 % and 6 % to future mortalities due to stable atmosphere and heat waves, respectively. Ten Hoeve and Jacobson (2012) applied GATOR-GCMOM and a human exposure model to estimate the local and worldwide health effects induced by the 2011 Fukushima nuclear accident and a hypothetical one in California of US.

5 Effects of aerosol feedbacks on model performance

Even though there are a certain number of research papers using two-way coupled models to quantify the effects of aerosol feedbacks on regional meteorology and air quality in Asia, model performances impacted by considering aerosol effects varied to some extent. This section provides a summary of model performance by presenting the SI of meteorology and air quality variables as shown in Table S2. These SI were collected from the selected papers that supplying these indices and being defined as papers with SI (PSI) (listed in Tables B2-B3 of Appendix B). As aforementioned in Section 3, investigations of ACI effects were very limited and no former studies simultaneously exploring aerosol feedbacks with and without both ARI and ACI turned on. Here, we only compared the SI for simulations with and without ARI in the same study, as summarized in Appendix Tables B4-B5. It should be pointed out that all the reported evaluation results either from individual model or inter-model comparison studies were extracted and put into the Table S2.

5.1 Model performance for meteorology variables

With certain emissions, accurate simulations of meteorological elements are critical to air quality modeling and prediction (Appel et al., 2017; Bauer et al., 2015; Saylor et al., 2019; Seaman, 2000). Targeting meteorological variables, we summarized their SI and further analyzed the variations of SI on different simulated time scales and among multiple models.

5.1.1 Overall performance

Figure 3 shows the compiled statistical indicators (correlation coefficient (R) is in black, and mean bias (MB) and root mean square error (RMSE) are in blue) of T2 (℃), RH2(%) and specific humidity (SH2, g·kg^{-1}) at 2 meters, and WS10 (m·s^{-1}) from PSI (a-d), and simulations with and without ARI (marked as ARI and NO-ARI in e-h). In this figure and following figures, NP and NS are number of publications and samples with SI, respectively and summed up in Appendix Table B2. In these two tables, we also listed the NS of positive (red upward arrow) and negative (blue downward arrow) biases for the meteorological and air quality variables in parentheses in the MB column. Note that NS in Fig. 3e-h and Appendix Table B4 counted the samples of SI provided by the simulations simultaneously with and without ARI. Also, the 5th, 25th, 75th and 95th percentiles of SI are illustrated in box-and-whisker plots, and the dashed line in the box is the mean value (not median) and the circles are outliers.

The evaluations for T2 (Fig. 3a) from PSI revealed that in Asia coupled models performed rather well for temperature (mean R = 0.90) with RMSE ranging from 0.64 to 5.90 ℃, but 60 % of samples showed the tendency towards temperature underestimations (mean value of MB = -0.20 ℃) with the largest average MB (-0.31 ℃) occurring during winter months (70 samples). The underestimations of temperature had been reported not only from modeling studies by using WRF or coupled models, but also in Asia, Europe and North America (Brunner et al., 2015; Gao et al., 2019; García-Díez et al., 2013; Makar et al., 2015a; Yahya et al., 2015). The WRF simulations in China (Gao et al., 2019) and US (EPA, 2018) also showed wintertime cold biases of T2 but in Europe warm biases were reported (García-Díez et al., 2013). This temperature bias was probably related to the impacts of model resolutions (Kuik et al., 2016), urban canopies (Liao et al., 2014) and PBL schemes (Hu et al., 2013). With the ARI turned on in the coupled models, modeled temperatures (limited papers with 12 samples) were improved somewhat and the mean correlation coefficient increased from 0.93 to 0.95 and RMSE decreased slightly (Fig. 3e), but average MB of temperature was decreased from -0.98 to -1.24 ℃. In short, temperatures from PSI or simulations with/without ARI turned on agreed well with observations but were mostly underestimated, and the negative bias of T2 simulated by models with ARI turned on got worse and reasons behind it will be explained in Section 6.

Figures 3b-c illustrate that RH2 was simulated reasonably well (mean R = 0.73) and the modeled SH2 was also well correlated with observations (R varied between 0.85 and 1.00). RH2 and SH2 from more than half of samples had slightly positive and negative mean biases with average MB values of 0.4 % and -0.01 g·kg^{-1}, respectively. The overestimations of RH2 could be caused by the negative bias of T2 (Cuchiara et al., 2014). Compared with results without ARI effects, statistics of RH2 and SH2 from simulations with ARI showed better R and RMSE. However, the increased positive mean biases (average MBs of RH2 and SH2 were from 6.4 % to 7.6 % and from 0.07 g·kg^{-1} to 0.11 g·kg^{-1}, respectively) indicated that turning on ARI could cause further overprediction of humidity variables. Overall, the modeled RH2 and SH2 were in good agreement with observations with slight over- and under-estimations, respectively, and the limited studies showed that RH2 and SH2 simulated by models with ARI turned on had marginally larger positive biases relative to the results without ARI.

Compared with the correlation coefficients of T2, RH2 and SH2, mean R (0.59) of WS10 was smallest with a large fluctuation ranging from 0.14 to 0.98 (Fig. 3d). The meta-analysis also indicated that most modeled WS10 tended to be overestimated (81 % of the samples) with the average MB value of 0.79 m·s^{-1}, and the mean RMSE value was 2.76 m·s^{-1}. The general overpredictions of WS10 by WRF (Mass and Ovens, 2011) and coupled models (Gao M. et al., 2018a; Gao Y. et al., 2015) had been explained with possible reasons such as out-of-date geographical data, coarse model resolutions and lacking of better representations of urban canopy physics. The PSI with ARI effects suggested that the correlation of wind speed was slightly improved (mean R from 0.56 to 0.57) and the average RMSE and positive MB decreased by 0.003 m·s^{-1} and 0.051 m·s^{-1}, respectively (Fig. 3h). The collected SI indicated relatively poor performance of modeled WS10 (most wind speeds were overestimated) compared to T2 and humidity, but turning on ARI in coupled models could improve WS10 simulations somewhat.

Besides the SI discussed above, very limited papers reported the normalized mean error (NME) (%) of surface meteorological variables (T2, SH2, RH2 and WS10) simulated by two-way coupled models (WRF-Chem and WRF-CMAQ) in Asia, which is summarized in Appendix Table B7. The evaluations with two-way coupled models in Asia showed that the overall mean percent errors of

T2, SH2, RH2 and WS10 were 22.71%, 10.32%, 13.94%, and 51.28%, respectively. The ranges of NME (%) values were quite wide for T2 (from -0.48 to 270.20 %) and WS10 (from 0.33 to 112.28%) reported by the limited studies. Note that no NME of surface meteorological variables simulated by two-way coupled models simultaneously with and without enabling the ARI effects was mentioned in these studies.

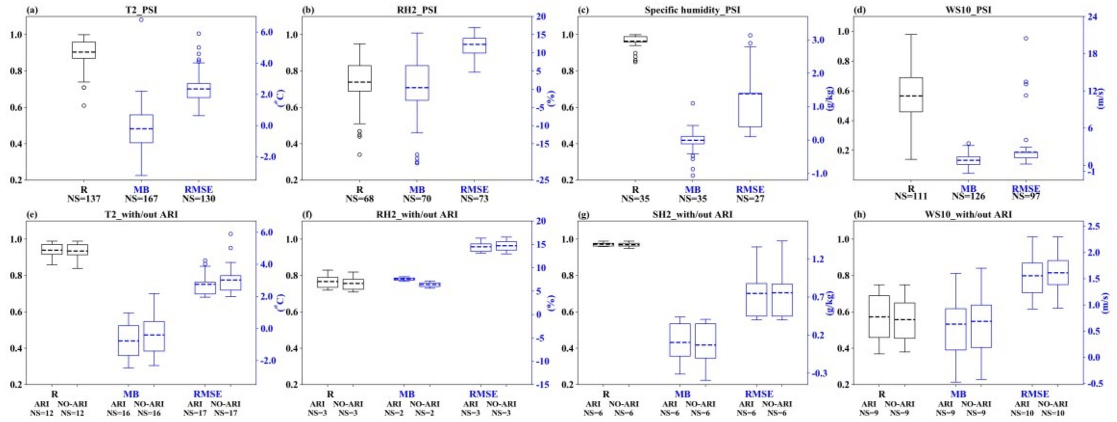

Figure 3. Quantile distributions of R, MB and RMSE for simulated surface meteorological variables by the five coupled models (WRF-Chem, WRF-CMAQ, GRAPES-CUACE, WRF-NAQPMS and GATOR-GCMOM) (a-d) and comparisons of statistical indices with/out ARI (e-h) in Asia.

5.1.2 Comparisons of SI for meteorology using different coupled models

Also, to examine how different coupled models (i.e., WRF-Chem, WRF-CMAQ, WRF-NAQPMS, GRAPES-CUACE and GATOR-GCMOM) performed in Asia with respect to meteorological variables, the SI were extracted from PSI in term of these five coupled models and displayed in Fig. 4. The SI for T2, RH2, SH2, and WS10 from WRF-NAQPMS, GRAPES-CUACE and GATOR-GCMOM simulations were missing or with rather limited samples so that the discussions here only focused on the WRF-Chem and WRF-CMAQ simulations. Moreover, the SI sample size from studies involving WRF-Chem was generally larger than that involving WRF-CMAQ, except for SH2.

As seen in Fig. 4a, the modeled T2 by both WRF-CMAQ and WRF-Chem was well correlated with observations but WRF-CMAQ (mean R = 0.95) outperformed WRF-Chem (mean R = 0.90) to some extent. On the other hand, WRF-CMAQ underestimated T2 (mean MB = -1.39 °C) but WRF-Chem slightly overestimated it (mean MB = 0.09 °C) (Fig. 4e). The RMSE of modeled T2 by both models was at the similar level with mean RMSE values of 2.51 °C and 2.31 °C by WRF-CMAQ and WRF-Chem simulations, respectively (Fig. 4i).

Both WRF-Chem and WRF-CMAQ performed better for SH2 (mean R = 0.96 and 0.97, respectively) than RH2 (mean R = 0.75 and 0.73, respectively) (Figures 4b and 4c), which might be due to the influence of temperature on RH2 (Bei et al., 2017). Also the modeled RH2 (SH2) by WRF-Chem correlated better (worsen) with observations than those by WRF-CMAQ. The mean RMSE of modeled RH2 (Fig. 4j) by WRF-Chem (11.1 %) was lower than that by WRF-CMAQ (14.3%) but the mean RMSE of modeled SH2 (Fig. 4k) by WRF-Chem (2.25 $g \cdot kg^{-1}$) higher than that by WRF-CMAQ (0.71 $g \cdot kg^{-1}$). It was seen in Figures 4f and 4d that WRF-CMAQ overestimated RH2 and SH2 (average MB were 5.30 % and 0.07 $g \cdot kg^{-1}$, respectively), and WRF-Chem underpredicted RH2 (average MB = -0.32 %) and SH2 (average MB = -0.06 $g \cdot kg^{-1}$). Generally, the modeled RH2 and SH2 were reproduced more reasonably by WRF-Chem than those by WRF-CMAQ.

The modeled WS10 by both WRF-Chem and WRF-CMAQ (Fig. 4d) correlated with observations on the same level with the mean R of 0.56. The mean RMSE of modeled WS10 by WRF-Chem and WRF-CMAQ were 1.54 $m \cdot s^{-1}$ and 2.28 $m \cdot s^{-1}$, respectively, as depicted in Fig. 4l. Both models overpredicted WS10 to some extend with average MBs of 0.55 $m \cdot s^{-1}$ (WRF-CAMQ) and 0.84 $m \cdot s^{-1}$ (WRF-Chem), respectively. These results demonstrated that overall WRF-CMAQ and WRF-Chem had similar model performance of WS10.

In general, WRF-CMAQ performed better than WRF-Chem for T2 but worse for humidity (RH2 and SH2), and both models' performance for WS10 was very similar. WRF-Chem overestimated T2, RH2 and WS10 and underestimated SH2 slightly, while WRF-CMAQ overpredicted humidity and WS10 but underpredicted T2. Compared to WRF-Chem and WRF-CMAQ, the very few SI samples indicated that for the meteorological variables excluding SH2, WRF-NAQPMS simulations matched with observations better than GRAPES-CUACE simulations but more applications and statistical analysis of these two models are needed to make this kind of comparison conclusive.

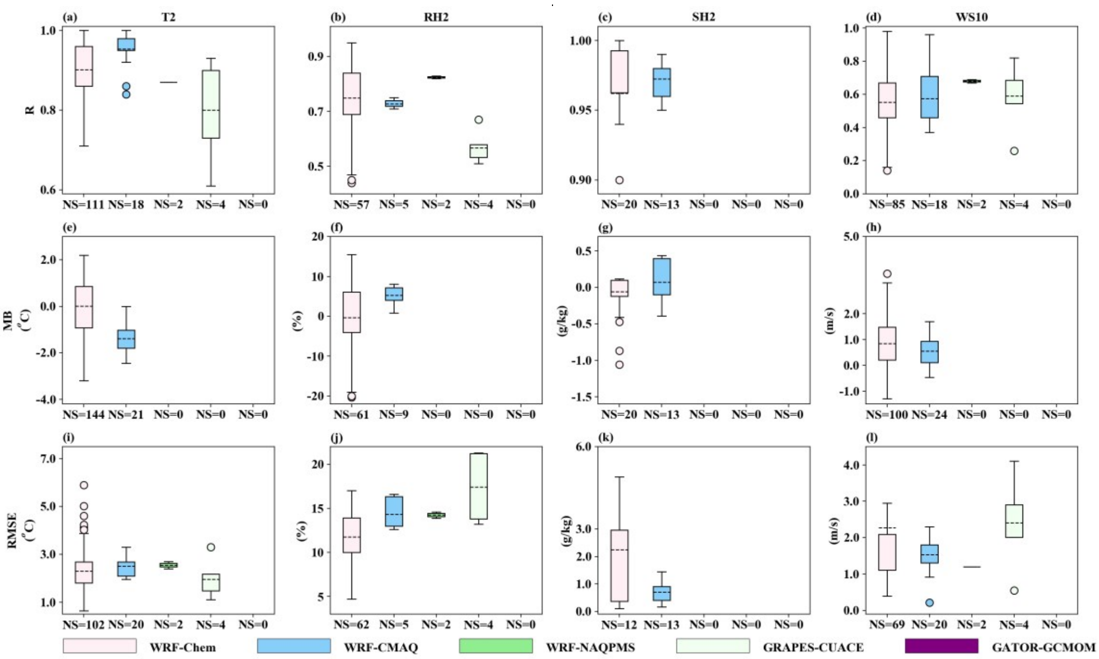

Figure 4. Quantile distributions of the statistical indices for simulated surface meteorological variables by WRF-Chem, WRF-CMAQ, GRAPES-CUACE, WRF-NAQPMS and GATOR-GCMOM in Asia.

5.2 Model performance for air quality variables

5.2.1 Overall performance

The results of the overall statistical evaluation for the online air quality simulations are presented in Figure 5, and all labels and colors indicating SI were the same as those for meteorological variables. In this figure and following figures, NP and NS are number of publications and samples with SI, respectively and summed up in Appendix Table B3. In Fig. 5a, the correlation between the simulated and observed $PM_{2.5}$ concentrations from PSI showed that in Asia coupled models performed relatively well for $PM_{2.5}$ (mean R = 0.63), but RMSE was between -87.60 and 80.90 and more than half of samples of simulated $PM_{2.5}$ were underestimated (mean MB = -2.08 $\mu g \cdot m^{-3}$). Note that NS in Fig. 5c-d and Appendix Table B5 counted the samples of SI provided by the simulations simultaneously with and without ARI. With the ARI turned on in the coupled models, modeled $PM_{2.5}$ concentrations (limited papers with 15 samples) were improved somewhat and the mean R slightly increased from 0.71 to 0.72 and mean absolute MB decreased from 4.10 to 1.33 $\mu g \cdot m^{-3}$ (Fig. 5c), but RMSE of $PM_{2.5}$ concentrations slightly increased from 35.40 to 36.20 $\mu g \cdot m^{-3}$. In short, $PM_{2.5}$ with/without ARI agreed well with observations but were mostly underestimated, and $PM_{2.5}$ bias simulated by models became overpredicted.

Compared with $PM_{2.5}$, mean R (0.59) of O_3 was relatively smaller (Fig. 5b). The statistical analysis also showed the most modeled O_3 concentrations tended to be overestimated (76 % of the samples) with the average MB value of 8.05 $\mu g \cdot m^{-3}$, and the mean RMSE value was 32.65 $\mu g \cdot m^{-3}$. The 14 PSI with ARI effects suggested that the correlation of O_3 was slightly improved (mean R from 0.58 to 0.64) and the average RMSE and MB were decreased by 15.93 $\mu g \cdot m^{-3}$ and 1.55 $\mu g \cdot m^{-3}$, respectively (Fig. 5d). The collected studies indicated relatively poor performance of modeled O_3 compared to $PM_{2.5}$, but turning on ARI in coupled models improved O_3 simulations somewhat.

In addition to the SI analyzed above and similar to the surface meteorological variables, the NME (%) of $PM_{2.5}$ and O_3 is listed in Table B7. The limited studies with WRF-Chem and WRF-CMAQ indicated that the overall mean percent errors of $PM_{2.5}$ and O_3 were 47.63% (from 29.55 to 104.70 %) and 43.03% (from 21.10 to 127.00 %), respectively. With the ARI effects enabled in WRF-Chem in different seasons over the China domain, the NME (%) of $PM_{2.5}$ increased slightly during most seasons, except during a spring month with little change (Zhang et al., 2018). Another study by Nguyen et al. (2019b) revealed that the NME (%) of $PM_{2.5}$ and O_3 simulated by WRF-CMAQ became a little worse in SEA comparing to the simulations without ARI.

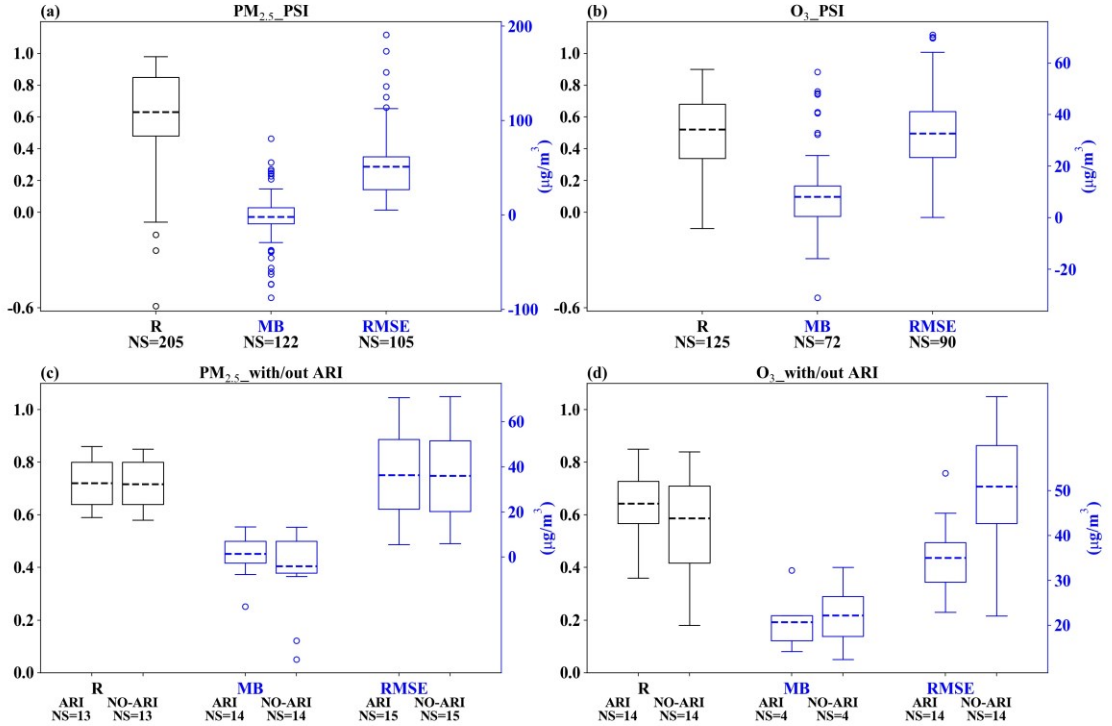

Figure 5. Quantile distributions of statistical indices for simulated $PM_{2.5}$ and O_3 (a-b) by the five two-way coupled models (WRF-Chem, WRF-CMAQ, GRAPES-CUACE, WRF-NAQPMS and GATOR-GCMOM) and comparisons of statistical indices with/out ARI (c-d) in Asia.

5.2.2 Comparisons of SI for air quality using different coupled models

Figure 6 showed the SI for $PM_{2.5}$ and O_3 from different coupled models, and only WRF-Chem and WRF-CMAQ simulations were discussed for the same reason as in Section 5.1.2. The modeled $PM_{2.5}$ by WRF-CMAQ (mean R = 0.69) outperformed WRF-Chem (mean R = 0.62) to some extent (Fig. 6a) and the RMSE of modeled $PM_{2.5}$ by WRF-CMAQ (33.24 $\mu g \cdot m^{-3}$) was smaller than that by WRF-Chem (56.16 $\mu g \cdot m^{-3}$). With respect to MB, WRF-CMAQ overestimated $PM_{2.5}$ (mean MB = +1.60 $\mu g \cdot m^{-3}$) but WRF-Chem slightly underestimated it (mean R = -3.12 $\mu g \cdot m^{-3}$) (Fig. 6c). Figure 6b showed that the modeled O_3 by WRF-CMAQ (0.60) correlated better with observations than those by WRF-Chem (0.47), but the mean RMSE of modeled O_3 (Fig. 6f) by WRF-Chem (27.13 $\mu g \cdot m^{-3}$) was lower than that by WRF-CMAQ (35.19 $\mu g \cdot m^{-3}$). It was seen in Figures 6d that both WRF-CMAQ and WRF-Chem overestimated O_3, with mean MBs as 11.98 and 7.21 $\mu g \cdot m^{-3}$, respectively. Generally, the modeled $PM_{2.5}$ and O_3 were reproduced more reasonably by WRF-CMAQ than by WRF-Chem, even though there were much more samples available from WRF-Chem simulations than WRF-CMAQ simulations.

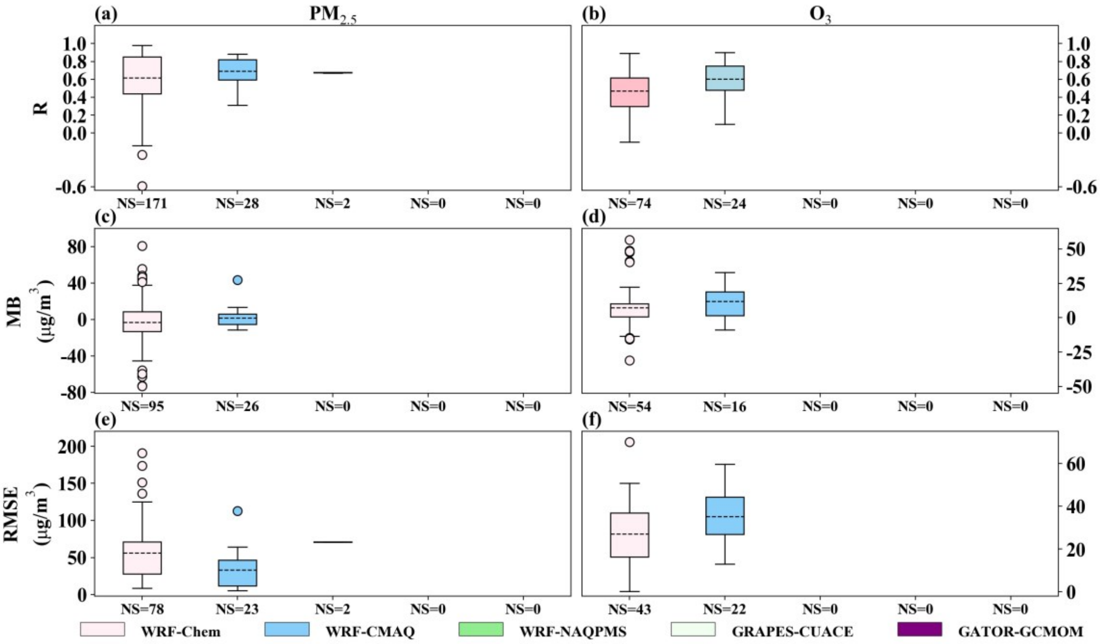

Figure 6. Quantile distributions of R, MB and RMSE of $PM_{2.5}$ and O_3 simulated by WRF-Chem, WRF-CMAQ, GRAPES-CUACE, WRF-NAQPMS and GATOR-GCMOM in Asia.

6 Impacts of aerosol feedbacks in Asia

Aerosol feedbacks not only impact the performances of two-way coupled models but also the simulated meteorological and air quality variables to a certain extent. In this section, we collected and quantified the variations (Table S3) of these variables induced by ARI or/and ACI from the modeling studies in Asia. Due to limited sample sizes in the collected papers, the target variables only include radiative forcing, surface meteorological parameters (T2, RH2, SH2 and WS10), PBLH, cloud, precipitation, and $PM_{2.5}$ and gaseous pollutants.

6.1 Impacts of aerosol feedbacks on meteorology

6.1.1 Radiative forcing

With regard to radiative forcing, most studies with two-way coupled models in Asia had focused on the effects of dust aerosols (Dust), BC emitted from ARB (ARB_BC) and anthropogenic sources (Anthro_BC), and total anthropogenic aerosols (Anthro). Figure 7 presents the variations of simulated SWRF and LWRF at the bottom (BOT) and TOA and in the ATM due to aerosol feedbacks, and detailed information of these variations are compiled in Table S5. In this figure, the color bars show the range of radiative forcing variations and the black tick marks inside the color bars represent these variations extracted from all the collected papers. It should be noted that in this figure all the radiative forcing variations were plotted regardless of temporal resolutions of data reporting and simulation durations. Apparently in Asia, most studies targeted the SWRF variations induced by anthropogenic aerosols at the BOT that exhibited the largest differences ranging from -140.00 to -0.45 $W\cdot m^{-2}$, with the most variations (88 % of samples) concentrated in the range of -50.00 to -0.45 $W\cdot m^{-2}$. The SWRF variations due to anthropogenic aerosols in the ATM and at the TOA were -2.00 to +120.00 $W\cdot m^{-2}$ and -6.50 to 20.00 $W\cdot m^{-2}$, respectively. There were much less studies reported LWRF variations caused by anthropogenic aerosols, which ranged from -10.00 to +5.78 $W\cdot m^{-2}$, -1.91 to +3.94 $W\cdot m^{-2}$, and -4.26 to +1.21 $W\cdot m^{-2}$ at the BOT and TOA, and in the ATM, respectively.

Considering BC from anthropogenic sources and ARB, they both led to positive SWRF at the TOA (with mean values of 2.69 and 7.55 $W\cdot m^{-2}$, respectively) and in the ATM (with mean values of 11.70 and 25.45 $W\cdot m^{-2}$, respectively) but negative SWRF at the BOT (with mean values of -18.43 and -14.39 $W\cdot m^{-2}$, respectively). The responses of LWRF to Anthro_BC and ARB_BC at the BOT (in the ATM) on average were 4.01 and 0.72 $W\cdot m^{-2}$ (-1.89 and -3.24 $W\cdot m^{-2}$), respectively, and weak at the TOA (+0.92 and -0.53 $W\cdot m^{-2}$, respectively). The SWRF variations induced by dust were in the range of -233.00 to -1.94 $W\cdot m^{-2}$ and -140.00 to +25.70 $W\cdot m^{-2}$, and +1.44 to +164.80 $W\cdot m^{-2}$ at the BOT and TOA, and in the ATM, respectively. The LWRF variations caused by dust were the largest (with mean values of 22.83 W·m^{-2} and +5.20 W·m^{-2}, and -22.12 W·m^{-2} at the BOT and TOA, and in the ATM, respectively), comparing to the ones caused by anthropogenic aerosols and BC aerosols from anthropogenic sources and ARB.

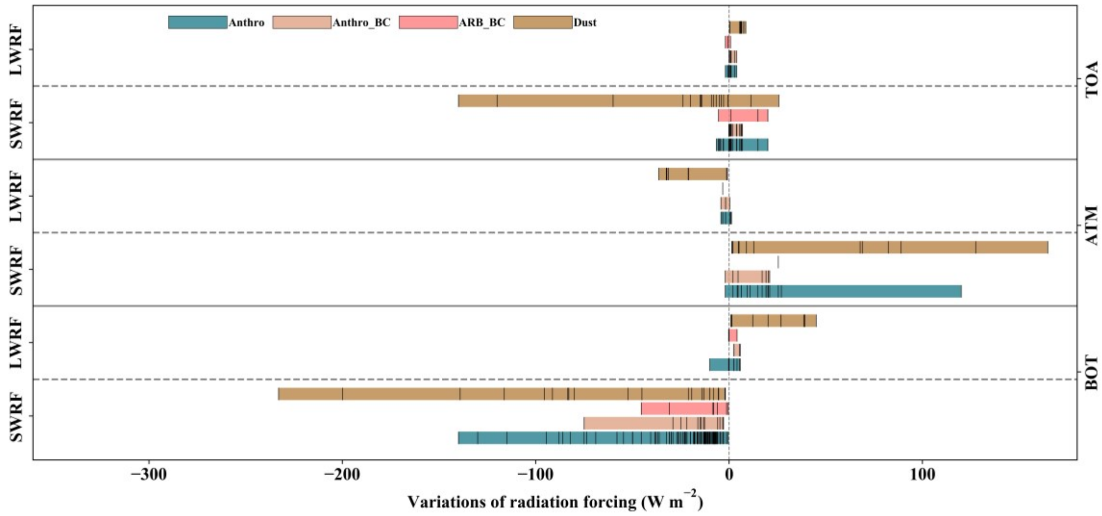

Figure 7. Variations of shortwave and longwave radiative forcing (SWRF and LWRF) simulated by two-way coupled models (WRF-Chem, WRF-CMAQ, GRAPES-CUACE, WRF-NAQPMS and GATOR-GCMOM) with aerosol feedbacks at the bottom and top of atmosphere (BOT and TOA), and in the atmosphere (ATM) in Asia.

As shown in Fig. 7, SWRF variations at the BOT caused by total aerosols (sum of Anthro, Anthro_BC, ARB_BC and Dust) had been widely assessed in Asia. Therefore, we further analyzed their spatiotemporal distributions and inter-regional differences, which are displayed in Fig. 8. Figure 8a presents the SWRF variations over different areas of Asia (the acronyms used in Fig. 8 are listed in Appendix Table B1) at different time scales. In Asia, almost 41 % of the selected papers investigated SWRF towards its monthly variations, 36 % towards its hourly and daily variations, and 23 % towards its seasonal and yearly variations. Most studies reported aerosol-induced SWRF variations were primarily conducted in NCP, EA, China, and India. At the hourly scale, the range of SWRF decreases was from -350.00 to -5.90 W·m^{-2} (mean value of -106.92 W·m^{-2}) during typical pollution episodes, and significant variations occurred in EA. The daily and monthly mean SWRF reductions varied from -73.71 to -5.58 W·m^{-2} and -82.20 to -0.45 W·m^{-2}, respectively, with relative large perturbations in NCP. At the seasonal and yearly scales, the SWRF changes ranged from -22.54 to -3.30 W·m^{-2} and -30.00 to -2.90 W·m^{-2} with mean value of -11.28 and -11.82 W·m^{-2}, respectively, with EA as the most researched area.

To identify the differences of aerosol-induced SWRF variations between high- (Asia) and low-polluted regions (Europe and North America), their inter-regional comparisons are depicted in Fig. 8b. This figure does not include information about temporal resolutions of data reporting and durations of model simulations with ARI or/and ACI, but intends to delineate the range of SWRF changes due to aerosol feedbacks. The SWRF variations fluctuated from -233.00 to -0.45 W·m^{-2}, -100.00 to -1.00 W·m^{-2}, and -600.00 to -1.00 W·m^{-2} in Asia, Europe, and North America, respectively. It should be pointed out that the two extreme values were caused by dust (-233.00 W·m^{-2}) in Asia and wildfire (-600.00 W·m^{-2}) in North America. Overall, the median value of SWRF reductions due to ARI or/and ACI in Asia (-15.92 W·m^{-2}) was larger than those in North America (-10.50 W·m^{-2}) and Europe (-7.00 W·m^{-2}).

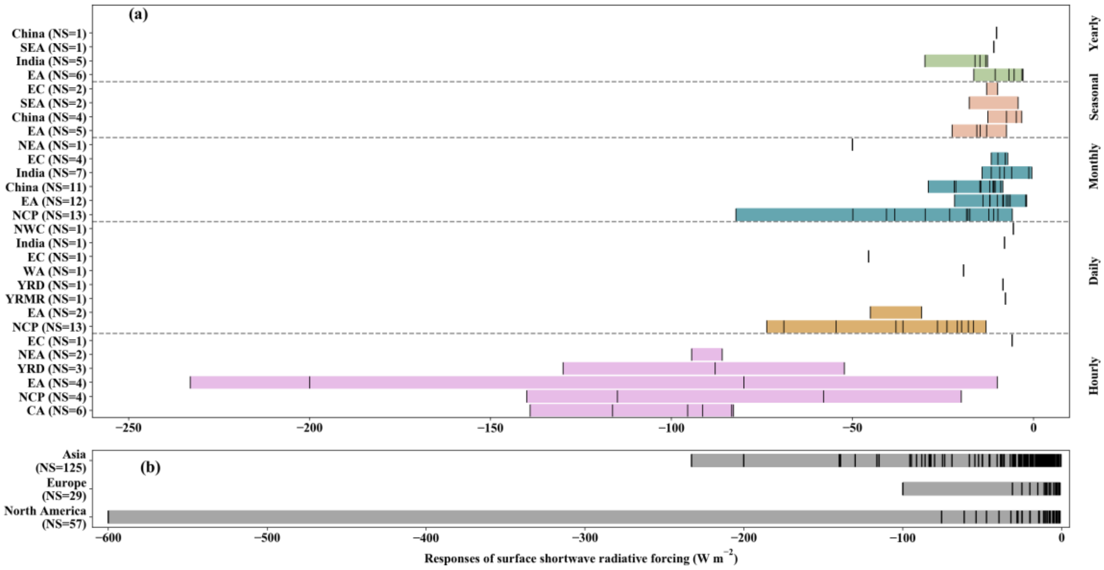

Figure 8. Responses of shortwave radiation forcing to aerosol feedbacks in different areas/periods in Asia (a) and the inter-regional comparisons of its variations in Asia, Europe and North America (b).

6.1.2 Temperature, wind speed, humidity and PBLH

The impact of aerosols on radiation can influence energy balance, which eventually alter other meteorological variables. The summary of aerosol-induced variations of T2, WS10, RH2, SH2 and PBLH in different regions of Asia as well as at different temporal scales are provided in Table 6. In this table, the minimum and maximum values were collected from the corresponding papers and the mean values were calculated with adding all the variations from these papers and then divided by the number of samples.

Overall, aerosol effects led to decreases of T2, WS10 and PBLH with average changes of -0.65 °C, -0.13 m·s^{-1} and -60.70 m, respectively, and increases of humidity (mean ΔRH2 = 2.56 %) in most regions of Asia. On average, the hourly aerosol-induced changes of surface meteorological variables (T2, WS10 and RH2) and PBLH were the largest among the different time scales. At the hourly time scale, the mean variations of T2, WS10, RH2 and PBLH due to ARI or/and ACI were -1.85 °C, -0.32 m·s^{-1}, 4.60 % and -165.84 m, respectively, and their absolute maximum values in EC, YRD, NCP and NCP, respectively. Compared to variations at the hourly time scale, smaller daily variations of T2, WS10, RH2 and PBLH were caused by aerosol effects, and their mean values were -0.63 °C, -0.15 m·s^{-1}, +2.89 % and -34.61 m, respectively. The largest daily variations of T2, WS10, RH2 and PBLH occurred in NCP, EC, EC and SEC, respectively. For other time scales (monthly, seasonal and yearly), the respective mean variations of T2, RH2 and PBLH induced by aerosol effects were comparable. However, the WS10 perturbations at the monthly time scale were about two to three times higher than those at the seasonal and yearly time scales. High variations at the monthly, seasonal and yearly time scales were reported in NCP (T2, RH2 and PBLH), EA (T2, WS10 and PBLH) and PRD (T2 and PBLH), respectively. In addition, comparing to T2 and PBLH, the aerosol-induced variations of WS10 and humidity were less revealed.

Table 6. Summary of variations of surface meteorological variables and planetary boundary layer height (PBLH) caused by aerosol feedbacks simulated by two-way coupled models (WRF-Chem, WRF-CMAQ, GRAPES-CUACE, WRF-NAQPMS and GATOR-GCMOM) in different regions of Asia and at different temporal scales.

Region	Time scale	ΔT2 [mean] (°C)	ΔWS10 [mean] (m·s^{-1})	ΔRH2/SH2 [mean]	ΔPBLH [mean] (m)
EC	hours	-8.00 to -0.20 [-2.68]			-300.00 to -50.00 [-175.00]
EA	hours	-3.00 to -2.00 [-2.50]			
YRD	hours	-1.40 to -1.00 [-1.15]	-0.80 to -0.10 [-0.41]		-276.00 to -29.90 [-105.42]
NCP	hours	-2.80 to -0.20 [-1.05]	-0.30 to -0.10 [-0.23]	1.00 % to 12.00 % [4.60 %]	-287.20 to -147.00 [-217.10]
Hourly mean		-1.85	-0.32	4.60%	-165.84
NCP	days	-2.00 to -0.10 [-0.88]	-0.4 to -0.01 [-0.17]	0.51 % to 4.10 % [2.52 %]	-111.40 to -10.00 [-49.07]

EC	days	-0.94 to -0.65 [-0.79]	-0.52 to -0.37 [-0.45]	1.92 % to 9.75 % [5.84 %]	
India	days	-1.60 to 0.10 [-0.75]			
SEC	days	-1.38 to -0.18 [-0.70]	-0.07 to 0.05 [-0.023]	-0.37 % to 6.57 % [2.63 %]	-84.1 to -27.55 [-53.62]
NEA	days	-0.52	-0.08		-46.39
MRYR	days	-0.16	-0.01	0.56 %	-16.46
India	days				-6.90
Daily mean		-0.63	-0.15	2.89 %	-34.61
India	months	-0.45			
NCP	months	-1.30 to -0.06 [-0.43]		1.30 % to 4.70 % [2.53 %]	-109.00 to -5.48 [-36.01]
NEA	months	-0.30	-0.10		-50.00
PRD	months	-0.60 to 0.13 [-0.16]			
EA	months	-0.45 to -0.03 [-0.13]			-35.70 to -13.00 [-24.35]
China	months	-0.89 to 0.60 [-0.12]			-66.60 to -2.30 [-25.67]
EC	months	-0.30 to -0.05 [-0.11]			-13.10 to -6.20 [-9.65]
Monthly mean		-0.24	-0.10	2.53 %	-29.13
EA	seasons	-0.58 to -0.30 [-0.40]	-0.05 to -0.02 [-0.035]		-64.62 to -30.70 [-43.27]
SEA	seasons	-0.39 to -0.03 [-0.21]	-0.06 to -0.01 [-0.035]		-48.33 to -6.71 [-27.52]
Seasonal mean		-0.31	-0.035		-34.61
PRD	years	-0.27			-45.00
TP	years	-0.24			
SEA	years	-0.21	-0.03		-27.25
EA	years		-0.03	0.13 $g\cdot kg^{-1}$	-46.47 to -45.00 [-45.74]
EC	years		-0.014	0.21 %	
Yearly mean		-0.24	-0.025	0.21 %	-39.33

6.1.3 Cloud and precipitation

In the included publications, only a few papers focusing on the effects of aerosol feedbacks on cloud properties (cloud fraction, LWP, ice water path (IWP), CDNC and cloud effective radius) and precipitation characteristics (amount, spatial distribution, peak occurrence and onset time) using two-way coupled models in Asia, as shown in Table 7. In this table, the abbreviations representing aerosol emission sources (Dust, ARB_BC, Anthro_BC, and Anthro) and regions in Asia are defined in Appendix Table B1. The plus and minus signs indicate increase and decrease, respectively.

The variations of cloud properties and precipitation characteristics induced by ARI or/and ACI are rather complex and not uniform in different parts of Asia and time periods. BC from both ARB and anthropogenic sources reduced cloud fraction through ARI and both ARI and ACI in several areas in China. ARI or/and ACI induced by anthropogenic aerosols could increase or decrease cloud fraction and affect cloud fraction differently in various atmospheric layers and time periods. Considering EA and subareas in China, anthropogenic aerosols tended to increase LWP through ARI and ACI as well as ACI alone but decrease LWP in some areas of SC (ARI and ACI) at noon and in afternoon during summertime and NC (ACI) in winter. ARI and ACI induced by anthropogenic BC aerosols had negative effects on LWP except at daytime in CC. Dust aerosols increased both LWP and IWP through ACI in EA, which was reported only by one study. The increase (decrease) of CDNC caused by the ARI and ACI effects of anthropogenic (anthropogenic BC) aerosols in EC during summertime was reported. Through ACI, anthropogenic aerosols affected CDNC positively in EA and China. Compared to anthropogenic aerosols, dust aerosols could have much larger positive impacts on CDNC via ACI in springtime over EA. The ACI effects of anthropogenic aerosols reduced cloud effective radius over China (January) and EA (July).

Among all the variables describing cloud properties and precipitation characteristics, the variations of precipitation amount were studied the most using two-way coupled models in Asia. How turning on ARI or/and ACI in coupled models can change precipitation amount is not unidirectional and depends on many factors, including different aerosol sources, areas, emission levels, atmospheric humidity, precipitation types, seasons, and time of a day. Under the high emission levels as well as at slightly different humidity levels of RH > 85 % with increasing emissions, the ACI effects of anthropogenic aerosols induced precipitation increase in the MRYR area of China. Over the same area, precipitation decreased due to the ACI effects of anthropogenic aerosols with the low emission levels and RH < 80 %. In PRD, wintertime precipitation was enhanced by the ACI effects of anthropogenic aerosols but inhibited by ARI. In SK, summertime precipitation was both enhanced and inhabited by the ACI and ARI effects of anthropogenic aerosols. In locations upwind (downwind) of Beijing, rainfall amount was raised (lowered) by the ARI effects of anthropogenic aerosols but lowered (raised) by ACI. Both ARI and ACI induced by anthropogenic aerosols had positive impacts on total, convective, and stratiform rain in India during the summer season and the increase of convective rain was larger than those of stratiform. Summertime precipitation amounts could be enhanced or inhibited at various subareas inside simulation domains over India, China, and Korea and during day- or night-time due to ARI and ACI of anthropogenic aerosols. Over China, dust-induced ACI decreased (increased) springtime precipitation in CC (western part of NC), and over India, dust aerosols from local sources and ME had positive impacts on total, convective, and stratiform rain through ARI and ACI. Simulations in India also revealed that precipitation could be increased in some subareas but decreased in another and absorptive (non-absorptive) dust enhanced (inhibited) summertime precipitation via ARI and ACI. The ARI (ACI) effects of BC from ARB caused precipitation reduction (increase) in SEC but CAs emitted from ARB (ARB_CAs) caused rainfall enhancement in Myanmmar. During pre-monsoon (monsoon) season, ARI induced by anthropogenic BC could lead to +42 % (-5 to -8 %) variations of precipitation in NEI (SI). Considering both ARI and ACI effects, BC from ARB and sea salt aerosols enhanced or inhibited precipitation in different parts of India and BC from anthropogenic sources enhanced (inhibited) nighttime (daytime) rainfall in CC (NC and SC) at the rate of +1 to +4 $mm \cdot day^{-1}$ (-2 to -6 $mm \cdot day^{-1}$) during summer season. With respect to spatial variations, 6.5 % larger rainfall area in PRD was caused by ARI and ACI effects under 50 % reduced anthropogenic emissions. ACI induced by anthropogenic aerosols tended to delay the peak occurrence time and onset time of precipitation by one to nine hours in China and South Korea.

Table 7. Summary of changes of cloud properties and precipitation characteristics due to aerosol feedbacks simulated by two-way coupled models (WRF-Chem, WRF-CMAQ, GRAPES-CUACE, WRF-NAQPMS and GATOR-GCMOM) in Asia.

	Variables	Variations (aerosol effects)	Simulation time period	Regions	References
Cloud properties	Cloud fraction	-7 % low-level cloud (ARB_BC ARI)	Apr., 2013	SEC	Huang et al., 2019
		+0.03 to +0.08 below 850 hPa and at 750 hPa (Anthro ARI & ACI), esp. at early morning and nighttime	Aug., 2008	EC	Gao and Zhang, 2018
		Max -0.06 between 750 hPa and 850 hPa (Anthro ARI & ACI), esp. in afternoon and evening	Aug., 2008	CC	Gao and Zhang, 2018
		-0.02 to -0.06 below 750 hPa (Anthro_BC ARI & ACI), esp. in afternoon	Aug., 2008	SC & NC	Gao and Zhang, 2018
		-0.04 to -0.06 between 750 hPa and 850 hPa (Anthro_BC ARI & ACI), esp. in afternoon	Aug., 2008	CC	Gao and Zhang, 2018
		-6.7 % to +3.8 % (Anthro ARI)	Jun. 6-9 & Jun. 11-14, 2015	SK	Park et al., 2018
		+22.7 % (Anthro ACI)	Jun. 6-9 & Jun. 11-14, 2015	SK	Park et al., 2018
		-0.03 % low-, -0.54 % middle- and -0.58 % high-level cloud (Anthro ACI)	2008 to 2012	PRD	Liu Z. et al., 2018
	LWP	+5 to +50 $g \cdot m^{-2}$ (Anthro ARI & ACI)	Aug., 2008	EC	Gao and Zhang, 2018
		+10 to +20 $g \cdot m^{-2}$ (Anthro_BC ARI & ACI) at daytime	Aug., 2008	CC	Gao and Zhang, 2018
		-5 to -40 $g \cdot m^{-2}$ (Anthro ARI & ACI) at noon and in afternoon	Aug., 2008	Part of SC	Gao and Zhang, 2018
		-2 to -20 $g \cdot m^{-2}$ (Anthro_BC ARI & ACI)	Aug., 2008	SC	Gao and Zhang, 2018
		-2 to -30 $g \cdot m^{-2}$ (Anthro_BC ARI & ACI)	Aug., 2008	NC	Gao and Zhang, 2018
		Max+18 $g \cdot m^{-2}$ (Dust ACI)	Mar.-May., 2010	EA	Wang et al., 2018
		+40 to +60 $g \cdot m^{-2}$ (Anthro ACI)	Jan., 2008	SC	Gao et al., 2012
		+40 $g \cdot m^{-2}$ (Anthro ACI)	Jan., 2008	CC	Gao et al., 2012
		Less than +5 g·m-2 or -5 $g \cdot m^{-2}$ (Anthro ACI)	Jan., 2008	NC	Gao et al., 2012
		+30 to +50 $g \cdot m^{-2}$ (Anthro ACI)	Jul., 2008	EA	Gao et al., 2012
	IWP	+5 to +10 $g \cdot m^{-2}$ (Dust ACI)	Mar. 17-Apr. 30, 2012	EA	Su and Fung, 2018a
	CDNC	+20 to +160 cm^{-3} (Anthro ARI & ACI)	Aug., 2008	EC	Gao and Zhang, 2018

		-5 to -60 cm^{-3} (Anthro_BC ARI & ACI)	Aug., 2008	EC	Gao and Zhang, 2018
		Max +10500 cm-3 (Dust ACI)	Mar.-May., 2010	EA	Wang et al., 2018
		+650 cm-3 (Anthro ACI)	Jan., 2008	EC	Gao et al., 2012
		+400 cm-3 (Anthro ACI)	Jan., 2008	CC & SWC	Gao et al., 2012
		Less than +200 cm-3 (Anthro ACI)	Jan., 2008	NC	Gao et al., 2012
		+250 to +400 cm-3 (Anthro ACI)	Jul., 2008	EA	Gao et al., 2012
	Cloud effective radius	More than -4 µm (Anthro ACI)	Jan., 2008	SWC, CC & SEC	Gao et al., 2012
		More than -2 µm (Anthro ACI)	Jan., 2008	NC	Gao et al., 2012
		-3 µm (Anthro ACI)	Jul., 2008	EA	Gao et al., 2012
		Enhancement/inhibition of precip. due to high/low Anthro emissions, ACI inhibited (enhanced) precip. at RH < 80 % (> 85 %) with increasing Anthro emissions	Jun. 18-19, 2018	MRYR	Bai et al., 2020
		-4.72 mm (Anthro ARI) and +33.7 mm (Anthro ACI)	Dec. 14-16, 2013	PRD	Liu Z. et al., 2020
		+2 to +5 % (ARB CAs ARI)	Mar.-Apr.,	Myanmar	Singh et al., 2020
		-1.09 mm·day^{-1} (ARB_BC ARI)	Apr., 2013	SEC	Huang et al., 2019
		+0.49 mm·day^{-1} (ARB_BC ACI)	Apr., 2013	SEC	Huang et al., 2019
		-0 to -4 mm·day^{-1} (Anthro ARI & ACI)	Jun.-Sep., 2010	Indus basin & eastern IGP	Kedia et al., 2019b
		+1 to +3 mm·day^{-1} non-convective rain (Anthro ARI & ACI)	Jun.-Sep., 2010	WG of India	Kedia et al., 2019b
		+5 mm·day^{-1} non-convective rain (Anthro ARI & ACI)	Jun.-Sep., 2010	NEI	Kedia et al., 2019b
		Increase of total rain (Dust ARI & ACI)	Jun.-Sep., 2010	NI, CI, WG, NEI & central IGP	Kedia et al., 2019b
		Decrease of total rain (Dust ARI & ACI)	Jun.-Sep., 2010	NWI & SPI	Kedia et al., 2019b
		Decrease of total rain (ARB_BC ARI & ACI)	Jun.-Sep., 2010	WG, SPI, NWI, EI & NEI	Kedia et al., 2019b
		Increase of total rain (ARB_BC ARI & ACI)	Jun.-Sep., 2010	CI, Central IGP & EPI	Kedia et al., 2019b
		Decrease of total rain (Sea salt ARI & ACI)	Jun.-Sep., 2010	EPI, WPI, CPI & SPI	Kedia et al., 2019b
		Increase of total rain (Sea salt ARI & ACI)	Jun.-Sep., 2010	NCI & central IGP	Kedia et al., 2019b
		-20 to -200mm (Anthro ARI & ACI)	Aug., 2008	SC & NC	Gao and Zhang, 2018
Precipitation (precip.)	Amount	+20 to +100 mm (Anthro_BC ARI & ACI)	Aug., 2008	CC	Gao and Zhang, 2018
		+1 to +4 mm·day^{-1} nighttime precip. (ARI & ACI of Anthro or Anthro_BC)	Aug., 2008	CC	Gao and Zhang, 2018
		-2 to -6 mm·day^{-1} daytime precip. (ARI & ACI of Anthro or Anthro_BC)	Aug., 2008	NC	Gao and Zhang, 2018
		-2 to -4 mm·day^{-1} daytime precip. (Anthro ARI & ACI)	Aug., 2008	SC	Gao and Zhang, 2018
		-2 to -6 mm·day^{-1} daytime precip. (Anthro_BC ARI & ACI)	Aug., 2008	SC	Gao and Zhang, 2018
		-54.6 to +24.1 mm (Anthro ARI)	Jun. 6-9, 2015	SK	Park et al., 2018
		-23.8 to +24.0 mm (Anthro ACI)	Jun. 6-9, 2015	SK	Park et al., 2018
		-63.2 to +27.1 mm (Anthro ARI & ACI)	Jun. 6-9, 2015	SK	Park et al., 2018
		Min -7.0 mm (Anthro ARI)	Jun. 11-14, 2015	SK	Park et al., 2018
		Min -36.6 mm (Anthro ACI)	Jun. 11-14, 2015	SK	Park et al., 2018
		+42 % (Anthro_BC ARI) during pre-monsoon season	Mar.-May., 2010	NEI	Soni et al., 2018
		-5 to -8 % (Anthro_BC ARI) during monsoon season	Jun.-Sep., 2010	SI	Soni et al., 2018
		+1 mm·day^{-1} precip. (Dust ACI)	Mar. 17-Apr. 30, 2012	Western part of NC	Su and Fung, 2018b
		-1 mm·day^{-1} precip. (Dust ACI)	Mar. 17-Apr. 30, 2012	CC	Su and Fung, 2018b
		+0.95 mm·day^{-1} precip. (absorptive Dust ARI & ACI)	Jun.-Aug., 2008	India	Jin et al., 2016a
		-0.4 mm·day^{-1} precip. (non-absorptive Dust ARI & ACI)	Jun.-Aug., 2008	India	Jin et al., 2016a
		+0.44 mm·day^{-1} total precip. (Dust ARI & ACI over whole study domain)	Jun.-Aug., 2008	India	Jin et al., 2016b

	+0.34 mm·day^{-1} total precip. (Dust ARI & ACI from ME)	Jun.-Aug., 2008	India	Jin et al., 2016b
	+0.31 mm·day^{-1} total precip. (Anthro ARI & ACI over whole study domain)	Jun.-Aug., 2008	India	Jin et al., 2016b
	+0.32 mm·day^{-1} convective precip. (Dust ARI & ACI over whole study domain)	Jun.-Aug., 2008	India	Jin et al., 2016b
	+0.24 mm·day^{-1} convective precip. (ARI & ACI of Dust from ME)	Jun.-Aug., 2008	India	Jin et al., 2016b
	+0.20 mm·day^{-1} convective precip. (Anthro ARI & ACI over whole study domain)	Jun.-Aug., 2008	India	Jin et al., 2016b
	+0.12 mm·day^{-1} stratiform precip. (Dust ARI & ACI over whole study domain)	Jun.-Aug., 2008	India	Jin et al., 2016b
	+0.10 mm·day^{-1} stratiform precip. (ARI & ACI of Dust from ME)	Jun.-Aug., 2008	India	Jin et al., 2016b
	+0.11 mm·day^{-1} stratiform precip. (Anthro ARI & ACI over whole study domain)	Jun.-Aug., 2008	India	Jin et al., 2016b
	-48.29 %/+24.87 % precip. in downwind/upwind regions (Anthro ARI)	Jun. 27-28, 2008	Beijing	Zhong et al. 2015
	+33.26 % /-4.64 % precip. in downwind/upwind regions (Anthro ACI)	Jun. 27-28, 2008	Beijing	Zhong et al. 2015
	+0.44 mm·day^{-1} precip. (Dust ARI & ACI)	Jun. 1-Aug. 31, 2008	India	Jin et al., 2015
Spatial variation	+6.5 % precip. area (ARI & ACI) with 50% Anthro emissions	Jun. 9-12, 2017	YRD	Liu C. et al., 2019
Peak occurrence time	1 to 2h delay (Anthro ACI)	Jun. 18-19, 2018	MRYR	Bai et al., 2020
	1h delay (ARI & ACI) with 50% Anthro emissions	Jun. 9-12, 2017	YRD	Liu C. et al., 2019
	9h delay (Anthro ACI)	Jun. 7, 2015	Gosan, SK	Park et al., 2018
	4h delay (Anthro ACI)	Jun. 7, 2015	Jinju, SK	Park et al., 2018
Onset time	9h delay (Anthro ACI)	Jun. 7, 2015	Gosan, SK	Park et al., 2018
	2h delay (Anthro ACI)	Jun. 7, 2015	Jinju, SK	Park et al., 2018

6.2 Impacts of aerosol feedbacks on air quality

Aerosol effects not only gave rise to changes in meteorological variables but also air quality. Table 8 (the minimum, maximum and mean values were defined in the same way as in Table 6) summarizes the variations of atmospheric pollutant concentrations induced by aerosol effects in different regions of Asia and at different time scales. In Asia, most modeling studies with coupled models targeted the impacts of aerosol feedbacks on surface $PM_{2.5}$ and O_3 concentrations, with only few focusing on other gaseous pollutants.

Simulation results showed that turning on aerosol feedbacks in coupled models generally made $PM_{2.5}$ concentrations increased in different regions of Asia at various time scales, which stemmed from decrease of shortwave radiation, T2, WS10 and PBLH and increase of RH2. Some studies did show negative impacts of aerosol effects on hourly, daily, and seasonal $PM_{2.5}$ at some areas that could be attributed to ACI effects, changes in transport and dispersion patterns, reductions in humidity levels and secondary aerosol formations (Zhang B. et al., 2015; Zhan et al., 2017; Yang et al., 2017; Wang K. et al., 2018). Similar to the perturbations of surface meteorological variables due to aerosol effects, the hourly $PM_{2.5}$ variations and the range were the largest compared to those at other time scales. The largest $PM_{2.5}$ increases were reported in NCP, SEC, EA, SEA and PRD at the hourly, daily, monthly, seasonal and yearly time scales with average values of 23.48 μg·m^{-3}, 14.73 μg·m^{-3}, 16.50 μg·m^{-3}, 1.12 μg·m^{-3} and 2.90 μg·m^{-3}, respectively.

In addition to $PM_{2.5}$, gaseous pollutants (O_3, NO_2, SO_2, CO and NH_3) are impacted by ARI or/and ACI effects as well. As shown in Table 8, general reductions of ozone concentrations were reported in Asia across all the modeling domains and time scales based on coupled models' simulations. However, the influences of aerosol feedbacks on atmospheric dynamics and stability, and photochemistry (photolysis rate and ozone formation regimes) could make ozone concentrations increase somewhat in summer months or during wet season (Jung et al., 2019; Nguyen et al., 2019b; Xing et al., 2017). The largest hourly, daily, monthly, seasonal, and annual variations of O_3 occurred in YRD (-32.80 μg·m^{-3}), EC (-5.97 μg·m^{-3}), China (-23.90 μg·m^{-3}), EA (-4.48 μg·m^{-3}) and EA (-2.76 μg·m^{-3}), respectively. Along with reduced O_3 due to ARI or/and ACI, NO_2 concentrations were enhanced with average changes of +12.30 μg·m^{-3} (YRD) at the hourly scale and +0.66 μg·m^{-3} (EA) at both the seasonal and yearly scales, which could be attributed to slower photochemical reactions, strengthened atmospheric stability and O_3 titration (Nguyen et al., 2019b). Regarding other gaseous pollutants, limited studies pointed out daily and annual SO_2 concentrations increased in NEA and

EA due to lower PBLH induced by the ARI effects of anthropogenic aerosols (Jung et al.,2019; Nguyen et al., 2019b). The seasonal SO_2 reduction was rather large, which related to higher PBLH induced by the ACI effects of dust aerosols in the NCP area of EA (Wang K. et al., 2018). The slight increase of seasonal SO_2 was reported in the whole domain of EA due to lower PBLH caused by ARI effects of anthropogenic aerosols (Nguyen et al., 2019b). There was only one study depicted increased CO (NH_3) concentration in EC (NEA) due to both the ARI and ACI (ARI) effects of anthropogenic aerosols but these results may not be conclusive.

Table 8. Compilation of aerosol-induced variations of $PM_{2.5}$ and gaseous pollutants simulated by two-way coupled models (WRF-Chem, WRF-CMAQ, GRAPES-CUACE, WRF-NAQPMS and GATOR-GCMOM) in different regions of Asia and at different temporal scales.

Region	Time scale	$\Delta PM_{2.5}$ [mean] ($\mu g \cdot m^{-3}$)	ΔO_3 [mean] ($\mu g \cdot m^{-3}$)	ΔNO_2 [mean] ($\mu g \cdot m^{-3}$)	ΔSO_2 [mean] ($\mu g \cdot m^{-3}$)	ΔCO [mean] ($\mu g \cdot m^{-3}$)	ΔNH_3 [mean] ($\mu g \cdot m^{-3}$)
NCP	hours	-3.50 to 90.00 [23.48]					
YRD	hours	7.00 to 30.50 [15.17]	-32.80 to -0.20 [-11.25]	12.30			
Hourly mean		19.32	-11.25	12.30			
SEC	days	-1.91 to 32.49 [14.73]					
NCP	days	-5.00 to 56.00 [14.51]					
EC	days	2.87 to 18.60 [10.74]	-5.97 to -1.45 [-3.71]				
NEA	days	1.75			0.97		0.11
Daily mean		10.43	-3.71		0.97		0.11
India	months	3.00 to 30.00 [16.50]					
EC	months	1.00 to 40.00 [16.33]	-2.40 to -1.00 [-1.70]			4.00 to 6.00 [5.00]	
China	months	1.60 to 33.20 [14.38]	-23.90 to 4.92 [-3.42]				
EA	months	3.60 to 10.20 [5.79]					
Monthly mean		13.25	-2.56			5.00	
SEA	seasons	0.15 to 2.09 [1.12]	-1.92 to 0.26 [-0.83]				
EA	seasons	-8.00 to 2.70 [-0.14]	-4.48 to -1.00 [-2.99]	0.43 to 0.88 [0.66]	-4.29 to 0.72 [-0.42]		
Seasonal mean		0.49	-1.91	0.66	-0.42		
PRD	years	2.90					
EA	years	1.82	-2.76	0.66	0.54		
NCP	years	0.10 to 5.10 [1.70]					
SEA	years	1.21	-0.80				
Yearly mean		1.91	-1.78	0.66	0.54		

7 Conclusions

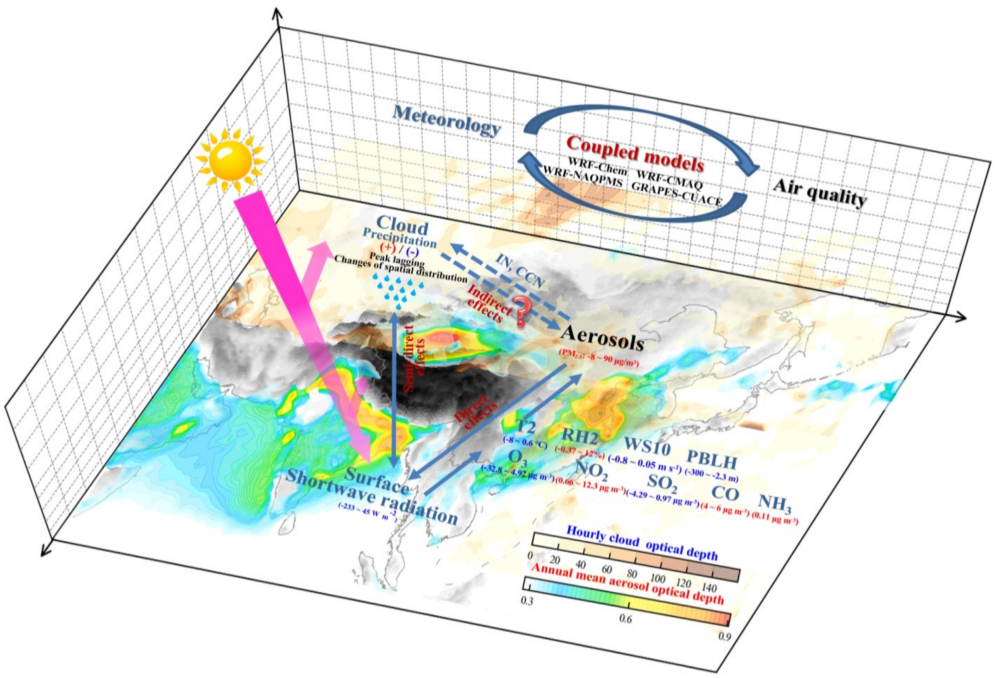

Figure 9. A schematic diagram depicting aerosol-radiation-cloud interactions and quantitative effects of aerosol feedbacks on meteorological and air quality variables simulated by two-way coupled models in Asia.

Two-way coupled models have been applied in US and Europe extensively and then in Asia due to frequent occurrences of severe air pollution events accompanied with rapid economic growth in the region. Until now, no comprehensive study is conducted to elucidate the recent advances in two-way coupled models' applications in Asia. This paper provides a critical overview of current status and research focuses of related modeling studies using two-way coupled models in Asia between 2010 and 2019, and summarizes the effects of aerosol feedbacks on meteorological and air quality variables from these studies.

Through systematically searching peer-reviewed publications with several scientific-based search engines and a variety of key word combinations and applying certain selection criteria, 160 relevant papers were identified. Our bibliometric analysis results (as schematically illustrated in Fig. 9) showed that in Asia, the research activities with two-way coupled models had increased gradually in the past decade and the five two-way coupled models (WRF-Chem, WRF-CMAQ, WRF-NAQPMS, GRAPES-CUACE and GATOR-GCMOM) were extensively utilized to explore the ARI or/and ACI effects in Asia with focusing on several high aerosol loading areas (e.g., EA, India, China and NCP) during wintertime or/and severe pollution events, with less investigations looking into other areas and seasons with low pollution levels. Among the 160 papers, nearly 82 % of them focused on ARI (72 papers) and both ARI and ACI effects (60 papers), but papers that only considering ACI effects were relatively limited. The ARI or/and ACI effects of natural mineral dust, BC and BrC from anthropogenic sources and BC from ARB were mostly investigated, while a few studies quantitatively assessed the health impacts induced by aerosol effects.

Meta-analysis results revealed that enabling aerosol effects in two-way coupled models could improve their simulation/forecast capabilities of meteorology and air quality in Asia, but a wide range of differences occurred among the previous studies perhaps due to various model configurations (selections of model versions and parameterization schemes) and largest uncertainties related to ACI processes and their treatments in models. Compared to US and Europe, the aerosol-induced decrease of the shortwave radiative forcing was larger because of higher air pollution levels in Asia. The overall decrease (increase) of T2, WS10, PBLH and O_3 (RH2, $PM_{2.5}$ and other gaseous pollutant concentrations) caused by ARI or/and ACI effects were reported from the modeling studies using two-way coupled models in Asia. The ranges of aerosol-induced variations of T2, PBLH, $PM_{2.5}$ and O_3 concentrations were larger than other meteorological and air quality variables. For variables of CO, SO_2, NO_2, and NH_3, reliable estimates could not be obtained due to insufficient numbers of samples in past studies.

Even though noticeable progresses toward the application of two-way coupled meteorology and air quality models have been made in Asia and the world during the last decade, several limitations are still presented. Enabling aerosol feedbacks lead to higher computational cost compared to offline models, but this shortcoming can be overcome with the new developments of cluster computing technology (i.e., Graphics Processing Unit (GPU)-accelerated computing and cloud computing). The latest advances in the measurements and research of cloud properties, precipitation characteristics, and physiochemical characteristics of aerosols that play pivotal roles in CCN or IN activation mechanisms can guide the improvements and enhancements in two-way coupled models, especially to abate the uncertainties in simulating ACI effects. Special attention needs to be paid to assess the accuracies of different methodologies in terms of ARI and ACI calculations in two-way coupled models in Asia and other regions. Besides the five two-way coupled models mentioned in this paper, more models capable of simulating aerosol feedbacks (such as WRF-CHIMERE and WRF-GEOS-Chem) have become available and projects covering more comprehensive intercomparisons of these coupled models should be conducted in Asia. Future assessments of the ARI or/and ACI effects should pay extra attention to their impacts on dry and wet depositions simulated by two-way coupled models. So far, the majority of two-way coupled models' simulations and evaluations focuses on episodic air pollution events occurring in certain areas, therefore their long-term applications and evaluations are necessary and their real-time forecasting capabilities should be explored as well.

Appendix A

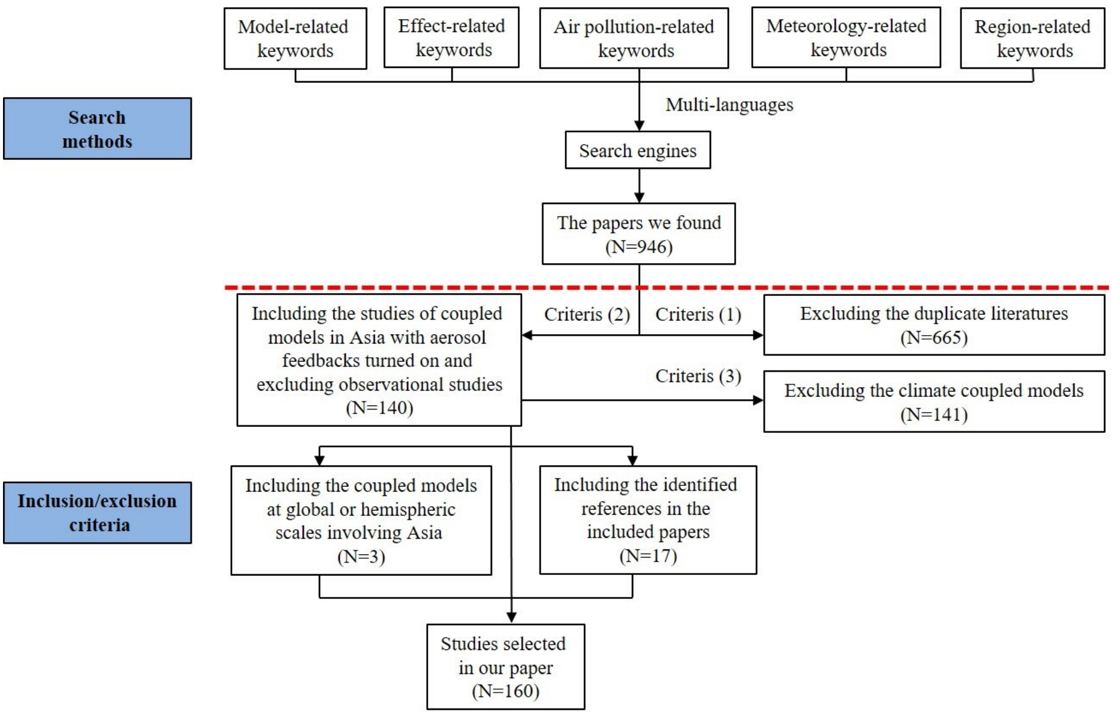

Figure A1. Flowchart of literature search and identification

Appendix B

Table B1. Lists of abbreviations and acronyms

ACI	Aerosol-cloud interactions
AOD	Aerosol optical depth
AQCHEM	the CMAQ's standard aqueous chemistry module
ARB	Agriculture residue burning
ARB_BC	BC emitted from agriculture residue burning
ARB_CAs	Carbonaceous aerosols emitted from agriculture residue burning
ARI	Aerosol-radiation interactions
ATM	In the atmosphere
BB	Biomass burning
BC	Black carbon
BCs	Boundary conditions
BOT	At the bottom

BrC	Brown carbon
CA	Central Asia
CAMx	Comprehensive Air quality Model with extensions
CAs	Carbonaceous aerosols
CC	Central China
CCN	Cloud condensation nuclei
CDNC	Cloud droplet number concentration
CHIMERE	A multi-scale chemistry-transport model for atmospheric composition analysis and forecast
CMAQ	Community Multiscale Air Quality model
CO	Carbon monoxide
CRFs	Concentration-response functions
DRF	Direct radiative forcing
EA	East Asia
EC	East China
EQUISOLV II	the EQUIlibrium SOLVer version 2
GATOR-GCMOM	Gas, aerosol, transport, radiation, general circulation, mesoscale, and ocean Model
GOCART	The Global Ozone Chemistry Aerosol Radiation and Transport
GPRAPES-CUACE	Global-regional assimilation and prediction system coupled with the Chinese Unified Atmospheric Chemistry Environment forecasting system
GSI	Gridpoint Statistical Interpolation
H_2O_2	Hydrogen peroxide
HNO_3	Nitric acid
$HO_2\cdot$	Hydroperoxyl
ICs	Initial conditions
IN	Ice nuclei
INPs	Ice nucleation parameterizations
IPCC	Intergovernmental Panel on Climate Change
IPR	Ice particle radius
IWP	Ice water path
LWP	Liquid water path
LWRF	Longwave radiative forcing
MARS-A	the Model for an Aerosol Reacting System-version A
MB	Mean bias
ME	Middle East
MESA-MTEM	the Multicomponent Equilibrium Solver for Aerosols with the Multicomponent Taylor Expansion Method
MICS-Asia	Model Inter-Comparison Study for Asia
MOZART	Model for Ozone and Related Chemical Tracer
MRYR	Middle reaches of the Yangtze River
N	Nitrate
N_2O_5	Nitrogen pentoxide
NAQPMS	Nested Air Quality Prediction Modeling System
NC	North China
NCP	North China Plain
NEA	Northeast Asia
NME	Normalized mean error
NO_2	Nitrogen dioxide
NU-WRF	National aeronautics and space administration Unified Weather Research and Forecasting model
NWC	Northwest China
O_3	Ozone
OA	Organic aerosols
OC	Organic carbon
$\cdot OH$	Hydroxyl radical
OPAC	Optical Properties of Aerosols and Clouds
PBL	Planetary boundary layer
PBLH	Planetary boundary layer height
$PM_{2.5}$	Fine particulate matter
PRD	Pearl River Delta
PSI	Papers with statistical indices
R	Correlation coefficient
RADM	the Regional Acid Deposition Mode
RH2	Relative humidity at 2 meters above the surface
RMSE	Root mean square error
RRTM	The Rapid Radiative Transfer Model
RRTMG	The Rapid Radiative Transfer Model for General Circulation Models
S	Sulfate
SA	South Asia
SC	South China
SEA	Southeast Asia
SEC	Southeast China
SH2	Specific humidity at 2 meters above the surface
SI	Statistical indices
SO_2	Sulfur dioxide
SOA	Secondary organic aerosol
SWC	Southwest China
SWRF	Shortwave radiative forcing
T2	Air temperature at 2 meters above the surface
TOA	At the top of atmosphere
TP	Tibetan Plateau
US	the United States
VBS	Volatility basis set

WA	West Asia
WRF	Weather Research and Forecasting model
WRF-Chem	Weather Research and Forecasting model coupled with Chemistry
WRF-CHIMERE	Weather Research and Forecasting model coupled with a multi-scale Chemistry-Transport Model (CTM) for air quality forecasting and simulation
WRF-CMAQ	Weather Research and Forecasting model coupled with Community Multiscale Air Quality model
WRF-NAQPMS	Weather Research and Forecasting model coupled with the Nested Air Quality Prediction Modeling System
WS10	Wind speed at 10 meters above the surface
YRD	Yangtze River Delta

Table B2. The compiled number of publications (NP) and number of samples (NS) for papers that providing statistical indices (SI) of meteorological variables.

No.*	Meteorological variables															
	T2				RH2				SH2				WS10			
	NP	NS			NP	NS			NP	NS			NP	NS		
		R	MB	RMSE		R	MB	RMSE		R	MB	RMSE		R	MB	RMSE
4	1	5	5 (4↑, 1↓)	5	1	5	5 (1↑, 4↓)	5								
5					1		3 (2↑, 1↓)	3								
7	1	4	4 (3↑, 1↓)													
13	1		1 (1↓)		1		1 (1↑)									
15	1	1			1	1							1	2		
16	1	1														
20	1	2	2 (1↑, 1↓)	2	1	2	2 (1↑, 1↓)	2					1	1	1 (1↑)	1
21	1	0	2 (2↓)	2									1		2 (1↑, 1↓)	2
22	1	1	1 (1↓)	1	1	1	1 (1↑)	1					1	1	1 (1↓)	1
23	1	1	1 (1↑)		1	1	1 (1↓)						1	1	1 (1↑)	
24	1	1	1 (1↑)		1	1	1 (1↓)						1	1	1 (1↑)	
25	1	1	1 (1↓)													
28	1		1 (1↑)	1	1		1 (1↓)	1					1		1 (1↑)	1
29	1	9	9 (6↑, 3↓)	9	1	8		9					1	9	9 (9↑)	9
33	1	6	6 (4↑, 2↓)	6												
34	1	2	2 (2↑)	2									1	2	2 (2↓)	2
35	1	2		2	1	1		1					1	1		1
38	1		4 (4↓)	4	1		4 (3↑, 1↓)	4								
50	1		8 (8↓)	8												
56	1	1	1 (1↓)	1	1	1	1 (1↓)	1					1	1	1 (1↑)	1
57	1	1			1	1							1	1		
61	1	4	4 (4↓)	4	1	4	4 (4↑)	4					1	4	4 (4↑)	4
62	1		5 (5↓)	5									1		5 (4↑, 1↓)	5
63	1	1														
71	1	1														
72	1	4	4 (3↑, 1↓)	4	1	4	4 (3↑, 1↓)	4								
73	1	1	1 (1↓)	1					1	1	1 (1↑)	1	1	1	1 (1↑)	1
75	1	4	4 (4↑)		1	4	4 (4↑)					0	1	4	4 (1↑, 3↓)	
77	1	4	4 (2↑, 2↓)						1	4	3 (3↑)	4	1	4	4 (4↑)	4
79	1		8 (6↑, 2↓)	8												
80	1	8	8 (8↑)	8	1	8	8 (8↓)	8					1	8	8 (6↑, 2↓)	8
85	1		4 (1↑, 3↓)	4	1		4 (2↑, 2↓)	4					1		4 (4↑)	4
87	1		3 (2↑, 1↓)	3									1		3 (2↑, 1↓)	3
88	1	3	3 (1↑, 2↓)	3	1	3	3 (2↑, 1↓)	3					1	3	3 (2↑, 1↓)	3
90	1	4	4 (1↑, 3↓)						1	4	4 (4↑)		1	4	4 (4↑)	
91	1	1	1 (1↓)	1					1	1	1 (1↑)	1	1	1	1 (1↑)	1
94	1	6	6 (4↑, 2↓)	6	1	6	6 (2↑, 4↓)	6					1	6	6 (6↑)	6
96	1	16	16 (11↑, 5↓)										1	16	16 (11↑, 5↓)	
97	1	1	1 (1↓)	1	1	1	1 (1↑)	1					1	1	1 (1↑)	1
106	1	6	6 (6↓)						1	6	5 (2↑, 3↓)		1	6	6 (6↑)	
109	1	2	2 (2↓)	2	1	3	3 (3↑)	3					1	2	2 (2↑)	2
112	1		2 (2↓)	2					1		2 (2↓)	2	1		2 (2↑)	2
116	1	2	2 (1↑, 1↓)	0	1	2	2 (1↑, 1↓)									
121	1	1	1 (1↓)	1									1	1	1 (1↑)	1
122	1		2 (2↓)	2	1		2 (2↑)	2					1		2 (2↑)	2
125	1	4	4 (4↓)	4	1	4	4 (4↑)	4					1	4	4 (4↓)	4
126	1	4	4 (4↓)	4					1	4	4 (2↑, 2↓)	4	1	4	4 (4↑)	4
127	1		2 (2↓)	2									1		2 (2↑)	2
128	1	8	8 (8↓)	8					1	8	8 (5↑, 3↓)	8	1	8	8 (8↑)	8
129	1	1	1 (1↓)	1	1	1	1 (1↑)	1					1	1	1 (1↑)	1
133	1		1 (1↓)	0	1		4 (4↑)						1		4 (3↑, 1↓)	
143	1	4		4	1	4		4					1	4		4
147	1	2		2	1	2		2					1	2		2
151	1	7	7 (7↓)	7					1	7	7 (3↑, 4↓)	7	1	7	7 (7↑)	7
Total	53	137	167 (67↑, 100↓)	130	30	68	70 (42↑, 28↓)	73	9	35	35 (21↑, 14↓)	27	40	111	126 (104↑, 22↓)	97

Note that the No.* is consistent with the No. in Table 1, and ↑ and ↓ mark over- and underestimations of variables, respectively, along with their number of samples.

Table B3. The compiled number of publications (NP) and number of samples (NS) for papers that providing statistical indices (SI) of air quality variables.

No.*	Air quality variables							
	$PM_{2.5}$				O_3			
	NP	NS			NP	NS		
		R	MB	RMSE		R	MB	RMSE
4	1	5	5 (5↓)	5				
5	1		1 (1↑)	1	1		1 (1↓)	1
11	1	60						
15	1	1						
21	1		2 (1↑, 1↓)					
22	1	1	1 (1↑)	1				
23	1	1	1 (1↑)		1	1	1 (1↓)	
24	1	1	1 (1↓)		1		1 (1↓)	
25	1	1	1 (1↑)		1	1	1 (1↑)	
29	1	9	9 (6↑, 3↓)	9				

33	1	4	4 (4↓)	4	1	4	4 (3↑, 1↓)	4
34	1	2	2 (1↑, 1↓)	2				
35					1	1		1
50	1		4 (1↑, 3↓)	4				
56	1	1	1 (1↑)	1				
57	1	1						
59	1	6	6 (6↓)	6	1	6	6 (6↑)	6
61	1	12	12 (12↑)	12				
67	1	10	2 (2↓)	10				
71	1	1						
73	1	2	2 (1↑, 1↓)		1	4	4 (4↑)	
77	1	4						
85	1	3	3 (3↓)					
86	1	4	4 (2↑, 2↓)	4				
88	1	3	3 (1↑, 2↓)	3				
90	1	8	8 (2↑, 6↓)		1	14	14 (14↑)	
91	1	4	4 (1↑, 3↓)	4	1	6	6 (4↑, 2↓)	6
94	1	4	4 (3↑, 1↓)	4				
97	1	1	1 (1↓)	1				
100	1	1			1	1		
106	1	6	6 (2↑, 4↓)		1	8	8 (4↑, 4↓)	
112	1				1			
121					1			5
122	1	4	4 (1↑, 3↓)					
125	1	4	4 (2↑, 2↓)	4	1	4	4 (4↑)	4
126	1	4	4 (2↑, 2↓)	4	1	4	4 (4↑)	4
127	1		1 (1↑)	1				
128	1	8	8 (3↑, 5↓)	8				
129	1	3	3 (2↑, 1↓)	3	1	2	2 (1↑, 1↓)	2
133					1	4	4 (3↑, 1↓)	4
136	1	5	5 (5↓)					
146	1	1			1	20		20
147	1	2		2				
149	1	6		6				
150					1	21		21
151	1	12	6 (6↑)	6	1	24	12 (7↑, 5↓)	12
Total	42	205	122 (55↑, 67↓)	105	21	125	72 (55↑, 17↓)	90

Note that the No.* is consistent with the No. in Table 1, and ↑ and ↓ mark over- and underestimations of variables, respectively, along with their number of samples.

Table B4. The compiled number of publications (NP) and number of samples (NS) for papers that simultaneously providing the statistical indices (SI) of meteorological variables simulated by coupled models (WRF-Chem, WRF-CMAQ, GRAPES-CUACE, WRF-NAQPMS and GATOR-GCMOM) with/out ARI.

No.*	Meteorological variables															
	T2				RH2				SH2				WS10			
	NP	NS			NP	NS			NP	NS			NP	NS		
		R	MB	RMSE		R	MB	RMSE		R	MB	RMSE		R	MB	RMSE
32	1	3	3 (2↑, 1↓)	3												
78	1		4 (3↑, 1↓)	4												
124	1	2	2 (2↓)	2	1	2	2 (2↑)	2					1	2	2 (2↓)	2
125	1	2	2 (2↓)	2					1	2	2 (1↑, 1↓)	2	1	2	2 (2↑)	2
126	1		1 (1↓)	1									1		1 (1↑)	1
127	1	4	4 (4↓)	4					1	4	4 (3↑, 1↓)	4	1	4	4 (4↑)	4
146	1	1		1	1	1		1					1	1		1
Total	7	12	16 (5↑, 11↓)	17	2	3	2 (2↑)	3	2	6	6 (4↑, 2↓)	6	5	9	9 (7↑, 2↓)	10

Note that the No.* is consistent with the No. in Table 1, and ↑ and ↓ mark over- and underestimations of variables, respectively, along with their number of samples.

Table B5. The compiled number of publications (NP) and number of samples (NS) for papers that simultaneously providing the statistical indices (SI) of air quality variables simulated by coupled models (WRF-Chem, WRF-CMAQ, GRAPES-CUACE, WRF-NAQPMS and GATOR-GCMOM) with/out ARI.

No.*	Air quality variables							
	$PM_{2.5}$				O_3			
	NP	NS			NP	NS		
		R	MB	RMSE		R	MB	RMSE
49	1		2 (1↑, 1↓)	2	1	10		10
60	1	4	4 (4↑)	4				
124	1	2	2 (1↑, 1↓)	2	1	2	2 (2↑)	2
125	1	2	2 (1↑, 1↓)	2	1	2	2 (2↑)	2
127	1	4	4 (2↑, 2↓)	4				
146	1	1		1				
Total	5	13	14 (9↑, 5↓)	15	3	14	4 (4↑)	14

Note that the No.* is consistent with the No. in Table 1, and ↑ and ↓ mark over- and underestimations of variables, respectively, along with their number of samples.

Table B6. Description of refractive indices and radiation schemes used in the WRF-Chem and WRF-CMAQ in Asia.

Model	Refractive indices of aerosol species groups		Radiation scheme	
	SW	LW	SW scheme (Spectral intervals)	LW scheme (Spectral intervals)
WRF-Chem	1. Water ($1.35+1.524^{-8}i$,	1. Water (1.532+0.336i,	GODDARD (0.175-0.225, 0.225-0.245, 0.245-	RRTMG (10-350, 350-500, 500-630, 630-700,

	1.34+2.494^{-9}i, 1.33+1.638^{-9}i, 1.33+3.128^{-6}i) 2. Dust (1.55+0.003i, 1.550+0.003i, 1.550+0.003i, 1.550+0.003i) 3. BC (1.95+0.79i, 1.95+0.79i, 1.95+0.79i, 1.95+0.79i) 4. OC (1.45+0i, 1.45+0i, 1.45+0i, 1.45+0i) 5. Sea salt (1.51+8.66^{-7}i, 1.5+7.019^{-8}i, 1.5+1.184^{-8}i, 1.47+1.5^{-4}i) 6. Sulfate (1.52+1.00^{-9}i, 1.52+1.00^{-9}i, 1.52+1.00^{-9}i, 1.52+1.75^{-6}i) in term of 4 spectral intervals in 0.25-0.35, 0.35-0.45, 0.55-0.65, 0.998-1.000 μm	1.524+0.360i, 1.420+0.426i, 1.274+0.403i, 1.161+0.321i, 1.142+0.115i, 1.232+0.0471i, 1.266+0.039i, 1.296+0.034i, 1.321+0.0344i, 1.342+0.092i, 1.315+0.012i, 1.330+0.013i, 1.339+0.01i, 1.350+0.0049i, 1.408+0.0142i) 2. Dust (2.34+0.7i, 2.904+0.857i, 1.748+0.462i, 1.508+0.263i, 1.911+0.319i, 1.822+0.26i, 2.917+0.65i, 1.557+0.373i, 1.242+0.093i, 1.447+0.105i, 1.432+0.061i, 1.473+0.0245i, 1.495+0.011i, 1.5+0.008i) 3. BC (1.95+0.79i, 1.95+0.79i, 1.95+0.79i, 1.95+0.79i, 1.95+0.79i, 1.95+0.79i, 1.95+0.79i, 1.95+0.79i, 1.95+0.79i, 1.95+0.79i, 1.95+0.79i, 1.95+0.79i, 1.95+0.79i, 1.95+0.79i,) 4. OC (1.86+0.5i, 1.91+0.268i, 1.988+0.185i, 1.439+0.198i, 1.606+0.059i, 1.7+0.0488i, 1.888+0.11i, 2.489+0.3345i, 1.219+0.065i, 1.419+0.058i, 1.426+0.0261i, 1.446+0.0142i, 1.457+0.013i, 1.458+0.01i) 5. Sea salt (1.74+0.1978i, 1.76+0.1978i, 1.78+0.129i, 1.456+0.038i, 1.41+0.019i, 1.48+0.014i, 1.56+0.016i, 1.63+0.03i, 1.4+0.012i, 1.43+0.0064i, 1.56+0.0196i, 1.45+0.0029i, 1.485+0.0017i, 1.486+0.0014i) 6. Sulfate (1.89+0.22i, 1.91+0.152i, 1.93+0.0846i, 1.586+0.2225i, 1.678+0.195i, 1.758+0.441i, 1.855+0.696i, 1.597+0.695i, 1.15+0.459i, 1.26+0.161i, 1.42+0.172i, 1.35+0.14i, 1.379+0.12i, 1.385+0.122i) in term of 16 spectral intervals in 10-350, 350-500, 500-630, 630-700, 700-820, 820-980, 980-1080, 1080-1180, 1180-1390, 1390-1480, 1480-1800, 1800-2080, 2080-2250, 2250-2390, 2390-2600, 2600-3250 cm^{-1}	0.260, 0.280-0.295, 0.295-0.310, 0.310-0.320, 0.325-0.400, 0.400-0.700, 0.700-1.220, 1.220-2.270, 2.270-10.00 μm) RRTMG (3.077-3.846, 2.500-3.077, 2.150-2.500, 1.942-2.150, 1.626-1.942, 1.299-1.626, 1.242-1.299, 0.778-1.242, 0.625-0.778, 0.442-0.625, 0.345-0.442, 0.263-0.345, 0.200-0.263, 3.846-12.195 μm)	700-820, 820-980, 980-1080, 1080-1180, 1180-1390, 1390-1480, 1480-1800, 1800-2080, 2080-2250, 2250-2390, 2390-2600, 2600-3250 cm^{-1})
WRF-CMAQ	1. Water (1.408+1.420^{-2}i, 1.324+1.577^{-1}i, 1.277+1.516^{-3}i, 1.302+1.159^{-3}i, 1.312+2.360^{-4}i, 1.321+1.713^{-4}i, 1.323+2.425^{-5}i, 1.327+3.125^{-6}i, 1.331+3.405^{-8}i, 1.334+1.639^{-9}i, 1.340+2.955^{-9}i, 1.349+1.635^{-8}i, 1.362+3.350^{-8}i, 1.260+6.220^{-2}i) 2. Water-soluble (1.443+5.718^{-3}i, 1.420+1.777^{-2}i, 1.420+1.060^{-2}i, 1.420+8.368^{-3}i, 1.463+1.621^{-2}i, 1.510+2.198^{-2}i, 1.510+1.929^{-2}i, 1.520+1.564^{-2}i, 1.530+7.000^{-3}i, 1.530+5.666^{-3}i, 1.530+5.000^{-3}i, 1.530+8.440^{-3}i, 1.530+3.000^{-2}i, 1.710+1.100^{-1}i) 3. BC (2.089+1.070i, 2.014+0.939i, 1.962+0.843i, 1.950+0.784i, 1.940+0.760i, 1.930+0.749i, 1.905+0.737i, 1.870+0.726i, 1.850+0.710i, 1.850+0.710i, 1.850+0.710i, 1.850+0.710i, 1.850+0.710i, 2.589+1.771i)	1. Water (1.160+0.321i, 1.140+0.117i, 1.232+0.047i, 1.266+0.038i, 1.300+0.034i) 2. Water-soluble (1.570+0.069i, 1.700+0.055i, 1.890+0.128i, 2.233+0.334i, 1.220+0.066i) 3. BC (1.570+2.200i, 1.700+2.200i, 1.890+2.200i, 2.233+2.200i, 1.220+2.200i) 4. Insoluble (1.482+0.096i, 1.600+0.107i, 1.739+0.162i, 1.508+0.117i, 1.175+0.042i) 5. Sea-salt (1.410+0.019i, 1.490+0.014i, 1.560+0.017i, 1.600+0.029i, 1.402+0.012i) in term of 5 thermal windows at 13.240, 11.20, 9.73, 8.870, 7.830 μm	RRTMG (3.077-3.846, 2.500-3.077, 2.150-2.500, 1.942-2.150, 1.626-1.942, 1.299-1.626, 1.242-1.299, 0.778-1.242, 0.625-0.778, 0.442-0.625, 0.345-0.442, 0.263-0.345, 0.200-0.263, 3.846-12.195 μm)	RRTMG (10-350, 350-500, 500-630, 630-700, 700-820, 820-980, 980-1080, 1080-1180, 1180-1390, 1390-1480, 1480-1800, 1800-2080, 2080-2250, 2250-2390, 2390-2600, 2600-3250 cm^{-1})

4. Insoluble ($1.272+1.165^{-2}i$, $1.168+1.073^{-2}i$, $1.208+8.650^{-3}i$, $1.253+8.092^{-3}i$, $1.329+8.000^{-3}i$, $1.418+8.000^{-3}i$, $1.456+8.000^{-3}i$, $1.518+8.000^{-3}i$, $1.530+8.000^{-3}i$, $1.530+8.000^{-3}i$, $1.530+8.000^{-3}i$, $1.530+8.440^{-3}i$, $1.530+3.000^{-2}i$, $1.470+9.000^{-2}i$)
5. Sea-salt ($1.480+1.758^{-3}i$, $1.534+7.462^{-3}i$, $1.437+2.950^{-3}i$, $1.448+1.276^{-3}i$, $1.450+7.944^{-4}i$, $1.462+5.382^{-4}i$, $1.469+3.754^{-4}i$, $1.470+1.498^{-4}i$, $1.490+2.050^{-7}i$, $1.500+1.184^{-8}i$, $1.502+9.938^{-8}i$, $1.510+2.060^{-6}i$, $1.510+5.000^{-6}i$, $1.510+1.000^{-2}i$) in term of 14 wavelengths at 3.4615, 2.7885, 2.325, 2.046, 1.784, 1.4625, 1.2705, 1.0101, 0.7016, 0.53325, 0.38815, 0.299, 0.2316, 8.24 μm

Table B7. Summary of normalized mean error (NME) (%) of surface meteorological and air quality variables using two-way coupled models (WRF-Chem and WRF-CMAQ).

T2	SH2	RH2	WS10	$PM_{2.5}$	O_3	$PM_{2.5}$ with ARI (ARI) or without ARI (NO)	O_3 with ARI (ARI) or without ARI (NO)	Model	Region	Reference
					23.60, 38.50, 55.70, 39.80			WRF-Chem	EA	Liu X. et al. (2016)
0.80, 0.60, 0.60, 0.60		19.10, 16.50, 10.00, 10.10	58.90, 41.60, 44.90, 49.50	37.31, 37.61, 35.77, 34.69, 35.34, 35.41, 45.22, 44.33, 43.09, 39.29, 39.49, 39.07		37.61, 35.34, 44.33, 39.49 (ARI) 35.77, 35.41, 43.09, 39.07 (NO)		WRF-Chem	China	Zhang et al. (2018)
270.20, 22.30, 12.50, 17.60								WRF-Chem	EA	Zhang Yang et al. (2016a)
				44.99, 29.55, 37.28				WRF-Chem	NCP	Yang et al. (2015)
15.50, 15.80, 13.90, 9.90	10.40, 10.40, 9.90, 9.90		31.30, 31.30, 32.50, 32.50	49.80, 65.30, 49.80, 65.60, 88.30, 56.90, 88.40, 57.00	127.00, 32.20, 25.40, 126.10, 32.10, 25.00, 79.90, 25.80, 21.40, 45.80, 77.90, 25.60, 21.10, 39.50			WRF-Chem	EA	Zhang Y. et al. (2015a)
14	11		32	52.70, 58.00, 104.70, 62.00	87.50, 28.60, 23.30, 52.90, 32.40, 28.20			WRF-Chem	EA	Chen Y. et al. (2015)
-0.48, 0.19, 0.21, 0.05, 0.08, 0.13, 0.05, 0.04, 0.04, 0.05, 0.02, 0.02, 0.06, 0.05, 0.04, 0.02			0.33, 1.92, 0.71, 0.78, 0.28, 1.72, 0.61, 0.64, 0.24, 1.76, 0.00, 0.45, 0.34, 1.29, 0.44, 0.56					WRF-Chem	NCP	Chen D. et al. (2015)
16.60, 10.50, 8.90, 12.90, 10.50, 10.20								WRF-Chem	EA	Wang K. et al. (2018)
6.52, 6.58		15.76, 12.15	112.28, 97.26					WRF-Chem	NEA	Park et al. (2018)
				36.00, 33.00	31.00, 22.00			WRF-Chem	China	Zhao et al. (2017)
				44.00, 44.60, 40.10, 54.30				WRF-Chem	NCP	Gao M. et al. (2015)
				41.48, 41.00, 51.77, 55.70	26.68, 26.71, 34.43, 34.64	41.00, 55.70 (ARI) 41.48, 51.77 (NO)	26.71, 34.64 (ARI) 26.68, 34.43 (NO)	WRF-CMAQ	SEA	Nguyen et al. (2019b)
				37.99, 35.06, 38.59, 35.44, 34.39				WRF-CMAQ	China	Chang (2018)

Appendix C

C1 Comparisons of SI at different temporal scales for meteorology

To probe the model performance of simulated T2, RH2, SH2 and WS2 at different temporal scales, the SI of these meteorological variables from PSI were grouped according to the simulation time (yearly, seasonal, monthly and daily) and plotted in Figure C1. Note that the seasonal results contained SI values from simulations lasting more than one month and less than or equal to 3 months. Here in Figure C1, NP and NS were the number of PSI and samples with SI at different time scales, respectively, and also their total values were the same as the ones listed in Table S2. The correlation between simulated and observed T2 (Figure C1a) at the seasonal (mean R= 0.97 with the smallest sample size), yearly (0.91) and monthly (0.90) scales were stronger than that at the daily scale (0.87), indicating that long-term simulations of T2 were well reproduced by coupled models. As shown in Figure C1e, T2 underestimation mentioned above (Fig. 3a) appeared also in the seasonal, monthly and yearly simulations (average MB = -0.87 ℃, -0.15 ℃ and -0.34 ℃, respectively), but the daily

T2 were overestimated (average MB = 0.07 °C). It should be noted that T2 at the monthly scale was underpredicted mainly during winter months (16 samples). Regarding the mean RMSE, its value (Figure C1i) at the daily scale was the largest (0.97 °C) in comparison with that at the other temporal scales.

Given that no SI was available for RH2 at the seasonal scale, results at other time scales were discussed here. Figure C1b presented that simulated RH2 at the daily scale had the best correlation coefficient (mean R= 0.74), followed by those at the monthly (0.73) and yearly (0.71) scales. Except overestimation (average MB = 3.6 %) at the yearly scale (Figure C1f), modeled RH2 were underestimated at the monthly (average MB = -1.1 %) and daily (average MB = -0.2 %) scales, respectively. Therefore, coupled models calculated RH2 reasonably well in short-term simulations. However, at the daily scale, RMSE of modeled RH2 (Figure C1j) was relatively large fluctuation ranging from 6.2 % to 21.3 %.

Lacking of SI for SH2 at the daily scale, only those at other time scales were compared. Even though NP and NS were very limited, the modeled SH2 (Figure C1c) exhibited especially good correlation with observations with the mean R values exceeding 0.95 at the yearly, seasonal and monthly scales (0.99, 0.97 and 0.96, respectively) but had the largest mean RMSE (2.09 $g \cdot kg^{-1}$) at the yearly scale (Figure C1k). Also, both over- and under-estimations of modeled SH2 (Fig. C1g) were reported at different time scales with average MB values as 0.15 $g \cdot kg^{-1}$, -0.02 $g \cdot kg^{-1}$, and -0.14 $g \cdot kg^{-1}$ for yearly, seasonal and monthly simulations, respectively. Generally, the long-term simulations of SH2 agreed better with observations than the short-term ones.

As seen in Figure C1d, the modeled WS10 at the monthly scale (mean R = 0.68) correlated with observations better than that at the daily, yearly and seasonal scales (mean R = 0.62, 0.48 and 0.46, respectively). The simulations at all temporal scales tended to overestimate WS10 comparing against observations (Figure C1h) and their average MB were 0.80 $m \cdot s^{-1}$ (seasonal), 0.86 $m \cdot s^{-1}$ (monthly), 0.64 $m \cdot s^{-1}$ (yearly) and 0.62 $m \cdot s^{-1}$ (daily), respectively. The short-term simulations of WS10 better matched with observations compared to the long-term ones. At the same time, the largest mean RMSE (1.79 $m \cdot s^{-1}$) of simulated WS10 (Figure C1l) appeared at the seasonal scale.

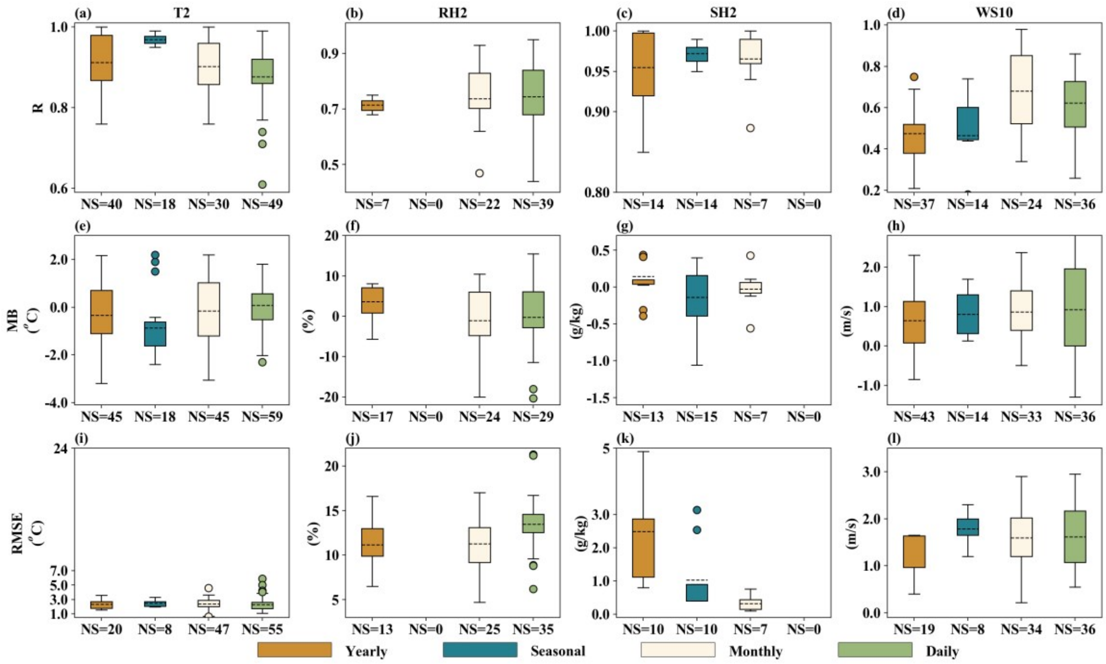

Figure C1. The statistical indices of modeled meteorological variables at different temporal scales (Yearly, Seasonal, Monthly and Daily) from past studies in Asia.

C2 Comparisons of SI at different temporal scales for air quality

Figure C2 depicted the SI of simulated $PM_{2.5}$ and O_3 at yearly, seasonal, monthly and daily scales. The correlation between simulated and observed $PM_{2.5}$ (Figure C2a) at the monthly scale (mean R= 0.68) was largest compared to those at the yearly (0.64), seasonal (0.59), daily (0.57) scales. All the simulated $PM_{2.5}$ were underestimated, with the average daily, monthly, seasonal, and yearly MB as -4.13, -1.46, -0.28, and -1.89 μg·m^{-3}, respectively (Figure C2c). As displayed in Figure C2e, the mean RMSE at the monthly scale was the largest (61.57 μg·m^{-3}).

Regarding to correlation between simulated and observed O_3 (Figure C2b), it was the best at the daily scale (mean R= 0.77). Modeled O_3 were overestimated at the seasonal (average MB = +4.12 μg·m^{-3}), monthly (average MB = +6.11 μg·m^{-3}) and yearly (average MB = +11.71 μg·m^{-3}) scales, but underestimated at the daily scale (average MB =-8.89 μg·m^{-3}) (Figure C2d). Note that no RMSE for O_3 simulation was available at the daily scale, and the RMSE at the yearly scale (Figure C2f) had relatively large fluctuation ranging from 0.21 to 71 μg·m^{-3}. Therefore, coupled models calculated O_3 matched well with observation in short-term simulations.

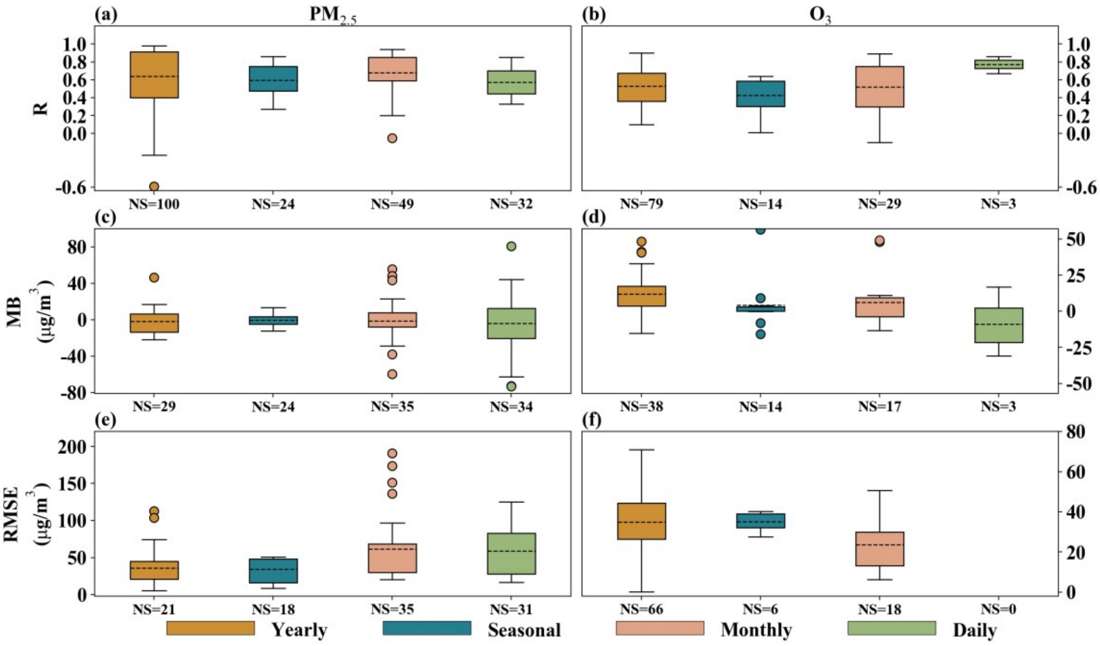

Figure C2. The quantile distributions of simulated $PM_{2.5}$ and O_3 performance metrics at different temporal scales from past studies in Asia.

Data availability

The related dataset can be downloaded from https://doi.org/10.5281/zenodo.5571076 (Gao et al., 2021), and this dataset includes basic information (Table S1), performance metrics (Table S2), quantitative effects of aerosol feedbacks on meteorological and air quality variables (Table S3), model configuration and setup (Table S4) and aerosol-induced variations of simulated shortwave and longwave radiative forcing (Table S5) extracted from collected studies of applications of two-way coupled meteorology and air quality models in Asia.

Author contribution

Chao Gao, Aijun Xiu, Xuelei Zhang and Qingqing Tong carried out the data collection, related analysis, figure plotting, and manuscript writing; Hongmei Zhao, Shichun Zhang, Guangyi Yang and Mengduo Zhang involved with the original research plan and made suggestions to the manuscript writing.

Competing interest

The authors declare that they have no conflict of interest.

Acknowledgement

This study was financially sponsored by National Key Research and Development Program of

China (No. 2017YFC0212304), Talent Program of Chinese Academy of Sciences, and National Natural Science Foundation of China (No. 41571063 and No. 41771071). The authors are very grateful to many researchers who provided detailed information on the two-way coupled models and related research work. The list includes but is not limited to Xueshun Chen, Zifa Wang, Yi Gao, Meigen Zhang and Baozhu Ge (Institute of Atmospheric Physics, Chinese Academy of Sciences), Chunhong Zhou (Chinese Academy of Meteorological Sciences), Yang Zhang (Northeastern University), Mark Zachary Jacobson (Stanford University), Tianliang Zhao (Nanjing University of Information Science & Technology), Xin Huang (Nanjing University), Chun Zhao (University of Science and Technology of China), Junhua Yang and Shichang Kang (Northwest Institute of Eco-Environment and Resources, Chinese Academy of Sciences), Sachin Ghude (Ministry of Earth Sciences Government of India) and Luke Conibear (University of Leeds). We would also like to express our deepest appreciation to the editor James Allan and two anonymous reviewers for their constructive comments and suggestions, which helped to improve the quality and readability of this article.

Reference

Albrecht, B.A., 1989. Aerosols, cloud microphysics, and fractional cloudiness. Science (80-.). 245, 1227-1230. https://doi.org/10.1126/science.245.4923.1227.

Ahmadov, R., McKeen, S.A., Robinson, A.L., Bahreini, R., Middlebrook, A.M., De Gouw, J.A., Meagher, J., Hsie, E., Edgerton, E., Shaw, S., 2012. A volatility basis set model for summertime secondary organic aerosols over the eastern United States in 2006. J. Geophys. Res. Atmos. 117. https://doi.org/10.1029/2011JD016831.

An, Z., Huang, R.-J., Zhang, R., Tie, X., Li, G., Cao, J., Zhou, W., Shi, Z., Han, Y., Gu, Z., 2019. Severe haze in northern China: A synergy of anthropogenic emissions and atmospheric processes. Proc. Natl. Acad. Sci. 116, 8657-8666. https://doi.org/10.1073/pnas.1900125116.

Andreae, M.O., Rosenfeld, D., 2008. Aerosol-cloud-precipitation interactions. Part 1. The nature and sources of cloud-active aerosols. Earth-Science Rev. 89, 13-41. https://doi.org/10.1016/j.earscirev.2008.03.001.

Appel, K.W., Bash, J.O., Fahey, K.M., Foley, K.M., Gilliam, R.C., Hogrefe, C., Hutzell, W.T., Kang, D., Mathur, R., Murphy, B.N., 2021. The Community Multiscale Air Quality (CMAQ) model versions 5.3 and 5.3.1: system updates and evaluation. Geosci. Model Dev. 14, 2867–2897. https://doi.org/10.5194/gmd-14-2867-2021.

Appel, K.W., Napelenok, S.L., Foley, K.M., Pye, H.O.T., Hogrefe, C., Luecken, D.J., Bash, J.O., Roselle, S.J., Pleim, J.E., Foroutan, H., Hutzell, W.T., Pouliot, G.A., Sarwar, G., Fahey, K.M., Gantt, B., Gilliam, R.C., Heath, N.K., Kang, D., Mathur, R., Schwede, D.B., Spero, T.L., Wong, D.C., Young, J.O., 2017. Description and evaluation of the Community Multiscale Air Quality (CMAQ) modeling system version 5.1. Geosci. Model Dev. 10, 1703-1732. https://doi.org/10.5194/gmd-10-1703-2017.

Appel, K.W., Pouliot, G.A., Simon, H., Sarwar, G., Pye, H.O.T., Napelenok, S.L., Akhtar, F., Roselle, S.J., 2013. Evaluation of dust and trace metal estimates from the Community Multiscale Air Quality (CMAQ) model version 5.0. Geosci. Model Dev. 6, 883–899. https://doi.org/10.5194/gmd-6-883-2013.

Archer-Nicholls, S., Lowe, D., Lacey, F., Kumar, R., Xiao, Q., Liu, Y., Carter, E., Baumgartner, J., Wiedinmyer, C., 2019. Radiative Effects of Residential Sector Emissions in China: Sensitivity to Uncertainty in Black Carbon Emissions. J. Geophys. Res. Atmos. 124, 5029-5044. https://doi.org/10.1029/2018JD030120.

Ashrafi, K., Motlagh, M.S., Neyestani, S.E., 2017. Dust storms modeling and their impacts on air quality and radiation budget over Iran using WRF-Chem. Air Qual. Atmos. Heal. 10, 1059-1076. https://doi.org/10.1007/s11869-017-0494-8.

Bai, Y., Qi, H., Zhao, T., Zhou, Y., Liu, L., Xiong, J., Zhou, Z., Cui, C., 2020. Simulation of the responses of rainstorm in the Yangtze River Middle Reaches to changes in anthropogenic aerosol emissions. Atmos. Environ. 220, 117081. https://doi.org/10.1016/j.atmosenv.2019.117081.

Baklanov, A., Schlünzen, K., Suppan, P., Baldasano, J., Brunner, D., Aksoyoglu, S., Carmichael, G., Douros, J., Flemming, J., Forkel, R., 2014. Online coupled regional meteorology chemistry models in Europe: current status and prospects. Atmos. Chem. Phys. 14, 317-398. https://doi.org/10.5194/acp-14-317-2014.

Baró, R., Jiménez-Guerrero, P., Balzarini, A., Curci, G., Forkel, R., Grell, G., Hirtl, M., Honzak, L., Langer, M., Pérez, J.L., 2015. Sensitivity analysis of the microphysics scheme in WRF-Chem contributions to AQMEII phase 2. Atmos. Environ. 115, 620-629. https://doi.org/10.1016/j.atmosenv.2015.01.047.

Barth, M.C., Rasch, P.J., Kiehl, J.T., Benkovitz, C.M., Schwartz, S.E., 2000. Sulfur chemistry in the NCAR CCM: Description, evaluation, features and sensitivity to aqueous chemistry. J. Geophys. Res 105, 1387–1415. https://doi.org/10.1029/1999JD900773.

Bauer, P., Thorpe, A., Brunet, G., 2015. The quiet revolution of numerical weather prediction. Nature 525, 47-55. https://doi.org/10.1038/nature14956.

Bei, N., Wu, J., Elser, M., Tian, F., Cao, J., El-Haddad, I., Li, X., Huang, R., Li, Z., Long, X., 2017. Impacts of meteorological uncertainties on the haze formation in Beijing-Tianjin-Hebei (BTH) during wintertime: a case study. Atmos. Chem. Phys. 17, 14579. https://doi.org/10.5194/acp-17-14579-2017.

Beig, G., Chate, D.M., Ghude, S.D., Mahajan, A.S., Srinivas, R., Ali, K., Sahu, S.K., Parkhi, N., Surendran, D., Trimbake, H.R., 2013. Quantifying the effect of air quality control measures during the 2010 Commonwealth Games at Delhi, India. Atmos. Environ. 80, 455-463. https://doi.org/10.1016/j.atmosenv.2013.08.012.

Bellouin, N., Jones, A., Haywood, J., Christopher, S.A., 2008. Updated estimate of aerosol direct radiative forcing from satellite observations and comparison against the Hadley Centre climate model. J. Geophys. Res. Atmos. 113. https://doi.org/10.1029/2007JD009385.

Benas, N., Meirink, J.F., Karlsson, K.-G., Stengel, M., Stammes, P., 2020. Satellite observations of aerosols and clouds over southern China from 2006 to 2015: analysis of changes and possible interaction mechanisms. Atmos. Chem. Phys. 20, 457-474. https://doi.org/10.5194/acp-20-457-2020.

Bennartz, R., Fan, J., Rausch, J., Leung, L.R., Heidinger, A.K., 2011. Pollution from China increases cloud droplet number, suppresses rain over the East China Sea. Geophys. Res. Lett. 38. https://doi.org/10.1029/2011GL047235.

Bharali, C., Nair, V.S., Chutia, L., Babu, S.S., 2019. Modeling of the effects of wintertime aerosols on boundary layer properties over the Indo Gangetic Plain. J. Geophys. Res. Atmos. 124, 4141-4157. https://doi.org/10.1029/2018JD029758.

Bhattacharya, A., Chakraborty, A., Venugopal, V., 2017. Role of aerosols in modulating cloud properties during active-break cycle of Indian summer monsoon. Clim. Dyn. 49, 2131-2145. https://doi.org/10.1007/s00382-016-3437-4.

Binkowski, F.S., Roselle, S.J., 2003. Models-3 Community Multiscale Air Quality (CMAQ) model aerosol component 1. Model description. J. Geophys. Res. Atmos. 108. https://doi.org/10.1029/2001JD001409.

Binkowski, F.S., Shankar, U., 1995. The regional particulate matter model: 1. Model description and preliminary results. J. Geophys. Res. Atmos. 100, 26191–26209. https://doi.org/10.1029/95JD02093.

Bollasina, M.A., Ming, Y., Ramaswamy, V., 2011. Anthropogenic aerosols and the weakening of the South Asian summer monsoon. Science (80-.). 334, 502-505. https://doi.org/10.1126/science.1204994.

Boucher, O., Randall, D., Artaxo, P., Bretherton, C., Feingold, G., Forster, P., Kerminen, V.M., Kondo, Y., Liao, H., Lohmann, U., 2013. Clouds and aerosols. Climate change 2013: The physical science basis. Contribution of working group I to the fifth assessment report of the intergovernmental panel on climate change. Cambridge Univ. Press. Cambridge, United Kingdom New York, NY, USA 571-657. https://doi.org/10.13140/2.1.1081.8883.

Bran, S.H., Jose, S., Srivastava, R., 2018. Investigation of optical and radiative properties of aerosols during an intense dust storm: A regional climate modeling approach. J. Atmos. Solar-Terrestrial Phys. 168, 21-31. https://doi.org/10.1016/j.jastp.2018.01.003.

Briant, R., Tuccella, P., Deroubaix, A., Khvorostyanov, D., Menut, L., Mailler, S., Turquety, S., 2017. Aerosol-radiation interaction modelling using online coupling between the WRF 3.7.1 meteorological model and the CHIMERE 2016 chemistry-transport model, through the OASIS3-MCT coupler. Geosci. Model Dev. 10, 927-944. https://doi.org/10.5194/gmd-10-927-2017.

Brunekreef, B., Holgate, S.T., 2002. Air pollution and health. Lancet 360, 1233-1242. https://doi.org/10.1016/S0140-6736(02)11274-8.

Brunner, D., Savage, N., Jorba, O., Eder, B., Giordano, L., Badia, A., Balzarini, A., Baro, R., Bianconi, R., Chemel, C., 2015. Comparative analysis of meteorological performance of coupled chemistry-meteorology models in the context of AQMEII phase 2. Atmos. Environ. 115, 470-498. https://doi.org/10.1016/j.atmosenv.2014.12.032.
Byun, D., Schere, K.L., 2006. Review of the governing equations, computational algorithms, and other components of the Models-3 Community Multiscale Air Quality (CMAQ) modeling system. Appl. Mech. Rev. 59, 51-77. https://doi.org/10.1115/1.2128636.
Campbell, P., Zhang, Y., Wang, K., Leung, R., Fan, J., Zheng, B., Zhang, Q., He, K., 2017. Evaluation of a multi-scale WRF-CAM5 simulation during the 2010 East Asian Summer Monsoon. Atmos. Environ. 169, 204-217. https://doi.org/10.1016/j.atmosenv.2017.09.008.
Campbell, P., Zhang, Y., Yahya, K., Wang, K., Hogrefe, C., Pouliot, G., Knote, C., Hodzic, A., San Jose, R., Perez, J.L., 2015. A multi-model assessment for the 2006 and 2010 simulations under the Air Quality Model Evaluation International Initiative (AQMEII) phase 2 over North America: Part I. Indicators of the sensitivity of O_3 and $PM_{2.5}$ formation regimes. Atmos. Environ. 115, 569-586. https://doi.org/10.1016/j.atmosenv.2014.12.026.
Carlton, A.G., Bhave, P. V, Napelenok, S.L., Edney, E.O., Sarwar, G., Pinder, R.W., Pouliot, G.A., Houyoux, M., 2010. Model representation of secondary organic aerosol in CMAQv4.7. Environ. Sci. Technol. 44, 8553–8560. https://doi.org/10.1021/es100636q.
Casazza, M., Lega, M., Liu, G., Ulgiati, S., Endreny, T.A., 2018. Aerosol pollution, including eroded soils, intensifies cloud growth, precipitation, and soil erosion: A review. J. Clean. Prod. 189, 135-144. https://doi.org/10.1016/j.jclepro.2018.04.004.
Chang, S., 2018. Characteristics of aerosols and cloud condensation nuclei (CCN) over China investigated by the two-way coupled WRF-CMAQ air quality model.
Chapman, E.G., Jr, W.I.G., Easter, R.C., Barnard, J.C., Ghan, S.J., Pekour, M.S., Fast, J.D., 2009. and Physics Coupling aerosol-cloud-radiative processes in the WRF-Chem model?: Investigating the radiative impact of elevated point sources 945-964. https://doi.org/10.5194/acp-9-945-2009.
Chen, D.-S., Ma, X., Xie, X., Wei, P., Wen, W., Xu, T., Yang, N., Gao, Q., Shi, H., Guo, X., 2015. Modelling the effect of aerosol feedbacks on the regional meteorology factors over China. Aerosol. Air. Qual. Res 15, 1559-1579. https://doi.org/10.4209/aaqr.2014.11.0272.
Chen, J., Li, C., Ristovski, Z., Milic, A., Gu, Y., Islam, M.S., Wang, S., Hao, J., Zhang, H., He, C., 2017. A review of biomass burning: Emissions and impacts on air quality, health and climate in China. Sci. Total Environ. 579, 1000-1034. https://doi.org/10.1016/j.scitotenv.2016.11.025.
Chen, L., Gao, Y., Zhang, M., Fu, J.S., Zhu, J., Liao, H., Li, J., Huang, K., Ge, B., Wang, X., 2019a. MICS-Asia III: Multi-model comparison and evaluation of aerosol over East Asia. Atmos. Chem. Phys. 19, 11911-11937. https://doi.org/10.5194/acp-19-11911-2019.
Chen, L., Zhu, J., Liao, H., Gao, Y., Qiu, Y., Zhang, M., Liu, Z., Li, N., Wang, Y., 2019b. Assessing the formation and evolution mechanisms of severe haze pollution in the Beijing-Tianjin-Hebei region using process analysis. Atmos. Chem. Phys. 19, 10845-10864. https://doi.org/10.5194/acp-19-10845-2019.
Chen, S., Huang, J., Kang, L., Wang, H., Ma, X., He, Y., Yuan, T., Yang, B., Huang, Z., Zhang, G., 2017a. Emission, transport, and radiative effects of mineral dust from the Taklimakan and Gobi deserts: comparison of measurements and model results. Atmos. Chem. Phys. 17. https://doi.org/10.5194/acp-17-2401-2017.
Chen, S., Huang, J., Qian, Y., Zhao, C., Kang, L., Yang, B., Wang, Y., Liu, Y., Yuan, T., Wang, T., 2017b. An overview of mineral dust modeling over East Asia. J. Meteorol. Res. 31, 633-653. https://doi.org/10.1007/s13351-017-6142-2.
Chen, S., Huang, J., Zhao, C., Qian, Y., Leung, L.R., Yang, B., 2013. Modeling the transport and radiative forcing of Taklimakan dust over the Tibetan Plateau: A case study in the summer of 2006. J. Geophys. Res. Atmos. 118, 797-812. https://doi.org/10.1002/jgrd.50122.
Chen, S., Zhao, C., Qian, Y., Leung, L.R., Huang, J., Huang, Z., Bi, J., Zhang, W., Shi, J., Yang, L., 2014. Regional modeling of dust mass balance and radiative forcing over East Asia using WRF-Chem. Aeolian Res. 15, 15-30. https://doi.org/10.1016/j.aeolia.2014.02.001.
Chen, X., Wang, Zifa, Yu, F., Pan, X., Li, J., Ge, B., Wang, Zhe, Hu, M., Yang, W., Chen, H., 2017. Estimation of atmospheric aging time of black carbon particles in the polluted atmosphere over central-eastern China using microphysical process analysis in regional chemical transport model. Atmos. Environ. 163, 44–56. https://doi.org/j.atmosenv.2017.05.016.

Chen, X., Yang, W., Wang, Zifa, Li, J., Hu, M., An, J., Wu, Q., Wang, Zhe, Chen, H., Wei, Y., 2019. Improving new particle formation simulation by coupling a volatility-basis set (VBS) organic aerosol module in NAQPMS+APM. Atmos. Environ. 204, 1–11. https://doi.org/j.atmosenv.2019.01.053.

Chen, X., Yu, F., Yang, W., Sun, Y., Chen, H., Du, W., Zhao, J., Wei, Y., Wei, L., Du, H., 2021. Global–regional nested simulation of particle number concentration by combing microphysical processes with an evolving organic aerosol module. Atmos. Chem. Phys. 21, 9343–9366.

Chen, Y., Zhang, Y., Fan, J., Leung, L.-Y.R., Zhang, Q., He, K., 2015. Application of an online-coupled regional climate model, WRF-CAM5, over East Asia for examination of ice nucleation schemes: Part I. Comprehensive model evaluation and trend analysis for 2006 and 2011. Climate 3, 627-667. https://doi.org/10.3390/cli3030627.

Choobari, O.A., Zawar-Reza, P., Sturman, A., 2014. The global distribution of mineral dust and its impacts on the climate system: A review. Atmos. Res. 138, 152-165. https://doi.org/10.1016/j.atmosres.2013.11.007.

Chung, C.E., 2012. Aerosol direct radiative forcing: a review, Atmospheric Aerosols-Regional Characteristics-Chemistry and Physics; Abdul-Razzak, H., Ed. https://doi.org/10.5772/50248.

Conibear, L., Butt, E.W., Knote, C., Arnold, S.R., Spracklen, D. V, 2018b. Residential energy use emissions dominate health impacts from exposure to ambient particulate matter in India. Nat. Commun. 9, 1-9. https://doi.org/10.1038/s41467-018-02986-7.

Conibear, L., Butt, E.W., Knote, C., Arnold, S.R., Spracklen, D. V., 2018a. Stringent Emission Control Policies Can Provide Large Improvements in Air Quality and Public Health in India. GeoHealth 2, 196-211. https://doi.org/10.1029/2018gh000139.

Conti, G.O., Heibati, B., Kloog, I., Fiore, M., Ferrante, M., 2017. A review of AirQ Models and their applications for forecasting the air pollution health outcomes. Environ. Sci. Pollut. Res. 24, 6426-6445. https://doi.org/10.1007/s11356-016-8180-1.

Corbin, J.C., Gysel-Beer, M., 2019. Detection of tar brown carbon with a single particle soot photometer (SP2). Atmos. Chem. Phys. 19, 15673–15690.

Craig, A., Valcke, S., Coquart, L., 2017. Development and performance of a new version of the OASIS coupler, OASIS3-MCT_3. 0. Geosci. Model Dev. 10, 3297. https://doi.org/10.5194/gmd-10-3297-2017.

Cuchiara, G.C., Li, X., Carvalho, J., Rappenglück, B., 2014. Intercomparison of planetary boundary layer parameterization and its impacts on surface ozone concentration in the WRF/Chem model for a case study in Houston/Texas. Atmos. Environ. 96, 175-185. https://doi.org/10.1016/j.atmosenv.2014.07.013.

Dahutia, P., Pathak, B., Bhuyan, P.K., 2019. Vertical distribution of aerosols and clouds over north-eastern South Asia: Aerosol-cloud interactions. Atmos. Environ. 215, 116882. https://doi.org/10.1016/j.atmosenv.2019.116882.

Ding, A.J., Huang, X., Nie, W., Sun, J.N., Kerminen, V., Pet?j?, T., Su, H., Cheng, Y.F., Yang, X., Wang, M.H., 2016. Enhanced haze pollution by black carbon in megacities in China. Geophys. Res. Lett. 43, 2873-2879. https://doi.org/10.1002/2016GL067745.

Ding, Q.J., Sun, J., Huang, X., Ding, A., Zou, J., Yang, X., Fu, C., 2019. Impacts of black carbon on the formation of advection-radiation fog during a haze pollution episode in eastern China. Atmos. Chem. Phys. 19, 7759-7774. https://doi.org/10.5194/acp-19-7759-2019.

Dipu, S., Prabha, T. V, Pandithurai, G., Dudhia, J., Pfister, G., Rajesh, K., Goswami, B.N., 2013. Impact of elevated aerosol layer on the cloud macrophysical properties prior to monsoon onset. Atmos. Environ. 70, 454-467. https://doi.org/10.1016/j.atmosenv.2012.12.036.

Donat, M.G., Lowry, A.L., Alexander, L. V, O'Gorman, P.A., Maher, N., 2016. More extreme precipitation in the world's dry and wet regions. Nat. Clim. Chang. 6, 508-513. https://doi.org/10.1038/nclimate2941.

Dong, X., Fu, J.S., Huang, K., Zhu, Q., Tipton, M., 2019. Regional Climate Effects of Biomass Burning and Dust in East Asia: Evidence From Modeling and Observation. Geophys. Res. Lett. 46, 11490-11499. https://doi.org/10.1029/2019GL083894.

Easter, R.C., Ghan, S.J., Zhang, Y., Saylor, R.D., Chapman, E.G., Laulainen, N.S., Abdul-Razzak, H., Leung, L.R., Bian, X., Zaveri, R.A., 2004. MIRAGE: Model description and evaluation of aerosols and trace gases. J. Geophys. Res. Atmos. 109. https://doi.org/10.1029/2004JD004571.

Eck, T.F., Holben, B.N., Reid, J.S., Xian, P., Giles, D.M., Sinyuk, A., Smirnov, A., Schafer, J.S., Slutsker, I., Kim, J., 2018. Observations of the interaction and transport of fine mode aerosols with cloud and/or fog in Northeast Asia from Aerosol Robotic Network and satellite remote sensing. J. Geophys. Res. Atmos. 123, 5560-5587. https://doi.org/10.1029/2018JD028313.

El-Harbawi, M., 2013. Air quality modelling, simulation, and computational methods: a review. Environ. Rev. 21, 149-179. https://doi.org/10.1139/er-2012-0056.

ENVIRON, U.G., 2008. Comprehensive Air Quality Model with Extensions (CAMx). Version 4.50. Env. Int. Corp. Novato.

EPA, 2018. Meteorological Model Performance for Annual 2016 Simulation WRF v3.8. United States Environ. Prot. Agency.

Fahey, K.M., Carlton, A.G., Pye, H.O.T., Baek, J., Hutzell, W.T., Stanier, C.O., Baker, K.R., Appel, K.W., Jaoui, M., Offenberg, J.H., 2017. A framework for expanding aqueous chemistry in the Community Multiscale Air Quality (CMAQ) model version 5.1. Geosci. Model Dev. 10, 1587–1605. https://doi.org/10.5194/gmd-10-1587-2017.

Fan, J., Rosenfeld, D., Yang, Y., Zhao, C., Leung, L.R., Li, Z., 2015. Substantial contribution of anthropogenic air pollution to catastrophic floods in Southwest China. Geophys. Res. Lett. 42, 6066-6075. https://doi.org/10.1002/2015GL064479.

Fan, J., Rosenfeld, D., Zhang, Y., Giangrande, S.E., Li, Z., Machado, L.A.T., Martin, S.T., Yang, Y., Wang, J., Artaxo, P., 2018. Substantial convection and precipitation enhancements by ultrafine aerosol particles. Science (80-.). 359, 411-418. https://doi.org/10.1126/science.aan8461.

Fan, J., Wang, Y., Rosenfeld, D., Liu, X., 2016. Review of aerosol-cloud interactions: Mechanisms, significance, and challenges. J. Atmos. Sci. 73, 4221-4252. https://doi.org/10.1175/JAS-D-16-0037.1.

Fast, J.D., Gustafson Jr, W.I., Easter, R.C., Zaveri, R.A., Barnard, J.C., Chapman, E.G., Grell, G.A., Peckham, S.E., 2006. Evolution of ozone, particulates, and aerosol direct radiative forcing in the vicinity of Houston using a fully coupled meteorology-chemistry-aerosol model. J. Geophys. Res. Atmos. 111. https://doi.org/10.1029/2005JD006721.

Feingold, G., Eberhard, W.L., Veron, D.E., Previdi, M., 2003. First measurements of the Twomey indirect effect using ground-based remote sensors. Geophys. Res. Lett. 30. https://doi.org/10.1029/2002GL016633.

Feng, Y., Kotamarthi, V.R., Coulter, R., Zhao, C., Cadeddu, M., 2016. Radiative and thermodynamic responses to aerosol extinction profiles during the pre-monsoon month over South Asia. Atmos. Chem. Phys. 16. https://doi.org/10.5194/acp-16-247-2016.

Foley, K.M., Roselle, S.J., Appel, K.W., Bhave, P. V, Pleim, J.E., Otte, T.L., Mathur, R., Sarwar, G., Young, J.O., Gilliam, R.C., 2010. Incremental testing of the Community Multiscale Air Quality (CMAQ) modeling system version 4.7. Geosci. Model Dev. 3, 205–226. https://doi.org/10.5194/gmd-3-205-2010.

Forkel, R., Brunner, D., Baklanov, A., Balzarini, A., Hirtl, M., Honzak, L., Jiménez-Guerrero, P., Jorba, O., Pérez, J.L., San José, R., 2016. A multi-model case study on aerosol feedbacks in online coupled chemistry-meteorology models within the cost action ES1004 EuMetChem, in: Air Pollution Modeling and Its Application XXIV. Springer, pp. 23-28. https://doi.org/10.1007/978-3-319-24478-5_4.

Fu, P., Aggarwal, S.G., Chen, J., Li, J., Sun, Y., Wang, Z., Chen, H., Liao, H., Ding, A., Umarji, G.S., 2016. Molecular markers of secondary organic aerosol in Mumbai, India. Environ. Sci. Technol. 50, 4659–4667. https://doi.org/10.1021/acs.est.6b00372.

Gao, C., Zhang, X., Xiu, A., Huang, L., Zhao, H., Wang, K., Tong, Q., 2019. Spatiotemporal distribution of biogenic volatile organic compounds emissions in China. Acta Sci. Circumstantiae 39, 4140-4151. https://doi.org/10.13671/j.hjkxxb.2019.0243.

Gao, J., Zhu, B., Xiao, H., Kang, H., Pan, C., Wang, D., Wang, H., 2018. Effects of black carbon and boundary layer interaction on surface ozone in Nanjing, China. Atmos. Chem. Phys. 18. https://doi.org/10.5194/acp-18-7081-2018.

Gao, M., Carmichael, G.R., Saide, P.E., Lu, Z., Yu, M., Streets, D.G., Wang, Z., 2016a. Response of winter fine particulate matter concentrations to emission and meteorology changes in North China. Atmos. Chem. Phys. 16, 11837. https://doi.org/10.5194/acp-16-11837-2016.

Gao, M., Carmichael, G.R., Wang, Y., Saide, P.E., Liu, Z., Xin, J., Shan, Y., Wang, Z., 2017a. Chemical and Meteorological Feedbacks in the Formation of Intense Haze Events, in: Air Pollution in Eastern Asia: An Integrated Perspective. Springer, pp. 437-452. https://doi.org/10.1007/978-3-319-59489-7_21.

Gao, M., Carmichael, G.R., Wang, Y., Saide, P.E., Yu, M., Xin, J., Liu, Z., Wang, Z., 2016b.

Modeling study of the 2010 regional haze event in the North China Plain. Atmos. Chem. Phys. 16, 1673. https://doi.org/10.5194/acp-16-1673-2016.
Gao, M., Guttikunda, S.K., Carmichael, G.R., Wang, Y., Liu, Z., Stanier, C.O., Saide, P.E., Yu, M., 2015. Health impacts and economic losses assessment of the 2013 severe haze event in Beijing area. Sci. Total Environ. 511, 553-561. https://doi.org/10.1016/j.scitotenv.2015.01.005.
Gao, M., Han, Z., Liu, Z., Li, M., Xin, J., Tao, Z., Li, J., Kang, J.E., Huang, K., Dong, X., Zhuang, B., Li, S., Ge, B., Wu, Q., Cheng, Y., Wang, Y., Lee, H.J., Kim, C.H., Fu, J.S., Wang, T., Chin, M., Woo, J.H., Zhang, Q., Wang, Z., Carmichael, G.R., 2018a. Air quality and climate change, Topic 3 of the Model Inter-Comparison Study for Asia Phase III (MICS-Asia III)- Part 1: Overview and model evaluation. Atmos. Chem. Phys. 18, 4859-4884. https://doi.org/10.5194/acp-18-4859-2018.
Gao, M., Ji, D., Liang, F., Liu, Y., 2018b. Attribution of aerosol direct radiative forcing in China and India to emitting sectors. Atmos. Environ. 190, 35-42. https://doi.org/10.1016/j.atmosenv.2018.07.011.
Gao, M., Liu, Z., Wang, Y., Lu, X., Ji, D., Wang, L., Li, M., Wang, Z., Zhang, Q., Carmichael, G.R., 2017b. Distinguishing the roles of meteorology, emission control measures, regional transport, and co-benefits of reduced aerosol feedbacks in "APEC Blue." Atmos. Environ. 167, 476-486. https://doi.org/10.1016/j.atmosenv.2017.08.054.
Gao, M., Saide, P.E., Xin, J., Wang, Yuesi, Liu, Z., Wang, Yuxuan, Wang, Z., Pagowski, M., Guttikunda, S.K., Carmichael, G.R., 2017c. Estimates of health impacts and radiative forcing in winter haze in eastern China through constraints of surface $PM_{2.5}$ predictions. Environ. Sci. Technol. 51, 2178-2185. https://doi.org/10.1021/acs.est.6b03745.
Gao, Y., Zhang, M., 2018. Changes in the diurnal variations of clouds and precipitation induced by anthropogenic aerosols over East China in August 2008. Atmos. Pollut. Res. 9, 513-525. https://doi.org/10.1016/j.apr.2017.11.013.
Gao, Y., Zhang, M., Liu, X., Wang, L., 2016. Change in diurnal variations of meteorological variables induced by anthropogenic aerosols over the North China Plain in summer 2008. Theor. Appl. Climatol. 124, 103-118. https://doi.org/10.1007/s00704-015-1403-4.
Gao, Y., Zhang, M., Liu, X., Zhao, C., 2012. Model Analysis of the Anthropogenic Aerosol Effect on Clouds over East Asia. Atmos. Ocean. Sci. Lett. 5, 1-7. https://doi.org/10.1080/16742834.2012.11446968.
Gao, Y., Zhang, M., Liu, Z., Wang, L., Wang, P., Xia, X., Tao, M., Zhu, L., 2015. Modeling the feedback between aerosol and meteorological variables in the atmospheric boundary layer during a severe fog-haze event over the North China Plain. Atmos. Chem. Phys. 15. https://doi.org/10.5194/acp-15-4279-2015.
Gao, Y., Zhao, C., Liu, X., Zhang, M., Leung, L.R., 2014. WRF-Chem simulations of aerosols and anthropogenic aerosol radiative forcing in East Asia. Atmos. Environ. 92, 250-266. https://doi.org/10.1016/j.atmosenv.2014.04.038.
García-Díez, M., Fernández, J., Fita, L., Yagüe, C., 2013. Seasonal dependence of WRF model biases and sensitivity to PBL schemes over Europe. Q. J. R. Meteorol. Soc. 139, 501-514. https://doi.org/10.1002/qj.1976.
Ge, C., Wang, J., Reid, J.S., 2014. Mesoscale modeling of smoke transport over the Southeast Asian Maritime Continent: coupling of smoke direct radiative effect below and above the low-level clouds. Atmos. Chem. Phys. 14, 159. https://doi.org/10.5194/acp-14-159-2014.
Gery, M.W., Whitten, G.Z., Killus, J.P., Dodge, M.C., 1989. A photochemical kinetics mechanism for urban and regional scale computer modeling. J. Geophys. Res. Atmos. 94, 12925–12956. https://doi.org/10.1029/JD094iD10p12925.
Ghan, S.J., Zaveri, R.A., 2007. Parameterization of optical properties for hydrated internally mixed aerosol. J. Geophys. Res. Atmos. 112, 1–10. https://doi.org/10.1029/2006JD007927.
Ghude, S.D., Chate, D.M., Jena, C., Beig, G., Kumar, R., Barth, M.C., Pfister, G.G., Fadnavis, S., Pithani, P., 2016. Premature mortality in India due to $PM_{2.5}$ and ozone exposure. Geophys. Res. Lett. 43, 4650-4658. https://doi.org/10.1002/2016GL068949.
Giorgi, F., Chameides, W.L., 1986. Rainout lifetimes of highly soluble aerosols and gases as inferred from simulations with a general circulation model. J. Geophys. Res. Atmos. 91, 14367–14376. https://doi.org/10.1029/JD091iD13p14367.
Gong, S.L., Barrie, L.A., Blanchet, J., 1997. Modeling sea-salt aerosols in the atmosphere: 1. Model development. J. Geophys. Res. Atmos. 102, 3805–3818. https://doi.org/10.1029/96JD02953.

Gong, S.L., Barrie, L.A., Blanchet, J., Von Salzen, K., Lohmann, U., Lesins, G., Spacek, L., Zhang, L.M., Girard, E., Lin, H., 2003. Canadian Aerosol Module: A size-segregated simulation of atmospheric aerosol processes for climate and air quality models 1. Module development. J. Geophys. Res. Atmos. 108, AAC-3. https://doi.org/10.1029/2001JD002002

Gong, S.L., Zhang, X.Y., Zhao, T.L., McKendry, I.G., Jaffe, D.A., Lu, N.M., 2003. Characterization of soil dust aerosol in China and its transport and distribution during 2001 ACE-Asia: 2. Model simulation and validation. J. Geophys. Res. Atmos. 108. https://doi.org/10.1029/2002JD002633.

Goren, T., Rosenfeld, D., 2014. Decomposing aerosol cloud radiative effects into cloud cover, liquid water path and Twomey components in marine stratocumulus. Atmos. Res. 138, 378-393. https://doi.org/10.1016/j.atmosres.2013.12.008.

Govardhan, G., Nanjundiah, R.S., Satheesh, S.K., Krishnamoorthy, K., Kotamarthi, V.R., 2015. Performance of WRF-Chem over Indian region: Comparison with measurements. J. Earth Syst. Sci. 124, 875-896. https://doi.org/10.1007/s12040-015-0576-7.

Govardhan, G.R., Nanjundiah, R.S., Satheesh, S.K., Moorthy, K.K., Takemura, T., 2016. Inter-comparison and performance evaluation of chemistry transport models over Indian region. Atmos. Environ. 125, 486-504. https://doi.org/10.1016/j.atmosenv.2015.10.065.

Gray, L.J., Beer, J., Geller, M., Haigh, J.D., Lockwood, M., Matthes, K., Cubasch, U., Fleitmann, D., Harrison, G., Hood, L., 2010. Solar influences on climate. Rev. Geophys. 48. https://doi.org/10.1029/2009RG000282.

Grell, G., Freitas, S.R., Stuefer, M., Fast, J., 2011. Inclusion of biomass burning in WRF-Chem: impact of wildfires on weather forecasts. Atmos. Chem. Phys 11, 5289-5303. https://doi.org/10.5194/acp-11-5289-2011.

Grell, G.A., Peckham, S.E., Schmitz, R., McKeen, S.A., Frost, G., Skamarock, W.C., Eder, B., 2005. Fully coupled “online” chemistry within the WRF model. Atmos. Environ. 39, 6957-6975. https://doi.org/10.1016/j.atmosenv.2005.04.027.

Gro?, S., Esselborn, M., Weinzierl, B., Wirth, M., Fix, A., Petzold, A., 2013. Aerosol classification by airborne high spectral resolution lidar observations. Atmos. Chem. Phys. 13, 2487. https://doi.org/10.5194/acp-13-2487-2013.

Guo, J., Deng, M., Fan, J., Li, Z., Chen, Q., Zhai, P., Dai, Z., Li, X., 2014. Precipitation and air pollution at mountain and plain stations in northern China: Insights gained from observations and modeling. J. Geophys. Res. Atmos. 119, 4793-4807. https://doi.org/10.1002/2013JD021161.

Guo, J., Liu, H., Li, Z., Rosenfeld, D., Jiang, M., Xu, W., Jiang, J.H., 2018. Aerosol-induced changes in the vertical structure of precipitation?: a perspective of TRMM precipitation radar 13329-13343. https://doi.org/10.5194/acp-18-13329-2018.

Gurjar, B.R., Ravindra, K., Nagpure, A.S., 2016. Air pollution trends over Indian megacities and their local-to-global implications. Atmos. Environ. 142, 475-495. https://doi.org/10.1016/j.atmosenv.2016.06.030.

Haywood, J., Boucher, O., 2000. Estimates of the direct and indirect radiative forcing due to tropospheric aerosols: A review. Rev. Geophys. 38, 513-543. https://doi.org/10.1029/1999RG000078.

He, J., Zhang, Y., 2014. Improvement and further development in CESM/CAM5: gas-phase chemistry and inorganic aerosol treatments. Atmos. Chem. Phys. 14, 9171–9200. https://doi.org/10.5194/acp-14-9171-2014.

He, J., Zhang, Y., Wang, K., Chen, Y., Leung, L.R., Fan, J., Li, M., Zheng, B., Zhang, Q., Duan, F., 2017. Multi-year application of WRF-CAM5 over East Asia-Part I: Comprehensive evaluation and formation regimes of O_3 and $PM_{2.5}$. Atmos. Environ. 165, 122-142. https://doi.org/10.1016/j.atmosenv.2017.06.015.

Hodshire, A.L., Akherati, A., Alvarado, M.J., Brown-Steiner, B., Jathar, S.H., Jimenez, J.L., Kreidenweis, S.M., Lonsdale, C.R., Onasch, T.B., Ortega, A.M., 2019. Aging effects on biomass burning aerosol mass and composition: A critical review of field and laboratory studies. Environ. Sci. Technol. 53, 10007-10022. https://doi.org/10.1021/acs.est.9b02588.

Hodzic, A., Jimenez, J.L., 2011. Modeling anthropogenically controlled secondary organic aerosols in a megacity: A simplified framework for global and climate models. Geosci. Model Dev. 4, 901–917. https://doi.org/10.5194/gmd-4-901-2011.

Hong, C., Zhang, Q., Zhang, Y., Davis, S.J., Tong, D., Zheng, Y., Liu, Z., Guan, D., He, K.,

Schellnhuber, H.J., 2019. Impacts of climate change on future air quality and human health in China. Proc. Natl. Acad. Sci. 116, 17193-17200. https://doi.org/10.1073/pnas.1812881116.
Hong, C., Zhang, Q., Zhang, Y., Tang, Y., Tong, D., He, K., 2017. Multi-year downscaling application of two-way coupled WRF v3.4 and CMAQ v5.0.2 over east Asia for regional climate and air quality modeling: model evaluation and aerosol direct effects. Geosci. Model Dev. 10. https://doi.org/10.5194/gmd-10-2447-2017.
Hu, X., Klein, P.M., Xue, M., 2013. Evaluation of the updated YSU planetary boundary layer scheme within WRF for wind resource and air quality assessments. J. Geophys. Res. Atmos. 118, 10-490. https://doi.org/10.1002/jgrd.50823.
Huang, J., Wang, T., Wang, W., Li, Z., Yan, H., 2014. Climate effects of dust aerosols over East Asian arid and semiarid regions. J. Geophys. Res. Atmos. 119, 11-398. https://doi.org/10.1002/2014JD021796.
Huang, L., Lin, W., Li, F., Wang, Y., Jiang, B., 2019. Climate impacts of the biomass burning in Indochina on atmospheric conditions over southern China. Aerosol Air Qual. Res. 19, 2707-2720. https://doi.org/10.4209/aaqr.2019.01.0028.
Huang, X., Ding, A., Liu, L., Liu, Q., Ding, K., Niu, X., Nie, W., Xu, Z., Chi, X., Wang, M., 2016. Effects of aerosol-radiation interaction on precipitation during biomass-burning season in East China. Atmos. Chem. Phys. 16. https://doi.org/10.5194/acp-16-10063-2016.
Huang, X., Song, Y., Zhao, C., Cai, X., Zhang, H., Zhu, T., 2015. Direct radiative effect by multicomponent aerosol over China. J. Clim. 28, 3472-3495. https://doi.org/10.1175/JCLI-D-14-00365.1.
Illingworth, A.J., Barker, H.W., Beljaars, A., Ceccaldi, M., Chepfer, H., Clerbaux, N., Cole, J., Delano?, J., Domenech, C., Donovan, D.P., 2015. The EarthCARE satellite: The next step forward in global measurements of clouds, aerosols, precipitation, and radiation. Bull. Am. Meteorol. Soc. 96, 1311-1332. https://doi.org/10.1175/BAMS-D-12-00227.1.
Im, U., Bianconi, R., Solazzo, E., Kioutsioukis, I., Badia, A., Balzarini, A., Baró, R., Bellasio, R., Brunner, D., Chemel, C., 2015a. Evaluation of operational online-coupled regional air quality models over Europe and North America in the context of AQMEII phase 2. Part II: Particulate matter. Atmos. Environ. 115, 421-441. https://doi.org/10.1016/j.atmosenv.2014.08.072.
Im, U., Bianconi, R., Solazzo, E., Kioutsioukis, I., Badia, A., Balzarini, A., Baró, R., Bellasio, R., Brunner, D., Chemel, C., 2015b. Evaluation of operational on-line-coupled regional air quality models over Europe and North America in the context of AQMEII phase 2. Part I: Ozone. Atmos. Environ. 115, 404-420. https://doi.org/10.1016/j.atmosenv.2014.09.042.
IPCC, 2007. Climate change 2007: Synthesis Report. Contribution of Working Groups I, II and III to the Fifth Assessment Report of the Intergovernmental Panel on Climate Change.
IPCC, 2014. Climate change 2014: Synthesis Report. Contribution of Working Groups I, II and III to the fifth assessment report of the Intergovernmental Panel on Climate Change.
Jacobson, M.Z., 2001. Strong radiative heating due to the mixing state of black carbon in atmospheric aerosols 409, 695-697. https://doi.org/10.1038/35055518.
Jacobson, M.Z., 2002. Analysis of aerosol interactions with numerical techniques for solving coagulation, nucleation, condensation, dissolution, and reversible chemistry among multiple size distributions. J. Geophys. Res. Atmos. 107, AAC-2. https://doi.org/10.1029/2001JD002044.
Jacobson, M.Z., 2003. Development of mixed-phase clouds from multiple aerosol size distributions and the effect of the clouds on aerosol removal. J. Geophys. Res. Atmos. 108. https://doi.org/10.1029/2002JD002691.
Jacobson, M.Z., 2012. Investigating cloud absorption effects: Global absorption properties of black carbon, tar balls, and soil dust in clouds and aerosols. J. Geophys. Res. Atmos. 117. https://doi.org/10.1029/2011JD017218.
Jacobson, M.Z., Jacobson, M.Z., 1999. Fundamentals of atmospheric modeling. Cambridge university press.
Jacobson, M.Z., Jadhav, V., 2018. World estimates of PV optimal tilt angles and ratios of sunlight incident upon tilted and tracked PV panels relative to horizontal panels. Sol. Energy 169, 55–66. https://doi.org/10.1016/j.solener.2018.04.030.
Jacobson, M.Z., Kaufman, Y.J., Rudich, Y., 2007. Examining feedbacks of aerosols to urban climate with a model that treats 3-D clouds with aerosol inclusions. J. Geophys. Res. Atmos. 112. https://doi.org/10.1029/2007JD008922.

Jacobson, M.Z., Nghiem, S. V, Sorichetta, A., 2019. Short-term impacts of the megaurbanizations of New Delhi and Los Angeles between 2000 and 2009. J. Geophys. Res. Atmos. 124, 35–56. https://doi.org/10.1029/2018JD029310.

Jacobson, M.Z., Nghiem, S. V, Sorichetta, A., Whitney, N., 2015. Ring of impact from the mega-urbanization of Beijing between 2000 and 2009. J. Geophys. Res. Atmos. 120, 5740–5756. https://doi.org/10.1002/2014JD023008.

Jacobson, M.Z., Turco, R.P., 1995. Simulating condensational growth, evaporation, and coagulation of aerosols using a combined moving and stationary size grid. Aerosol Sci. Technol. 22, 73–92. https://doi.org/10.1080/02786829408959729.

Jacobson, M.Z., Turco, R.P., Jensen, E.J., Toon, O.B., 1994. Modeling coagulation among particles of different composition and size. Atmos. Environ. 28, 1327–1338. https://doi.org/10.1016/1352-2310(94)90280-1.

Jena, C., Ghude, S.D., Pfister, G.G., Chate, D.M., Kumar, R., Beig, G., Surendran, D.E., Fadnavis, S., Lal, D.M., 2015. Influence of springtime biomass burning in South Asia on regional ozone (O_3): A model based case study. Atmos. Environ. 100, 37-47. https://doi.org/10.1016/j.atmosenv.2014.10.027.

Jeong, J.I., Park, R.J., 2017. Winter monsoon variability and its impact on aerosol concentrations in East Asia. Environ. Pollut. 221, 285-292. https://doi.org/10.1016/j.envpol.2016.11.075.

Jia, X., Guo, X., 2012. Impacts of Anthropogenic Atmospheric Pollutant on Formation and Development of a Winter Heavy Fog Event. Chinese J. Atmos. Sci. 36, 995-1008. https://doi.org/10.1007/s11783-011-0280-z.

Jia, X., Quan, J., Zheng, Z., Liu, X., Liu, Q., He, H., Liu, Y., 2019. Impacts of Anthropogenic Aerosols on Fog in North China Plain. J. Geophys. Res. Atmos. 124, 252-265. https://doi.org/10.1029/2018JD029437.

Jiang, B., Huang, B., Lin, W., Xu, S., 2016. Investigation of the effects of anthropogenic pollution on typhoon precipitation and microphysical processes using WRF-Chem. J. Atmos. Sci. 73, 1593-1610. https://doi.org/10.1175/JAS-D-15-0202.1.

Jiang, B., Lin, W., Li, F., Chen, B., 2019a. Simulation of the effects of sea-salt aerosols on cloud ice and precipitation of a tropical cyclone. Atmos. Sci. Lett. 20, e936. https://doi.org/10.1002/asl.936.

Jiang, B., Lin, W., Li, F., Chen, J., 2019b. Sea-salt aerosol effects on the simulated microphysics and precipitation in a tropical cyclone. J. Meteorol. Res. 33, 115-125. https://doi.org/10.1007/s13351-019-8108-z.

Jiang, X., Wiedinmyer, C., Carlton, A.G., 2012. Aerosols from fires: An examination of the effects on ozone photochemistry in the Western United States. Environ. Sci. Technol. 46, 11878–11886. https://doi.org/10.1021/es301541k.

Jimenez, P.A., Hacker, J.P., Dudhia, J., Haupt, S.E., Ruiz-Arias, J.A., Gueymard, C.A., Thompson, G., Eidhammer, T., Deng, A., 2016. WRF-Solar: Description and clear-sky assessment of an augmented NWP model for solar power prediction. Bull. Am. Meteorol. Soc. 97, 1249-1264. https://doi.org/10.1175/BAMS-D-14-00279.1.

Jin, Q., Wei, J., Yang, Z.-L., Pu, B., Huang, J., 2015. Consistent response of Indian summer monsoon to Middle East dust in observations and simulations. Atmos. Chem. Phys. 15, 9897-9915. https://doi.org/10.5194/acp-15-9897-2015.

Jin, Q., Yang, Z.-L., Wei, J., 2016a. Seasonal responses of Indian summer monsoon to dust aerosols in the Middle East, India, and China. J. Clim. 29, 6329-6349. https://doi.org/10.1175/JCLI-D-15-0622.1.

Jin, Q., Yang, Z.-L., Wei, J., 2016b. High sensitivity of Indian summer monsoon to Middle East dust absorptive properties. Sci. Rep. 6, 1-8. https://doi.org/10.1038/srep30690.

Jung, J., Souri, A.H., Wong, D.C., Lee, S., Jeon, W., Kim, J., Choi, Y., 2019. The Impact of the Direct Effect of Aerosols on Meteorology and Air Quality Using Aerosol Optical Depth Assimilation During the KORUS-AQ Campaign. J. Geophys. Res. Atmos. 124, 8303-8319. https://doi.org/10.1029/2019JD030641.

Kajino, M., Ueda, H., Han, Z., Kudo, R., Inomata, Y., Kaku, H., 2017. Synergy between air pollution and urban meteorological changes through aerosol-radiation-diffusion feedback—A case study of Beijing in January 2013. Atmos. Environ. 171, 98-110. https://doi.org/10.1016/j.atmosenv.2017.10.018.

Kant, S., Panda, J., Gautam, R., 2019. A seasonal analysis of aerosol-cloud-radiation interaction

over Indian region during 2000-2017. Atmos. Environ. 201, 212-222. https://doi.org/10.1016/j.atmosenv.2018.12.044.
Kedia, S., Cherian, R., Islam, S., Das, S.K., Kaginalkar, A., 2016. Regional simulation of aerosol radiative effects and their influence on rainfall over India using WRFChem model. Atmos. Res. 182, 232-242. https://doi.org/10.1016/j.atmosres.2016.07.008.
Kedia, S., Kumar, S., Islam, S., Hazra, A., Kumar, N., 2019a. Aerosols impact on the convective and non-convective rain distribution over the Indian region?: Results from WRF-Chem simulation. Atmos. Environ. 202, 64-74. https://doi.org/10.1016/j.atmosenv.2019.01.020.
Kedia, S., Vellore, R.K., Islam, S., Kaginalkar, A., 2019b. A study of Himalayan extreme rainfall events using WRF-Chem. Meteorol. Atmos. Phys. 131, 1133-1143. https://doi.org/10.1007/s00703-018-0626-1.
Keita, S.A., Girard, E., Raut, J.-C., Leriche, M., Blanchet, J.-P., Pelon, J., Onishi, T., Cirisan, A., 2020. A new parameterization of ice heterogeneous nucleation coupled to aerosol chemistry in WRF-Chem model version 3.5.1: evaluation through ISDAC measurements. Geosci. Model Dev. 13, 5737–5755. https://doi.org/10.5194/gmd-13-5737-2020.
Kim, B., Schwartz, S.E., Miller, M.A., Min, Q., 2003. Effective radius of cloud droplets by ground-based remote sensing: Relationship to aerosol. J. Geophys. Res. Atmos. 108. https://doi.org/10.1029/2003JD003721.
Knote, C., Hodzic, A., Jimenez, J.L., Volkamer, R., Orlando, J.J., Baidar, S., Brioude, J., Fast, J., Gentner, D.R., Goldstein, A.H., 2014. Simulation of semi-explicit mechanisms of SOA formation from glyoxal in aerosol in a 3-D model. Atmos. Chem. Phys. 14, 6213–6239. https://doi.org/10.5194/acp-14-6213-2014.
Koch, D., Del Genio, A.D., 2010. Black carbon semi-direct effects on cloud cover: review and synthesis. Atmos. Chem. Phys. 10. https://doi.org/10.5194/acp-10-7685-2010.
Kong, X., Forkel, R., Sokhi, R.S., Suppan, P., Baklanov, A., Gauss, M., Brunner, D., Barò, R., Balzarini, A., Chemel, C., Curci, G., Jiménez-Guerrero, P., Hirtl, M., Honzak, L., Im, U., Pérez, J.L., Pirovano, G., San Jose, R., Schlünzen, K.H., Tsegas, G., Tuccella, P., Werhahn, J., ?abkar, R., Galmarini, S., 2015. Analysis of meteorology-chemistry interactions during air pollution episodes using online coupled models within AQMEII phase-2. Atmos. Environ. 115, 527-540. https://doi.org/10.1016/j.atmosenv.2014.09.020.
Kuik, F., Lauer, A., Churkina, G., Denier van der Gon, H., Fenner, D., Mar, K., Butler, T., 2016. Air quality modelling in the Berlin-Brandenburg region using WRF-Chem v3. 7.1: sensitivity to resolution of model grid and input data. Geosci. Model Dev. 4339-4363. https://doi.org/10.5194/gmd-9-4339-2016.
Kulmala, M., Laaksonen, A., Pirjola, L., 1998. Parameterizations for sulfuric acid/water nucleation rates. J. Geophys. Res. Atmos. 103, 8301–8307. https://doi.org/10.1029/97JD03718.
Kumar, P., Sokolik, I.N., Nenes, A., 2009. Parameterization of cloud droplet formation for global and regional models: including adsorption activation from insoluble CCN. Atmos. Chem. Phys. 9. https://doi.org/10.5194/acp-9-2517-2009.
Kumar, R., Barth, M.C., Pfister, G.G., Naja, M., Brasseur, G.P., 2014. WRF-Chem simulations of a typical pre-monsoon dust storm in northern India: influences on aerosol optical properties and radiation budget. Atmos. Chem. Phys 14, 2431-2446. https://doi.org/10.5194/acp-14-2431-2014.
Kumar, R., Naja, M., Pfister, G.G., Barth, M.C., Brasseur, G.P., 2012a. Simulations over South Asia using the Weather Research and Forecasting model with Chemistry (WRF-Chem): set-up and meteorological evaluation. Geosci. Model Dev. 5, 321-343. https://doi.org/10.5194/gmd-5-321-2012.
Kumar, R., Naja, M., Pfister, G.G., Barth, M.C., Wiedinmyer, C., Brasseur, G.P., 2012b. Simulations over South Asia using the Weather Research and Forecasting model with Chemistry (WRF-Chem): chemistry evaluation and initial results. Geosci. Model Dev. 5, 619-648. https://doi.org/10.5194/gmd-5-619-2012.
Kuniyal, J.C., Guleria, R.P., 2019. The current state of aerosol-radiation interactions: a mini review. J. Aerosol Sci. 130, 45-54. https://doi.org/10.1016/j.jaerosci.2018.12.010.
Lau, W.K.M., Kim, K.-M., Shi, J.-J., Matsui, T., Chin, M., Tan, Q., Peters-Lidard, C., Tao, W.-K., 2017. Impacts of aerosol-monsoon interaction on rainfall and circulation over Northern India and the Himalaya Foothills. Clim. Dyn. 49, 1945-1960. https://doi.org/10.1007/s00382-016-3430-y.

Lee, H.-H., Chen, S.-H., Kumar, A., Zhang, H., Kleeman, M.J., 2020. Improvement of aerosol activation/ice nucleation in a source-oriented WRF-Chem model to study a winter Storm in California. Atmos. Res. 235, 104790. https://doi.org/10.1016/j.atmosres.2019.104790.

Lee, Y.C., Yang, X., Wenig, M., 2010. Transport of dusts from East Asian and non-East Asian sources to Hong Kong during dust storm related events 1996-2007. Atmos. Environ. 44, 3728-3738. https://doi.org/10.1016/j.atmosenv.2010.03.034.

Lelieveld, J., Bourtsoukidis, E., Brühl, C., Fischer, H., Fuchs, H., Harder, H., Hofzumahaus, A., Holland, F., Marno, D., Neumaier, M., 2018. The South Asian monsoon-pollution pump and purifier. Science (80-.). 361, 270-273. https://doi.org/10.1126/science.aar2501.

Lelieveld, J., Evans, J.S., Fnais, M., Giannadaki, D., Pozzer, A., 2015. The contribution of outdoor air pollution sources to premature mortality on a global scale. Nature 525, 367. https://doi.org/10.1038/nature15371.

Li, J., Chen, X., Wang, Z., Du, H., Yang, W., Sun, Y., Hu, B., Li, Jianjun, Wang, W., Wang, T., 2018. Radiative and heterogeneous chemical effects of aerosols on ozone and inorganic aerosols over East Asia. Sci. Total Environ. 622, 1327-1342. https://doi.org/10.1016/j.scitotenv.2017.12.041.

Li, J., Nagashima, T., Kong, L., Ge, B., Yamaji, K., Fu, J.S., Wang, X., Fan, Q., Itahashi, S., Hyo-Jung, L., 2019. Model evaluation and intercomparison of surface-level ozone and relevant species in East Asia in the context of MICS-Asia Phase III-Part 1: Overview. Atmos. Chem. Phys. 19, 12993-13015. https://doi.org/10.5194/acp-19-12993-2019.

Li, J., Wang, Z., Wang, X., Yamaji, K., Takigawa, M., Kanaya, Y., Pochanart, P., Liu, Y., Irie, H., Hu, B., 2011. Impacts of aerosols on summertime tropospheric photolysis frequencies and photochemistry over Central Eastern China. Atmos. Environ. 45, 1817–1829. https://doi.org/10.1016/j.atmosenv.2011.01.016.

Li, Jie, Chen, X., Wang, Z., Du, H., Yang, W., Sun, Y., Hu, B., Li, Jianjun, Wang, W., Wang, T., 2018. Radiative and heterogeneous chemical effects of aerosols on ozone and inorganic aerosols over East Asia. Sci. Total Environ. 622, 1327–1342. https://doi.org/10.1016/j.scitotenv.2017.12.041.

Li, L., Hong, L., 2014. Role of the Radiative Effect of Black Carbon in Simulated $PM_{2.5}$ Concentrations during a Haze Event in China. Atmos. Ocean. Sci. Lett. 7, 434-440. https://doi.org/10.3878/j.issn.1674-2834.14.0023.

Li, L., Sokolik, I.N., 2018. The Dust Direct Radiative Impact and Its Sensitivity to the Land Surface State and Key Minerals in the WRF-Chem-DuMo Model: A Case Study of Dust Storms in Central Asia. J. Geophys. Res. Atmos. 123, 4564-4582. https://doi.org/10.1029/2017JD027667.

Li, L., Sokolik, I.N., 2018. The Dust Direct Radiative Impact and Its Sensitivity to the Land Surface State and Key Minerals in the WRF-Chem-DuMo Model: A Case Study of Dust Storms in Central Asia. J. Geophys. Res. Atmos. 123, 4564–4582. https://doi.org/10.1029/2017JD027667.

Li, M., Wang, T., Xie, M., Li, S., Zhuang, B., Chen, P., Huang, X., Han, Y., 2018. Agricultural fire impacts on ozone photochemistry over the Yangtze River Delta region, East China. J. Geophys. Res. Atmos. https://doi.org/10.1029/2018JD028582.

Li, M., Wang, T., Xie, M., Li, S., Zhuang, B., Huang, X., Chen, P., Zhao, M., Liu, J., 2019. Formation and evolution mechanisms for two extreme haze episodes in the Yangtze River Delta region of China during winter 2016. J. Geophys. Res. Atmos. 124, 3607-3623. https://doi.org/10.1029/2019JD030535.

Li, M., Zhang, Q., Kurokawa, J., Woo, J.-H., 2017. MIX: a mosaic Asian anthropogenic emission inventory under the international collaboration framework of the MICS-Asia and HTAP. Atmos. Chem. Phys. 17, 935-963. https://doi.org/10.5194/acp-17-935-2017.

Li, M.M., Wang, T., Han, Y., Xie, M., Li, S., Zhuang, B., Chen, P., 2017a. Modeling of a severe dust event and its impacts on ozone photochemistry over the downstream Nanjing megacity of eastern China. Atmos. Environ. 160, 107-123. https://doi.org/10.1016/j.atmosenv.2017.04.010.

Li, M.M., Wang, T., Xie, M., Zhuang, B., Li, S., Han, Y., Chen, P., 2017b. Impacts of aerosol-radiation feedback on local air quality during a severe haze episode in Nanjing megacity, eastern China. Tellus, Ser. B Chem. Phys. Meteorol. 69, 1-16. https://doi.org/10.1080/16000889.2017.1339548.

Li, Z., Guo, J., Ding, A., Liao, H., Liu, J., Sun, Y., Wang, T., Xue, H., Zhang, H., Zhu, B., 2017. Aerosol and boundary-layer interactions and impact on air quality. Natl. Sci. Rev. 4, 810-833. https://doi.org/10.1093/nsr/nwx117.

Li, Z., Lau, W.K.M., Ramanathan, V., Wu, G., Ding, Y., Manoj, M.G., Liu, J., Qian, Y., Li, J., Zhou, T., Fan, J., Rosenfeld, D., Ming, Y., Wang, Y., Huang, J., Wang, B., Xu, X., Lee, S.S., Cribb, M., Zhang, F., Yang, X., Zhao, C., Takemura, T., Wang, K., Xia, X., Yin, Y., Zhang, H., Guo, J., Zhai, P.M., Sugimoto, N., Babu, S.S., Brasseur, G.P., 2016. Aerosol and monsoon climate interactions over Asia. Rev. Geophys. 54, 866-929. https://doi.org/10.1002/2015RG000500.

Li, Z., Niu, F., Fan, J., Liu, Y., Rosenfeld, D., Ding, Y., 2011. Long-term impacts of aerosols on the vertical development of clouds and precipitation. Nat. Geosci. 4, 888-894. https://doi.org/10.1038/ngeo1313.

Li, Z., Wang, Y., Guo, J., Zhao, C., Cribb, M.C., Dong, X., Fan, J., Gong, D., Huang, J., Jiang, M., 2019. East Asian study of tropospheric aerosols and their impact on regional clouds, precipitation, and climate (EAST-AIRCPC). J. Geophys. Res. Atmos. 124, 13026-13054. https://doi.org/10.1029/2019JD030758.

Liao, J., Wang, T., Wang, X., Xie, M., Jiang, Z., Huang, X., Zhu, J., 2014. Impacts of different urban canopy schemes in WRF/Chem on regional climate and air quality in Yangtze River Delta, China. Atmos. Res. 145, 226-243. https://doi.org/10.1016/j.atmosres.2014.04.005.

Lin, C.-Y., Zhao, C., Liu, X., Lin, N.-H., Chen, W.-N., 2014. Modelling of long-range transport of Southeast Asia biomass-burning aerosols to Taiwan and their radiative forcings over East Asia. Tellus B Chem. Phys. Meteorol. 66, 23733. https://doi.org/10.3402/tellusb.v66.23733.

Lin, N.-H., Sayer, A.M., Wang, S.-H., Loftus, A.M., Hsiao, T.-C., Sheu, G.-R., Hsu, N.C., Tsay, S.-C., Chantara, S., 2014. Interactions between biomass-burning aerosols and clouds over Southeast Asia: Current status, challenges, and perspectives. Environ. Pollut. 195, 292-307. https://doi.org/10.1016/j.envpol.2014.06.036.

Liu, C., Wang, T., Chen, P., Li, M., Zhao, M., Zhao, K., Wang, M., Yang, X., 2019. Effects of Aerosols on the Precipitation of Convective Clouds: A Case Study in the Yangtze River Delta of China. J. Geophys. Res. Atmos. 124, 7868-7885. https://doi.org/10.1029/2018JD029924.

Liu, G., Shao, H., Coakley Jr, J.A., Curry, J.A., Haggerty, J.A., Tschudi, M.A., 2003. Retrieval of cloud droplet size from visible and microwave radiometric measurements during INDOEX: Implication to aerosols' indirect radiative effect. J. Geophys. Res. Atmos. 108, AAC-2. https://doi.org/10.1029/2001JD001395.

Liu, L., Bai, Y., Lin, C., Yang, H., 2018. Evaluation of Regional Air Quality Numerical Forecasting System in Central China and Its Application for Aerosol Radiative Effect. Meteorol. Mon. 44, 1179-1190. https://doi.org/10.7519/j.issn.1000-0526.2018.09.006.

Liu, L., Huang, X., Ding, A., Fu, C., 2016. Dust-induced radiative feedbacks in north China?: A dust storm episode modeling study using WRF-Chem. Atmos. Environ. 129, 43-54. https://doi.org/10.1016/j.atmosenv.2016.01.019.

Liu, Q., Jia, X., Quan, J., Li, J., Li, X., Wu, Y., Chen, D., Wang, Z., Liu, Y., 2018. New positive feedback mechanism between boundary layer meteorology and secondary aerosol formation during severe haze events. Sci. Rep. 8, 1-8. https://doi.org/10.1038/s41598-018-24366-3.

Liu, X., Easter, R.C., Ghan, S.J., Zaveri, R., Rasch, P., Shi, X., Lamarque, J.-F., Gettelman, A., Morrison, H., Vitt, F., 2012. Toward a minimal representation of aerosols in climate models: Description and evaluation in the Community Atmosphere Model CAM5. Geosci. Model Dev. 5, 709–739. https://doi.org/10.5194/gmd-5-709-2012.

Liu, X., Zhang, Y., Zhang, Q., He, K., 2016. Application of online-coupled WRF/Chem-MADRID in East Asia?: Model evaluation and climatic effects of anthropogenic aerosols. Atmos. Environ. 124, 321-336. https://doi.org/10.1016/j.atmosenv.2015.03.052.

Liu, Z., Yi, M., Zhao, C., Lau, N.C., Guo, J., Bollasina, M., Yim, S.H.L., 2020. Contribution of local and remote anthropogenic aerosols to a record-breaking torrential rainfall event in Guangdong Province, China. Atmos. Chem. Phys. 20, 223-241. https://doi.org/10.5194/acp-20-223-2020.

Liu, Z., Yim, S.H.L., Wang, C., Lau, N.C., 2018. The Impact of the Aerosol Direct Radiative Forcing on Deep Convection and Air Quality in the Pearl River Delta Region. Geophys. Res. Lett. 45, 4410-4418. https://doi.org/10.1029/2018GL077517.

Lohmann, U., Diehl, K., 2006. Sensitivity studies of the importance of dust ice nuclei for the indirect aerosol effect on stratiform mixed-phase clouds. J. Atmos. Sci. 63, 968-982. https://doi.org/10.1175/JAS3662.1.

Lohmann, U., Feichter, J., 2005. Global indirect aerosol effects: a review. Atmos. Chem. Phys. 5, 715-737. https://doi.org/10.5194/acp-5-715-2005.

Ma, X., Chen, D., Wen, W., Sheng, L., Hu, J., Tong, H., Wei, P., 2016. Effect of Particle Pollution on Regional Meteorological Factors in China. J. Beijing Univ. Technol. 285-295.

https://doi.org/10.11936/bjutxb2015040075.
Ma, X., Wen, W., 2017. Modelling the Effect of Black Carbon and Sulfate Aerosol on the Regional Meteorology Factors, in: IOP Conf. Ser. Earth Environ. Sci. p. 12002. https://doi.org/10.1088/1755-1315/78/1/012002.
Mailler, S., Menut, L., Khvorostyanov, D., Valari, M., Couvidat, F., Siour, G., Turquety, S., Briant, R., Tuccella, P., Bessagnet, B., 2017. CHIMERE-2017: from urban to hemispheric chemistry-transport modeling. Geosci. Model Dev. 10, 2397-2423. https://doi.org/10.5194/gmd-10-2397-2017.
Makar, P.A., Gong, W., Hogrefe, C., Zhang, Y., Curci, G., ?abkar, R., Milbrandt, J., Im, U., Balzarini, A., Baró, R., Bianconi, R., Cheung, P., Forkel, R., Gravel, S., Hirtl, M., Honzak, L., Hou, A., Jiménez-Guerrero, P., Langer, M., Moran, M.D., Pabla, B., Pérez, J.L., Pirovano, G., San José, R., Tuccella, P., Werhahn, J., Zhang, J., Galmarini, S., 2015a. Feedbacks between air pollution and weather, part 2: Effects on chemistry. Atmos. Environ. 115, 499-526. https://doi.org/10.1016/j.atmosenv.2014.10.021.
Makar, P.A., Gong, W., Milbrandt, J., Hogrefe, C., Zhang, Y., Curci, G., ?abkar, R., Im, U., Balzarini, A., Baró, R., Bianconi, R., Cheung, P., Forkel, R., Gravel, S., Hirtl, M., Honzak, L., Hou, A., Jiménez-Guerrero, P., Langer, M., Moran, M.D., Pabla, B., Pérez, J.L., Pirovano, G., San José, R., Tuccella, P., Werhahn, J., Zhang, J., Galmarini, S., 2015b. Feedbacks between air pollution and weather, Part 1: Effects on weather. Atmos. Environ. 115, 442-469. https://doi.org/10.1016/j.atmosenv.2014.12.003.
Manisalidis, I., Stavropoulou, E., Stavropoulos, A., Bezirtzoglou, E., 2020. Environmental and health impacts of air pollution: A review. Front. public Heal. 8. https://doi.org/10.3389/fpubh.2020.00014.
Marelle, L., Raut, J.-C., Law, K.S., Berg, L.K., Fast, J.D., Easter, R.C., Shrivastava, M., Thomas, J.L., 2017. Improvements to the WRF-Chem 3.5. 1 model for quasi-hemispheric simulations of aerosols and ozone in the Arctic. Geosci. Model Dev. 10, 3661–3677. https://doi.org/10.5194/gmd-10-3661-2017.
Martin, D.E., Leight, W.G., 1949. Objective temperature estimates from mean circulation patterns. Mon. Weather Rev. 77, 275-283. https://doi.org/10.1175/1520-0493(1949)077<0275:OTEFMC>2.0.CO;2.
Martin, S.T., Schlenker, J.C., Malinowski, A., Hung, H., Rudich, Y., 2003. Crystallization of atmospheric sulfate-nitrate-ammonium particles. Geophys. Res. Lett. 30. https://doi.org/10.1029/2003GL017930.
Mass, C., Ovens, D., 2011. Fixing WRF's high speed wind bias: A new subgrid scale drag parameterization and the role of detailed verification, in: 24th Conference on Weather and Forecasting and 20th Conference on Numerical Weather Prediction, Preprints, 91st American Meteorological Society Annual Meeting.
McCormick, R.A., Ludwig, J.H., 1967. Climate modification by atmospheric aerosols. Science (80-.). 156, 1358-1359. https://doi.org/10.1126/science.156.3780.1358.
McMurry, P.H., Friedlander, S.K., 1979. New particle formation in the presence of an aerosol. Atmos. Environ. 13, 1635–1651. https://doi.org/10.1016/0004-6981(79)90322-6.
Miao, Y., Guo, J., Liu, S., Zhao, C., Li, X., Zhang, G., Wei, W., Ma, Y., 2018. Impacts of synoptic condition and planetary boundary layer structure on the trans-boundary aerosol transport from Beijing-Tianjin-Hebei region to northeast China. Atmos. Environ. 181, 1-11. https://doi.org/10.1016/j.atmosenv.2018.03.005.
Miao, Y., Liu, S., Zheng, Y., Wang, S., 2016. Modeling the feedback between aerosol and boundary layer processes: a case study in Beijing, China. Environ. Sci. Pollut. Res. 23, 3342-3357. https://doi.org/10.1007/s11356-015-5562-8.
Morrison, H., van Lier-Walqui, M., Fridlind, A.M., Grabowski, W.W., Harrington, J.Y., Hoose, C., Korolev, A., Kumjian, M.R., Milbrandt, J.A., Pawlowska, H., 2020. Confronting the challenge of modeling cloud and precipitation microphysics. J. Adv. Model. earth Syst. 12, e2019MS001689. https://doi.org/10.1029/2019MS001689.
Napari, I., Noppel, M., Vehkam?ki, H., Kulmala, M., 2002. Parametrization of ternary nucleation rates for H_2SO_4-NH_3-H_2O vapors. J. Geophys. Res. Atmos. 107, AAC-6. https://doi.org/10.1029/2002JD002132.
Nenes, A., Pandis, S.N., Pilinis, C., 1998. ISORROPIA: A new thermodynamic equilibrium model for multiphase multicomponent inorganic aerosols. Aquat. geochemistry 4, 123–152.

https://doi.org/10.1023/A:1009604003981.
Nguyen, G.T.H., Shimadera, H., Sekiguchi, A., Matsuo, T., Kondo, A., 2019a. Investigation of aerosol direct effects on meteorology and air quality in East Asia by using an online coupled modeling system. Atmos. Environ. 207, 182-196. https://doi.org/10.1016/j.atmosenv.2019.03.017.
Nguyen, G.T.H., Shimadera, H., Uranishi, K., Matsuo, T., Kondo, A., Thepanondh, S., 2019b. Numerical assessment of $PM_{2.5}$ and O_3 air quality in continental Southeast Asia: Baseline simulation and aerosol direct effects investigation. Atmos. Environ. 219, 117054. https://doi.org/10.1016/j.atmosenv.2019.117054.
North, G.R., Pyle, J.A., Zhang, F., 2014. Encyclopedia of atmospheric sciences. Elsevier.
Odum, J.R., Jungkamp, T.P.W., Griffin, R.J., Flagan, R.C., Seinfeld, J.H., 1997. The atmospheric aerosol-forming potential of whole gasoline vapor. Science (80-.). 276, 96–99. https://doi.org/10.1126/science.276.5309.96.
Park, S.-Y., Lee, H.-J., Kang, J.-E., Lee, T., Kim, C.-H., 2018. Aerosol radiative effects on mesoscale cloud-precipitation variables over Northeast Asia during the MAPS-Seoul 2015 campaign. Atmos. Environ. 172, 109-123. https://doi.org/10.1016/j.atmosenv.2017.10.044.
Penner, J.E., Dong, X., Chen, Y., 2004. Observational evidence of a change in radiative forcing due to the indirect aerosol effect. Nature 427, 231-234. https://doi.org/10.1038/nature02234.
Pye, H.O.T., Murphy, B.N., Xu, L., Ng, N.L., Carlton, A.G., Guo, H., Weber, R., Vasilakos, P., Appel, K.W., Budisulistiorini, S.H., 2017. On the implications of aerosol liquid water and phase separation for organic aerosol mass. Atmos. Chem. Phys. 17, 343–369. https://doi.org/10.5194/acp-17-343-2017.
Qiu, Y., Liao, H., Zhang, R., Hu, J., 2017. Simulated impacts of direct radiative effects of scattering and absorbing aerosols on surface layer aerosol concentrations in China during a heavily polluted event in february 2014. J. Geophys. Res. 122, 5955-5975. https://doi.org/10.1002/2016JD026309.
Quaas, J., Boucher, O., Bellouin, N., Kinne, S., 2008. Satellite-based estimate of the direct and indirect aerosol climate forcing. J. Geophys. Res. Atmos. 113. https://doi.org/10.1029/2007JD008962.
Reid, J.S., Koppmann, R., Eck, T.F., Eleuterio, D.P., 2005. A review of biomass burning emissions part II: intensive physical properties of biomass burning particles. Atmos. Chem. Phys. 5, 799-825. https://doi.org/10.5194/acp-5-799-2005.
Rohde, R.A., Muller, R.A., 2015. Air pollution in China: mapping of concentrations and sources. PLoS One 10, e0135749. https://doi.org/10.1371/journal.pone.0135749.
Rosenfeld, D., 2000. Suppression of rain and snow by urban and industrial air pollution. Science (80-.). 287, 1793-1796. https://doi.org/10.1126/science.287.5459.1793.
Rosenfeld, D., Andreae, M.O., Asmi, A., Chin, M., de Leeuw, G., Donovan, D.P., Kahn, R., Kinne, S., Kivek?s, N., Kulmala, M., 2014. Global observations of aerosol-cloud-precipitation-climate interactions. Rev. Geophys. 52, 750-808. https://doi.org/10.1002/2013RG000441.
Rosenfeld, D., Lohmann, U., Raga, G.B., O'Dowd, C.D., Kulmala, M., Fuzzi, S., Reissell, A., Andreae, M.O., 2008. Flood or drought: How do aerosols affect precipitation? Science (80-.). 321, 1309-1313. https://doi.org/10.1126/science.1160606.
Rosenfeld, D., Zhu, Y., Wang, M., Zheng, Y., Goren, T., Yu, S., 2019. Aerosol-driven droplet concentrations dominate coverage and water of oceanic low-level clouds. Science (80-.). 363. https://doi.org/10.1126/science.aav0566.
Saleh, R., Robinson, E.S., Tkacik, D.S., Ahern, A.T., Liu, S., Aiken, A.C., Sullivan, R.C., Presto, A.A., Dubey, M.K., Yokelson, R.J., 2014. Brownness of organics in aerosols from biomass burning linked to their black carbon content. Nat. Geosci. 7, 647-650. https://doi.org/10.1038/ngeo2220.
Sanchez-Romero, A., Sanchez-Lorenzo, A., Calbó, J., González, J.A., Azorin-Molina, C., 2014. The signal of aerosol-induced changes in sunshine duration records: A review of the evidence. J. Geophys. Res. Atmos. 119, 4657-4673. https://doi.org/10.1002/2013JD021393.
Sarangi, C., Tripathi, S.N., Tripathi, S., Barth, M.C., 2015. Aerosol-cloud associations over Gangetic Basin during a typical monsoon depression event using WRF-Chem simulation. J. Geophys. Res. Atmos. 120, 10-974. https://doi.org/10.1002/2015JD023634.
Satheesh, S.K., Moorthy, K.K., 2005. Radiative effects of natural aerosols: A review. Atmos. Environ. 39, 2089-2110. https://doi.org/10.1016/j.atmosenv.2004.12.029.

Sato, Y., Suzuki, K., 2019. How do aerosols affect cloudiness? Science (80-.). 363, 580-581. https://doi.org/10.1126/science.aaw3720.
Saylor, R.D., Baker, B.D., Lee, P., Tong, D., Pan, L., Hicks, B.B., 2019. The particle dry deposition component of total deposition from air quality models: right, wrong or uncertain? Tellus B Chem. Phys. Meteorol. 71, 1550324. https://doi.org/10.1080/16000889.2018.1550324.
Seaman, N.L., 2000. Meteorological modeling for air-quality assessments. Atmos. Environ. 34, 2231-2259. https://doi.org/10.1016/S1352-2310(99)00466-5.
Seethala, C., Pandithurai, G., Fast, J.D., Polade, S.D., Reddy, M.S., Peckham, S.E., 2011. Evaluating WRF-Chem multi-scale model in simulating aerosol radiative properties over the tropics-a case study over India. Mapan 26, 269-284. https://doi.org/10.1007/s12647-011-0025-2.
Seinfeld, J., Pandis, S., 1998. Atmospheric chemistry and physics: atmospheric chemistry and physics.
Sekiguchi, A., Shimadera, H., Kondo, A., 2018. Impact of aerosol direct effect on wintertime $PM_{2.5}$ simulated by an online coupled meteorology-air quality model over east asia. Aerosol Air Qual. Res. 18, 1068-1079. https://doi.org/10.4209/aaqr.2016.06.0282.
Sekiguchi, M., Nakajima, T., Suzuki, K., Kawamoto, K., Higurashi, A., Rosenfeld, D., Sano, I., Mukai, S., 2003. A study of the direct and indirect effects of aerosols using global satellite data sets of aerosol and cloud parameters. J. Geophys. Res. Atmos. 108. https://doi.org/10.1029/2002JD003359.
Shahid, M.Z., Shahid, I., Chishtie, F., Shahzad, M.I., Bulbul, G., 2019. Analysis of a dense haze event over North-eastern Pakistan using WRF-Chem model and remote sensing. J. Atmos. Solar-Terrestrial Phys. 182, 229-241. https://doi.org/10.1016/j.jastp.2018.12.007.
Shao, Y., Dong, C.H., 2006. A review on East Asian dust storm climate, modelling and monitoring. Glob. Planet. Change 52, 1-22. https://doi.org/10.1016/j.gloplacha.2006.02.011.
Shen, H., Shi, Huawei, Shi, Huading, Ma, X., 2015. Simulation Study of Influence of Aerosol Pollution on Regional Meteorological Factors in Beijing-Tianjin-Hebei Region. J. Anhui Agric. Sci. 43, 207-210. https://doi.org/10.13989/j.cnki.0517-6611.2015.25.217.
Shen, X., Jiang, X., Liu, D., Zu, F., Fan, S., 2017. Simulations of Anthropogenic Aerosols Effects on the Intensity and Precipitation of Typhoon Fitow (1323) Using WRF-Chem Model. Chinese J. Atmos. Sci. 41, 960-974. https://doi.org/10.3878/j.issn.1006-9895.1703.16216.
Siméon, A., Waquet, F., Péré, J.-C., Ducos, F., Thieuleux, F., Peers, F., Turquety, S., Chiapello, I., 2021. Combining POLDER-3 satellite observations and WRF-Chem numerical simulations to derive biomass burning aerosol properties over the southeast Atlantic region. Atmos. Chem. Phys. 21, 17775–17805. https://doi.org/10.5194/acp-21-17775-2021.
Singh, P., Sarawade, P., Adhikary, B., 2020. Carbonaceous Aerosol from Open Burning and its Impact on Regional Weather in South Asia. Aerosol Air Qual. Res. 20, 419-431. https://doi.org/10.4209/aaqr.2019.03.0146.
Slinn, W.G.N., 1984. Precipitation scavenging, in atmospheric sciences and power production-1979. Div. Biomed. Environ. Res. US Dep. Energy, Washingt. DC.
Soni, P., Tripathi, S.N., Srivastava, R., 2018. Radiative effects of black carbon aerosols on Indian monsoon: a study using WRF-Chem model. Theor. Appl. Climatol. 132, 115-134. https://doi.org/10.1007/s00704-017-2057-1.
Srinivas, R., Panicker, A.S., Parkhi, N.S., Peshin, S.K., Beig, G., 2016. Sensitivity of online coupled model to extreme pollution event over a mega city Delhi. Atmos. Pollut. Res. 7, 25-30. https://doi.org/10.1016/j.apr.2015.07.001.
Stephens, G.L., Li, J., Wild, M., Clayson, C.A., Loeb, N., Kato, S., L'ecuyer, T., Stackhouse, P.W., Lebsock, M., Andrews, T., 2012. An update on Earth's energy balance in light of the latest global observations. Nat. Geosci. 5, 691-696. https://doi.org/10.1038/ngeo1580.
Su, L., Fung, J.C.H., 2018a. Investigating the role of dust in ice nucleation within clouds and further effects on the regional weather system over East Asia--Part 2: modification of the weather system. Atmos. Chem. Phys. 18. https://doi.org/10.5194/acp-18-11529-2018.
Su, L., Fung, J.C.H., 2018b. Investigating the role of dust in ice nucleation within clouds and further effects on the regional weather system over East Asia--Part 1: model development and validation. Atmos. Chem. Phys. 18. https://doi.org/10.5194/acp-18-8707-2018.
Sud, Y.C., Walker, G.K., 1990. A review of recent research on improvement of physical parameterizations in the GLA GCM.
Sun, K., Liu, H., Wang, X., Peng, Z., Xiong, Z., 2017. The aerosol radiative effect on a severe haze

episode in the Yangtze River Delta. J. Meteorol. Res. 31, 865-873. https://doi.org/10.1007/s13351-017-7007-4.
Takemura, T., Nakajima, T., Higurashi, A., Ohta, S., Sugimoto, N., 2003. Aerosol distributions and radiative forcing over the Asian Pacific region simulated by Spectral Radiation-Transport Model for Aerosol Species (SPRINTARS). J. Geophys. Res. Atmos. 108. https://doi.org/10.1029/2002JD003210.
Tang, Y., Han, Y., Ma, X., Liu, Z., 2018. Elevated heat pump effects of dust aerosol over Northwestern China during summer. Atmos. Res. 203, 95-104. https://doi.org/10.1016/j.atmosres.2017.12.004.
Ten Hoeve, J.E., Jacobson, M.Z., 2012. Worldwide health effects of the Fukushima Daiichi nuclear accident. Energy Environ. Sci. 5, 8743–8757. https://doi.org/10.1039/c2ee22019a.
Thompson, G., Eidhammer, T., 2014. A study of aerosol impacts on clouds and precipitation development in a large winter cyclone. J. Atmos. Sci. 71, 3636-3658. https://doi.org/10.1175/JAS-D-13-0305.1.
Toon, O.B., McKay, C.P., Ackerman, T.P., Santhanam, K., 1989. Rapid calculation of radiative heating rates and photodissociation rates in inhomogeneous multiple scattering atmospheres. J. Geophys. Res. Atmos. 94, 16287–16301. https://doi.org/10.1029/JD094iD13p16287.
Tremback, C., Tripoli, G., Arritt, R., Cotton, W.R., Pielke, R.A., 1986. The regional atmospheric modeling system, in: Proceedings of an International Conference on Development Applications of Computer Techniques Environmental Studies. Computational Mechanics Publication, Rewood Burn Ltd, pp. 601-607.
Tsay, S.-C., Hsu, N.C., Lau, W.K.-M., Li, C., Gabriel, P.M., Ji, Q., Holben, B.N., Welton, E.J., Nguyen, A.X., Janjai, S., 2013. From BASE-ASIA toward 7-SEAS: A satellite-surface perspective of boreal spring biomass-burning aerosols and clouds in Southeast Asia. Atmos. Environ. 78, 20-34. https://doi.org/10.1016/j.atmosenv.2012.12.013.
Twomey, S., 1977. The influence of pollution on the shortwave albedo of clouds. J. Atmos. Sci. 34, 1149-1152. https://doi.org/10.1175/1520-0469(1977)034<1149:TIOPOT>2.0.CO;2.
Uno, I., Wang, Z., Chiba, M., Chun, Y.S., Gong, S.L., Hara, Y., Jung, E., Lee, S., Liu, M., Mikami, M., 2006. Dust model intercomparison (DMIP) study over Asia: Overview. J. Geophys. Res. Atmos. 111. https://doi.org/10.1029/2005JD006575.
Vehkam?ki, H., Kulmala, M., Napari, I., Lehtinen, K.E.J., Timmreck, C., Noppel, M., Laaksonen, A., 2002. An improved parameterization for sulfuric acid-water nucleation rates for tropospheric and stratospheric conditions. J. Geophys. Res. Atmos. 107, AAC-3. https://doi.org/10.1029/2002JD002184.
Wang, D., Jiang, B., Lin, W., Gu, F., 2019. Effects of aerosol-radiation feedback and topography during an air pollution event over the North China Plain during December 2017. Atmos. Pollut. Res. 10, 587-596. https://doi.org/10.1016/j.apr.2018.10.006.
Wang, H., Niu, T., 2013. Sensitivity studies of aerosol data assimilation and direct radiative feedbacks in modeling dust aerosols. Atmos. Environ. 64, 208-218. https://doi.org/10.1016/j.atmosenv.2012.09.066.
Wang, H., Peng, Y., Zhang, X., Liu, H., Zhang, M., Che, H., Cheng, Y., Zheng, Y., 2018. Contributions to the explosive growth of $PM_{2.5}$ mass due to aerosol-radiation feedback and decrease in turbulent diffusion during a red alert heavy haze in Beijing-Tianjin-Hebei, China. Atmos. Chem. Phys. 18, 17717-17733. https://doi.org/10.5194/acp-18-17717-2018.
Wang, H., Shi, G., Zhu, J., Chen, B., Che, H., Zhao, T., 2013. Case study of longwave contribution to dust radiative effects over East Asia. Chinese Sci. Bull. 58, 3673-3681. https://doi.org/10.1007/s11434-013-5752-z.
Wang, H., Shi, G.Y., Zhang, X.Y., Gong, S.L., Tan, S.C., Chen, B., Che, H.Z., Li, T., 2015a. Mesoscale modelling study of the interactions between aerosols and PBL meteorology during a haze episode in China Jing-Jin-Ji and its near surrounding region-Part 2: Aerosols' radiative feedback effects. Atmos. Chem. Phys. 15, 3277-3287. https://doi.org/10.5194/acp-15-3277-2015.
Wang, H., Xue, M., Zhang, X.Y., Liu, H.L., Zhou, C.H., Tan, S.C., Che, H.Z., Chen, B., Li, T., 2015b. Mesoscale modeling study of the interactions between aerosols and PBL meteorology during a haze episode in Jing-Jin-Ji (China) and its nearby surrounding region-Part 1: Aerosol distributions and meteorological features. Atmos. Chem. Phys. 15, 3257-3275. https://doi.org/10.5194/acp-15-3257-2015.

Wang, H., Zhang, X., Gong, S., Chen, Y., Shi, G., Li, W., 2010. Radiative feedback of dust aerosols on the East Asian dust storms. J. Geophys. Res. Atmos. 115. https://doi.org/10.1029/2009JD013430.

Wang, J., Allen, D.J., Pickering, K.E., Li, Z., He, H., 2016. Impact of aerosol direct effect on East Asian air quality during the EAST-AIRE campaign. J. Geophys. Res. Atmos. 121, 6534-6554. https://doi.org/10.1002/2016JD025108.

Wang, J., Wang, S., Jiang, J., Ding, A., Zheng, M., Zhao, B., Wong, D.C., Zhou, W., Zheng, G., Wang, L., Pleim, J.E., Hao, J., 2014. Impact of aerosol-meteorology interactions on fine particle pollution during China's severe haze episode in January 2013. Environ. Res. Lett. 9. https://doi.org/10.1088/1748-9326/9/9/094002.

Wang, J., Xing, J., Mathur, R., Pleim, J.E., Wang, S., Hogrefe, C., Gan, C.-M., Wong, D.C., Hao, J., 2017. Historical trends in $PM_{2.5}$-related premature mortality during 1990-2010 across the northern hemisphere. Environ. Health Perspect. 125, 400-408. https://doi.org/10.1289/EHP298.

Wang, K., Yahya, K., Zhang, Y., Hogrefe, C., Pouliot, G., Knote, C., Hodzic, A., San Jose, R., Perez, J.L., Jiménez-Guerrero, P., 2015. A multi-model assessment for the 2006 and 2010 simulations under the Air Quality Model Evaluation International Initiative (AQMEII) Phase 2 over North America: Part II. Evaluation of column variable predictions using satellite data. Atmos. Environ. 115, 587-603. https://doi.org/10.1016/j.atmosenv.2014.07.044.

Wang, K., Zhang, Y., Zhang, X., Fan, J., Leung, L.R., Zheng, B., Zhang, Q., He, K., 2018. Fine-scale application of WRF-CAM5 during a dust storm episode over East Asia: Sensitivity to grid resolutions and aerosol activation parameterizations. Atmos. Environ. 176, 1-20. https://doi.org/0.1016/j.atmosenv.2017.12.014.

Wang, L., Fu, J.S., Wei, W., Wei, Z., Meng, C., Ma, S., Wang, J., 2018. How aerosol direct effects influence the source contributions to $PM_{2.5}$ concentrations over Southern Hebei, China in severe winter haze episodes. Front. Environ. Sci. Eng. 12, 13. https://doi.org/10.1007/s11783-018-1014-2.

Wang, Z., Huang, X., Ding, A., 2018. Dome effect of black carbon and its key influencing factors: a one-dimensional modelling study. Atmos. Chem. Phys. 18, 2821. https://doi.org/10.5194/acp-18-2821-2018.

Wang, Z., Huang, X., Ding, A., 2019. Optimization of vertical grid setting for air quality modelling in China considering the effect of aerosol-boundary layer interaction. Atmos. Environ. 210, 1-13. https://doi.org/10.1016/j.atmosenv.2019.04.042.

Wang, Z., Wang, Zhe, Li, Jie, Zheng, H., Yan, P., Li, J, 2014. Development of a meteorology-chemistry two-way coupled numerical model (WRF? NAQPMS) and its application in a severe autumn haze simulation over the Beijing-Tianjin-Hebei area, China. Clim. Environ. Res 19, 153-163. https://doi.org/10.3878/j.issn.1006-9585.2014.13231.

Wang, Z.F., Li, J., Wang, Z., Yang, W., Tang, X., Ge, B., Yan, P., Zhu, L., Chen, X., Chen, H., 2014. Modeling study of regional severe hazes over mid-eastern China in January 2013 and its implications on pollution prevention and control. Sci. China Earth Sci. 57, 3-13. https://doi.org/10.1007/s11430-013-4793-0.

Wendisch, M., Keil, A., Müller, D., Wandinger, U., Wendling, P., Stifter, A., Petzold, A., Fiebig, M., Wiegner, M., Freudenthaler, V., 2002. Aerosol-radiation interaction in the cloudless atmosphere during LACE 98 1. Measured and calculated broadband solar and spectral surface insolations. J. Geophys. Res. Atmos. 107, LAC-6. https://doi.org/10.1029/2000JD000226.

Wexler, A.S., Lurmann, F.W., Seinfeld, J.H., 1994. Modelling urban and regional aerosols-I. Model development. Atmos. Environ. 28, 531–546. https://doi.org/10.1016/1352-2310(94)90129-5.

Whitby, K.T., 1978. The physical characteristics of sulfur aerosols, in: Sulfur in the Atmosphere. Elsevier, pp. 135–159. https://doi.org/10.1016/B978-0-08-022932-4.50018-5.

Wilcox, E.M., 2012. Direct and semi-direct radiative forcing of smoke aerosols over clouds. Atmos. Chem. Phys. 12, 139. https://doi.org/10.5194/acp-12-139-2012.

Wong, D.C., Pleim, J., Mathur, R., Binkowski, F., Otte, T., Gilliam, R., Pouliot, G., Xiu, A., Young, J.O., Kang, D., 2012. WRF-CMAQ two-way coupled system with aerosol feedback: software development and preliminary results. Geosci. Model Dev. 5, 299. https://doi.org/10.5194/gmd-5-299-2012.

Wu, J., Bei, N., Hu, B., Liu, S., Zhou, M., Wang, Q., Li, X., Lang, L., Tian, F., Liu, Z., 2019a. Aerosol-radiation feedback deteriorates the wintertime haze in the North China Plain. Atmos. Chem. Phys. 19, 8703-8719. https://doi.org/10.5194/acp-19-8703-2019.

Wu, J., Bei, N., Hu, B., Liu, S., Zhou, M., Wang, Q., Li, X., Liu, L., Feng, T., Liu, Z., Wang, Y., Cao, J., Tie, X., Wang, J., Molina, L.T., Li, G., 2019b. Is water vapor a key player of the wintertime haze in North China Plain? Atmos. Chem. Phys. 19, 8721-8739. https://doi.org/10.5194/acp-19-8721-2019

Wu, L., Su, H., Jiang, J.H., 2013. Regional simulation of aerosol impacts on precipitation during the East Asian summer monsoon. J. Geophys. Res. Atmos. 118, 6454-6467. https://doi.org/10.1002/jgrd.50527.

Wu, W., Zhang, Y., 2018. Effects of particulate matter ($PM_{2.5}$) and associated acidity on ecosystem functioning: response of leaf litter breakdown. Environ. Sci. Pollut. Res. 25, 30720-30727. https://doi.org/10.1007/s11356-018-2922-1.

Wu, Y., Han, Y., Voulgarakis, A., Wang, T., Li, M., Wang, Y., Xie, M., Zhuang, B., Li, S., 2017. An agricultural biomass burning episode in eastern China: Transport, optical properties, and impacts on regional air quality. J. Geophys. Res. Atmos. 122, 2304-2324. https://doi.org/10.1002/2016JD025319.

Xie, M., Liao, J., Wang, T., Zhu, K., Zhuang, B., Han, Y., Li, M., Li, S., 2016. Modeling of the anthropogenic heat flux and its effect on regional meteorology and air quality over the Yangtze River Delta region, China. Atmos. Chem. Phys. 16, 6071. https://doi.org/10.5194/acp-16-6071-2016.

Xing, J., Mathur, R., Pleim, J., Hogrefe, C., Gan, C., Wong, D.C., Wei, C., Wang, J., 2015b. Air pollution and climate response to aerosol direct radiative effects: A modeling study of decadal trends across the northern hemisphere. J. Geophys. Res. Atmos. 120, 12-221. https://doi.org/10.1002/2015JD023933.

Xing, J., Mathur, R., Pleim, J., Hogrefe, C., Gan, C.M., Wong, D.C., Wei, C., 2015c. Can a coupled meteorology-chemistry model reproduce the historical trend in aerosol direct radiative effects over the Northern Hemisphere? Atmos. Chem. Phys. 15, 9997-10018. https://doi.org/10.5194/acp-15-9997-2015.

Xing, J., Mathur, R., Pleim, J., Hogrefe, C., Gan, C.-M., Wong, D.-C., Wei, C., Gilliam, R., Pouliot, G., 2015a. Observations and modeling of air quality trends over 1990-2010 across the Northern Hemisphere: China, the United States and Europe. Atmos. Chem. Phys. 15. https://doi.org/10.5194/acp-15-2723-2015.

Xing, J., Wang, J., Mathur, R., Pleim, J., Wang, S., Hogrefe, C., Gan, C.-M., Wong, D.C., Hao, J., 2016. Unexpected benefits of reducing aerosol cooling effects. Environ. Sci. Technol. 50, 7527-7534. https://doi.org/10.1021/acs.est.6b00767.

Xing, J., Wang, J., Mathur, R., Wang, S., Sarwar, G., Pleim, J., Hogrefe, C., Zhang, Y., Jiang, J., Wong, D.C., 2017. Impacts of aerosol direct effects on tropospheric ozone through changes in atmospheric dynamics and photolysis rates. Atmos. Chem. Phys. 17, 9869. https://doi.org/10.5194/acp-17-9869-2017.

Yahya, K., Wang, K., Gudoshava, M., Glotfelty, T., Zhang, Y., 2015. Application of WRF/Chem over North America under the AQMEII Phase 2: Part I. Comprehensive evaluation of 2006 simulation. Atmos. Environ. 115, 733-755. https://doi.org/10.1016/j.atmosenv.2014.08.063.

Yan, J., Wang, X., Gong, P., Wang, C., Cong, Z., 2018. Review of brown carbon aerosols: Recent progress and perspectives. Sci. Total Environ. 634, 1475-1485. https://doi.org/10.1016/j.scitotenv.2018.04.083.

Yang, J., Duan, K., Kang, S., Shi, P., Ji, Z., 2017. Potential feedback between aerosols and meteorological conditions in a heavy pollution event over the Tibetan Plateau and Indo-Gangetic Plain. Clim. Dyn. 48, 2901-2917. https://doi.org/10.1007/s00382-016-3240-2.

Yang, J., Kang, S., Ji, Z., Chen, D., 2018. Modeling the origin of anthropogenic black carbon and its climatic effect over the Tibetan Plateau and surrounding regions. J. Geophys. Res. Atmos. 123, 671-692. https://doi.org/10.1002/2017JD027282.

Yang, T., Liu, Y., 2017a. Mechanism analysis of the impacts of aerosol direct effects on a rainstorm. J. Trop. Meteorol. 33, 762-773. https://doi.org/10.16032/j.issn.1004-4965.2017.05.019.

Yang, T., Liu, Y., 2017b. Impact of anthropogenic pollution on “7.21” extreme heavy rainstorm. J. Meteorol. Sci. 742-752. https://doi.org/10.3969/2016jms.0074.

Yang, Y., Fan, J., Leung, L.R., Zhao, C., Li, Z., Rosenfeld, D., 2016. Mechanisms contributing to suppressed precipitation in Mt. Hua of central China. Part I: Mountain valley circulation. J. Atmos. Sci. 73, 1351-1366. https://doi.org/10.1175/JAS-D-15-0233.1.

Yang, Y., Tang, J., Sun, J., Wang, L., Wang, X., Zhang, Y., Qu, Q., Zhao, W., 2015. Synoptic Effect

of a Heavy Haze Episode over North China. Clim. Environ. Res. https://doi.org/10.3878/j.issn.1006-9585.2015.15018.
Yang, Y., Zhao, C., Dong, X., Fan, G., Zhou, Y., Wang, Y., Zhao, L., Lv, F., Yan, F., 2019. Toward understanding the process-level impacts of aerosols on microphysical properties of shallow cumulus cloud using aircraft observations. Atmos. Res. 221, 27-33. https://doi.org/10.1016/j.atmosres.2019.01.027.
Yao, H., Song, Y., Liu, M., Archer-Nicholls, S., Lowe, D., McFiggans, G., Xu, T., Du, P., Li, J., Wu, Y., 2017. Direct radiative effect of carbonaceous aerosols from crop residue burning during the summer harvest season in East China. Atmos. Chem. Phys. 17, 5205. https://doi.org/10.5194/acp-17-5205-2017.
Yasunari, T.J., Yamazaki, K., 2009. Impacts of Asian dust storm associated with the stratosphere-to-troposphere transport in the spring of 2001 and 2002 on dust and tritium variations in Mount Wrangell ice core, Alaska. Atmos. Environ. 43, 2582-2590. https://doi.org/10.1016/j.atmosenv.2009.02.025.
Yi?it, E., Kní?ová, P.K., Georgieva, K., Ward, W., 2016. A review of vertical coupling in the Atmosphere-Ionosphere system: Effects of waves, sudden stratospheric warmings, space weather, and of solar activity. J. Atmos. Solar-Terrestrial Phys. 141, 1-12. https://doi.org/10.1016/j.jastp.2016.02.011.
Yoo, J.-W., Jeon, W., Park, S.-Y., Park, C., Jung, J., Lee, S.-H., Lee, H.W., 2019. Investigating the regional difference of aerosol feedback effects over South Korea using the WRF-CMAQ two-way coupled modeling system. Atmos. Environ. 218, 116968. https://doi.org/10.1016/j.atmosenv.2019.116968.
Yoon, J., Chang, D.Y., Lelieveld, J., Pozzer, A., Kim, J., Yum, S.S., 2019. Empirical evidence of a positive climate forcing of aerosols at elevated albedo. Atmos. Res. 229, 269-279. https://doi.org/10.1016/j.atmosres.2019.07.001.
Yu, F., 2006. From molecular clusters to nanoparticles: second-generation ion-mediated nucleation model. Atmos. Chem. Phys. 6, 5193–5211. https://doi.org/10.5194/acp-6-5193-2006.
Yu, F., Luo, G., 2009. Simulation of particle size distribution with a global aerosol model: contribution of nucleation to aerosol and CCN number concentrations. Atmos. Chem. Phys. 9, 7691–7710. https://doi.org/10.5194/acp-9-7691-2009.
Yu, H., Kaufman, Y.J., Chin, M., Feingold, G., Remer, L.A., Anderson, T.L., Balkanski, Y., Bellouin, N., Boucher, O., Christopher, S., 2006. A review of measurement-based assessments of the aerosol direct radiative effect and forcing. Atmos. Chem. Phys. 6, 613-666. https://doi.org/10.5194/acp-6-613-2006.
Yuan, Q., Xu, J., Liu, L., Zhang, A., Liu, Y., Zhang, J., Wan, X., Li, M., Qin, K., Cong, Z., 2020. Evidence for large amounts of brown carbonaceous tarballs in the himalayan atmosphere. Environ. Sci. Technol. Lett. 8, 16–23. https://doi.org/10.1021/acs.estlett.0c00735.
Yuan, T., Chen, S., Huang, J., Wu, D., Lu, H., Zhang, G., Ma, Xiaojun, Chen, Z., Luo, Y., Ma, Xiaohui, 2019. Influence of dynamic and thermal forcing on the meridional transport of Taklimakan Desert dust in spring and summer. J. Clim. 32, 749-767. https://doi.org/10.1175/JCLI-D-18-0361.1.
Zaveri, R.A., Easter, R.C., Fast, J.D., Peters, L.K., 2008. Model for simulating aerosol interactions and chemistry (MOSAIC). J. Geophys. Res. Atmos. 113. https://doi.org/10.1029/2007JD008782.
Zhan, J., Chang, W., Li, W., Wang, Y., Chen, L., Yan, J., 2017. Impacts of meteorological conditions, aerosol radiative feedbacks, and emission reduction scenarios on the coastal haze episodes in southeastern China in December 2013. J. Appl. Meteorol. Climatol. 56, 1209-1229. https://doi.org/10.1175/JAMC-D-16-0229.1.
Zhang, B., Wang, Y., Hao, J., 2015. Simulating aerosol-radiation-cloud feedbacks on meteorology and air quality over eastern China under severe haze conditionsin winter. Atmos. Chem. Phys. 15, 2387-2404. https://doi.org/10.5194/acp-15-2387-2015.
Zhang, H., Cheng, S., Li, J., Yao, S., Wang, X., 2019. Investigating the aerosol mass and chemical components characteristics and feedback effects on the meteorological factors in the Beijing-Tianjin-Hebei region, China. Environ. Pollut. 244, 495-502. https://doi.org/10.1016/j.envpol.2018.10.087.
Zhang, H., DeNero, S.P., Joe, D.K., Lee, H.-H., Chen, S.-H., Michalakes, J., Kleeman, M.J., 2014. Development of a source oriented version of the WRF/Chem model and its application to the

California regional $PM_{10}/PM_{2.5}$ air quality study. Atmos. Chem. Phys. 14, 485–503. https://doi.org/10.5194/acp-14-485-2014.
Zhang, L., Gong, S., Zhao, T., Zhou, C., Wang, Y., Li, J., Ji, D., He, J., Liu, H., Gui, K., 2021. Development of WRF/CUACE v1.0 model and its preliminary application in simulating air quality in China. Geosci. Model Dev. 14, 703–718. https://doi.org/10.5194/gmd-14-703-2021.
Zhang, L., Wang, T., Lv, M., Zhang, Q., 2015. On the severe haze in Beijing during January 2013: Unraveling the effects of meteorological anomalies with WRF-Chem. Atmos. Environ. 104, 11–21. https://doi.org/10.1016/j.atmosenv.2015.01.001.
Zhang, X.Y., Gong, S.L., Shen, Z.X., Mei, F.M., Xi, X.X., Liu, L.C., Zhou, Z.J., Wang, D., Wang, Y.Q., Cheng, Y., 2003a. Characterization of soil dust aerosol in China and its transport and distribution during 2001 ACE-Asia: 1. Network observations. J. Geophys. Res. Atmos. 108. https://doi.org/10.1029/2002JD002632.
Zhang, X.Y., Gong, S.L., Zhao, T.L., Arimoto, R., Wang, Y.Q., Zhou, Z.J., 2003b. Sources of Asian dust and role of climate change versus desertification in Asian dust emission. Geophys. Res. Lett. 30. https://doi.org/10.1029/2003GL018206.
Zhang, Xin, Zhang, Q., Hong, C., Zheng, Y., Geng, G., Tong, D., Zhang, Y., Zhang, Xiaoye, 2018. Enhancement of $PM_{2.5}$ Concentrations by Aerosol-Meteorology Interactions Over China. J. Geophys. Res. Atmos. 123, 1179-1194. https://doi.org/10.1002/2017JD027524.
Zhang, Y., 2008. Online-coupled meteorology and chemistry models: history, current status, and outlook. Atmos. Chem. Phys 8, 2895-2932. https://doi.org/10.5194/acp-8-2895-2008.
Zhang, Y., Chen, Y., Fan, J., Leung, L.-Y.R., 2015a. Application of an online-coupled regional climate model, WRF-CAM5, over East Asia for examination of ice nucleation schemes: part II. Sensitivity to heterogeneous ice nucleation parameterizations and dust emissions. Climate 3, 753-774. https://doi.org/10.3390/cli3030753.
Zhang, Y., He, J., Zhu, S., Gantt, B., 2016. Sensitivity of simulated chemical concentrations and aerosol-meteorology interactions to aerosol treatments and biogenic organic emissions in WRF/Chem. J. Geophys. Res. Atmos. 121, 6014–6048. https://doi.org/10.1002/2016JD024882.
Zhang, Y., Hu, X.M., Howell, G.W., Sills, E., Fast, J.D., Gustafson Jr, W.I., Zaveri, R.A., Grell, G.A., Peckham, S.E., McKeen, S.A., 2005. Modeling atmospheric aerosols in WRF/CHEM, in: WRF/MM5 Users's Workshop. National Center for Atmospheric Research.
Zhang, Y., Karamchandani, P., Glotfelty, T., Streets, D.G., Grell, G., Nenes, A., Yu, F., Bennartz, R., 2012. Development and initial application of the global-through-urban weather research and forecasting model with chemistry (GU-WRF/Chem). J. Geophys. Res. Atmos. 117. https://doi.org/10.1029/2012JD017966.
Zhang, Y., Pan, Y., Wang, K., Fast, J.D., Grell, G.A., 2010. WRF/Chem-MADRID: Incorporation of an aerosol module into WRF/Chem and its initial application to the TexAQS2000 episode. J. Geophys. Res. Atmos. 115. https://doi.org/10.1029/2009JD013443.
Zhang, Y., Pun, B., Vijayaraghavan, K., Wu, S., Seigneur, C., Pandis, S.N., Jacobson, M.Z., Nenes, A., Seinfeld, J.H., 2004. Development and application of the model of aerosol dynamics, reaction, ionization, and dissolution (MADRID). J. Geophys. Res. Atmos. 109. https://doi.org/10.1029/2003JD003501.
Zhang, Y., Wang, K., He, J., 2017. Multi-year application of WRF-CAM5 over East Asia-Part II: Interannual variability, trend analysis, and aerosol indirect effects. Atmos. Environ. 165, 222-239. https://doi.org/10.1016/j.atmosenv.2017.06.029.
Zhang, Y., Zhang, X., Cai, C., Wang, K., Wang, L., 2014. Studying Aerosol-Cloud-Climate Interactions over East Asia Using WRF/Chem, in: Air Pollution Modeling and Its Application XXIII. Springer, pp. 61-66. https://doi.org/10.1007/978-3-319-04379-1_10.
Zhang, Y., Zhang, X., Wang, K., He, J., Leung, L.R., Fan, J., Nenes, A., 2015b. Incorporating an advanced aerosol activation parameterization into WRF-CAM5: Model evaluation and parameterization intercomparison. J. Geophys. Res. Atmos. 120, 6952-6979. https://doi.org/10.1002/2014JD023051.
Zhang, Yang, Zhang, X., Wang, K., Zhang, Q., Duan, F., He, K., 2016a. Application of WRF/Chem over East Asia: Part II. Model improvement and sensitivity simulations. Atmos. Environ. 124, 301-320. https://doi.org/10.1016/j.atmosenv.2015.07.023.
Zhang, Yang, Zhang, X., Wang, L., Zhang, Q., Duan, F., He, K., 2016b. Application of WRF/Chem over East Asia: Part I. Model evaluation and intercomparison with MM5/CMAQ. Atmos. Environ. 124, 285-300. https://doi.org/10.1016/j.atmosenv.2015.07.022.

Zhang, Yue, Fan Shuxian, Li Hao, Kang Boshi, 2016. Effects of aerosol radiative feedback during a severe smog process over eastern China. Acta Meteorol. 74. https://doi.org/10.11676/qxxb2016.028.
Zhao, B., Liou, K., Gu, Y., Li, Q., Jiang, J.H., Su, H., He, C., Tseng, H.-L.R., Wang, S., Liu, R., 2017. Enhanced $PM_{2.5}$ pollution in China due to aerosol-cloud interactions. Sci. Rep. 7, 1-11. https://doi.org/10.1038/s41598-017-04096-8.
Zhao, B., Wang, Y., Gu, Y., Liou, K.-N., Jiang, J.H., Fan, J., Liu, X., Huang, L., Yung, Y.L., 2019. Ice nucleation by aerosols from anthropogenic pollution. Nat. Geosci. 12, 602-607. https://doi.org/10.1038/s41561-019-0389-4.
Zhong, M., Chen, F., Saikawa, E., 2019. Sensitivity of projected $PM_{2.5}$- and O_3-related health impacts to model inputs: A case study in mainland China. Environ. Int. 123, 256-264. https://doi.org/10.1016/j.envint.2018.12.002.
Zhong, M., Saikawa, E., Liu, Y., Naik, V., Horowitz, L.W., Takigawa, M., Zhao, Y., Lin, N.-H., Stone, E.A., 2016. Air quality modeling with WRF-Chem v3.5 in East Asia: sensitivity to emissions and evaluation of simulated air quality. Geosci. Model Dev. 9, 1201-1218. https://doi.org/10.5194/gmd-9-1201-2016.
Zhong, S., Qian, Y., Zhao, C., Leung, R., Wang, H., Yang, B., Fan, J., Yan, H., Yang, X.-Q., Liu, D., 2017. Urbanization-induced urban heat island and aerosol effects on climate extremes in the Yangtze River Delta region of China. Atmos. Chem. Phys. 17. https://doi.org/10.5194/acp-17-5439-2017.
Zhong, S., Qian, Y., Zhao, C., Leung, R., Yang, X., 2015. A case study of urbanization impact on summer precipitation in the Greater Beijing Metropolitan Area: Urban heat island versus aerosol effects. J. Geophys. Res. Atmos. 120, 10-903. https://doi.org/10.1002/2015JD023753.
Zhou, C., Gong, S., Zhang, X., Liu, H., Xue, M., Cao, G., An, X., Che, H., Zhang, Y., Niu, T., 2012. Towards the improvements of simulating the chemical and optical properties of Chinese aerosols using an online coupled model-CUACE/Aero. Tellus B Chem. Phys. Meteorol. 64, 18965. https://doi.org/10.3402/tellusb.v64i0.18965.
Zhou, C., Gong, S.L., Zhang, X.Y., Wang, Y.Q., Niu, T., Liu, H.L., Zhao, T.L., Yang, Y.Q., Hou, Q., 2008. Development and evaluation of an operational SDS forecasting system for East Asia: CUACE/Dust. Atmos. Chem. Phys. 8, 787-798. https://doi.org/10.5194/acp-8-787-2008.
Zhou, C., Zhang, X., Gong, S., Wang, Y., Xue, M., 2016. Improving aerosol interaction with clouds and precipitation in a regional chemical weather modeling system 145-160. https://doi.org/10.5194/acp-16-145-2016.
Zhou, D., Ding, K., Huang, X., Liu, L., Liu, Q., Xu, Z., Jiang, F., Fu, C., Ding, A., 2018. Transport, mixing and feedback of dust, biomass burning and anthropogenic pollutants in eastern Asia: a case study. Atmos. Chem. Phys. 18, 16345-16361. https://doi.org/10.5194/acp-18-16345-2018.
Zhou, M., Zhang, L., Chen, D., Gu, Y., Fu, T.-M., Gao, M., Zhao, Y., Lu, X., Zhao, B., 2019. The impact of aerosol-radiation interactions on the effectiveness of emission control measures. Environ. Res. Lett. 14, 24002. https://doi.org/10.1088/1748-9326/aaf27d.
Zhou, Y., Gong, S., Zhou, C., Zhang, L., He, J., Wang, Y., Ji, D., Feng, J., Mo, J., Ke, H., 2021. A new parameterization of uptake coefficients for heterogeneous reactions on multi-component atmospheric aerosols. Sci. Total Environ. 781, 146372. https://doi.org/10.1016/j.scitotenv.2021.146372.
Zhuang, B., Jiang, F., Wang, T., Li, S., Zhu, B., 2011. Investigation on the direct radiative effect of fossil fuel black-carbon aerosol over China. Theor. Appl. Climatol. 104, 301-312. https://doi.org/10.1007/s00704-010-0341-4.